AFFDL-TR-67-187

AN OPTIMAL CONTROL METHOD FOR PREDICTING CONTROL CHARACTERISTICS AND DISPLAY REQUIREMENTS OF MANNED-VEHICLE SYSTEMS

JEROME I. ELKIND
PETER L. FALB
DAVID KLEINMAN
WILLIAM H. LEVISON

Bolt Beranek and Newman Inc.

FOREWORD

The studies reported here are part of a U.S. Air Force research program to develop methods for the design and analysis of piloted-vehicle systems. This report summarizes theoretical and experimental investigations performed under Contract No. AF33(615) 5160, Project No. 8219, Task No. 821910, sponsored by the Flight Control Division of the Air Force Flight Dynamics Laboratory. The principal investigators for the contract were J.I. Elkind and J. W. Senders of Bolt Beranek and Newman Inc. The project engineer for the Flight Control Division was A.J. Connors.

Many have contributed to the results reported here. J.W. Senders' work on human instrument monitoring provided the basis for display analysis procedures that were developed. He was a major contributor to the formulation of the research program and was a sympathetic critic of the results obtained. D.T. McRuer and his colleagues at Systems Technology, Inc. did much of the basic work on human controller characteristics and we have drawn heavily upon their results in this study. Mrs. Jane Ward had a major responsibility for performing the simulator experiments and contributed greatly to the success of the program. Robert Wenning, James Martin, and Wesley Warner of the Naval Air Station, South Weymouth, Massachusetts served most willingly and cooperatively as subjects for the experiments. R.O. Anderson, A.J. Connors, P. Pietrzak, and R. J. Woodcock of the Flight Control Division contributed greatly to the planning of the program and were exceedingly helpful in their careful review of the report. They are responsible for many improvements to the report made as a result of their suggestions.

The manuscript was released by the authors April 1968 for publication as an RTD Technical Report.

This technical report has been reviewed and is approved.

C. B. Westbrook

Chief, Control Criteria Branch
Flight Control Division
AF Flight Dynamics Laboratory

ABSTRACT

An analytic procedure for determining information display requirements and human control and instrument monitoring characteristics for complex multivariable vehicular control systems is developed. The method is based upon the assumption that, subject to certain internal limitations, the human controller will act in a near optimal manner. Because of the multidimensionality of the system and the near optimality of the human controller, it is appropriate to use modern optimal control theory and its associated state-space representation as the basis for the analytic procedure.

A model for the human controller is developed in which the controller's inherent limitations are approximated by a time delay. The model also includes a prediction process for compensating for this time delay, a control process for producing the control inputs to the vehicle and a cost functional that is to be minimized. The control process is assumed to be optimal. Several suboptimal prediction processes are investigated. Only quadratic cost functionals are considered.

The analytic procedure assumes that the human operator's control characteristics can be represented by a set of gains operating on the delayed state variables of the system. These gains are predicted from the gains of optimal control process of the model and from the characteristics of the prediction process. It is further postulated that the information display requirements and instrument monitoring behavior can be determined from the sensitivity of the cost (or performance of the system) to changes in gain of the controller.

To validate the analytic procedure and model an analysis of a V/STOL vehicle in hovering flight under several conditions was performed. The vehicle chosen was the XV-5A. Information display requirements and control and monitoring characteristics were predicted. The vehicle was simulated and experiments were performed with several heliocopter pilot's as subjects and with several different display configurations. Good agreement was achieved between the analytic and experimental results.

The experiments and the analyses that we performed suggested several important modifications and refinements that should be made to the model. These include an explicit representation of the noise associated with observation of system state and a representation of the controllers visual scanning process.

TABLE OF CONTENTS

Table of Contents (Continued)

LIST OF FIGURES

LIST OF TABLES

List of Tables (continued) PAGE

LIST OF SYMBOLS

A_i	time per unit time allocated to i^{th} variable
$\underline{A}$	matrix representing system dynamics
$\underline{\bar{A}}$	matrix representing closed-loop dynamics, equal to $\underline{A}-\underline{B}\ \underline{R}^{-1}\ \underline{B}'\ \underline{K}$
$\underline{B}$	matrix representing effects of control on system
C	minimum time per sample of fixation
D	ratio of actual gain to optimum gain
D_i	duration of fixation of the i^{th} display
E[ ]	expected value
E	variance of filtered disturbance
E_i	variance of the permissible error in reading the i^{th} variable
F_i	sampling frequency for i^{th} display
$\underline{G}$	nonoptimal feedback gain matrix
H(s)	human operator describing function
$\underline{H}(s)$	compensator for optimal controller configuration
$H_e(s)$	describing function of human operator equalizer dynamics
$H_E(s)$	equivalent human operator describing function
$H_I(s)$	describing function of invariant dynamics of human operator
i	subscript

$\underline{I}$	identity matrix
J	cost
J*	optimal cost
K	gain
K	time per bit spent acquiring and processing information
$\underline{K}$	matrix solution to Riccati Equation
K'	constant in scanning model for control tasks
$\underline{L}^*$	optimal feedback gain matrix
$\underline{L}_c$	matrix of cross-correlated gains
$\underline{L}_s$	matrix of simple predictor feedback gains
$\underline{L}_{HE}$	equivalent gain matrix for human operator
$\underline{L}_{HEi}$	gain matrix for human operator for i^{th} display
P_i	variance in the i^{th} signal being monitored
q	pitch rate
$\underline{Q}$	weighting matrix for $\underline{x}(t)$ in cost functional
$\underline{R}$	weighting matrix for $\underline{u}(t)$ in cost functional
s	complex frequency
$s_i(D)$	sensitivity coefficient
$s_i^o(D)$	normalized sensitivity coefficient
$\underline{S}_G$	sensitivity matrix
$S_i(f)$	power density spectrum of i^{th} variable

t	time
T	time delay
u	translational velocity along X axis of aircraft
$\dot{u}$	translational acceleration along X axis of aircraft
$\underline{u}^*$	optimal control
$\underline{u}_G$	nonoptimal control
$\underline{u}(t)$	control inputs
$u_w(t)$	filtered disturbance
$v(t)$	observation noise
$\underline{v}_\omega(t)$	vector observation noise with scanning
$\underline{V}_\omega$	observation noise covariance matrix
$w_1(t)$	first element of $\underline{w}(t)$
w_{11}	variance of w_1
$\underline{w}(t)$	disturbance vector
$W_{1/2}$	half-power bandwidth
W_i	bandwidth of i^{th} variable
W_{ei}	effective bandwidth of i^{th} variable
x	position along X axis
$\underline{x}^*$	optimal trajectory
$\underline{x}(t)$	vehicle state vector

$\hat{x}(t)$	estimate of x(t)
$y(t)$	output of $H_I(s)$
$\underline{y}_d(t)$	display information
$\underline{Z}(s)$	transfer matrix of plant augmented by time delay
α	bandwidth of disturbance
$\delta(t-\tau)$	delta or impulse function
$\delta_\theta(t)$	control deflection
ΔJ	cost increase
$\Lambda_1(D)$	diagonal matrix for deviations of gain from optimum
$\underline{\Sigma}_{\hat{x}}$	covariance matrix of $\hat{\underline{x}}(t)$
θ	pitch angle
τ	time
ω	sampling strategy

CHAPTER I

INTRODUCTION

During the past decade there has been developed a good basic understanding of the human operator as a controller of relatively simple dynamic systems and as a monitor of instruments that portray the behavior of such systems.† Although models of human control behavior derived from studies of simple systems occasionally have been applied in the design and analysis of complex systems, a well tested and reasonably coherent theory of the human controller of complex systems has not yet emerged. Development of such a theory, naturally enough, is the focus of several research projects that are currently in process.

The study that we discuss in this report is one of these projects. The objectives of our research were to develop and test a method for determining information display requirements, for predicting human operator control characteristics, and for predicting human operator instrument monitoring behavior in realistically complex aircraft systems. Our strategy was to build upon existing models for control and monitoring behavior that for the most part were derived from studies of simple systems. To provide a structure for extending these simple models to complex situations, we have relied heavily upon the techniques of modern control theory. This theory is well suited for the analysis of complex multivariable dynamic systems.[5,6]

---

†The results of these attempts to uncover the properties of the human operator have been summarized by McRuer and Krendel,[1] Senders,[2] Elkind,[3] and McRuer, Graham, Krendel and Reisner.[4]

The systems analysis method that we developed is presented in Chapter II. A brief review of the relevant human operator models and certain results from modern control theory are also in this chapter. In Chapter III we apply the method to the analysis of a V/STOL vehicle in hovering flight. Experiments were performed to validate the analysis method. They are described in Chapter IV and the results obtained are presented there. In Chapter V the experimental results are discussed. We evaluate the analysis method, point out its deficiencies, and suggest a more promising approach to the analysis of complex systems.

We are continuing our work toward the development of a theory of manual control of complex systems. Thus, this is actually an interim report on one phase of this development. Research on other phases are in process and reports on the results obtained will be forthcoming.

CHAPTER II

SYSTEM ANALYSIS METHOD

We are given the manned-vehicle system shown in Fig. 1. The vehicle's state is represented by the vector $\underline{x}(t)$. The vehicle is subjected to random disturbances $\underline{w}(t)$. The pilot has the task of controlling the vehicle so that it follows some desired flight path. To do this he must regulate the system state to counteract the effects of the disturbances as well as establish the desired flight path.

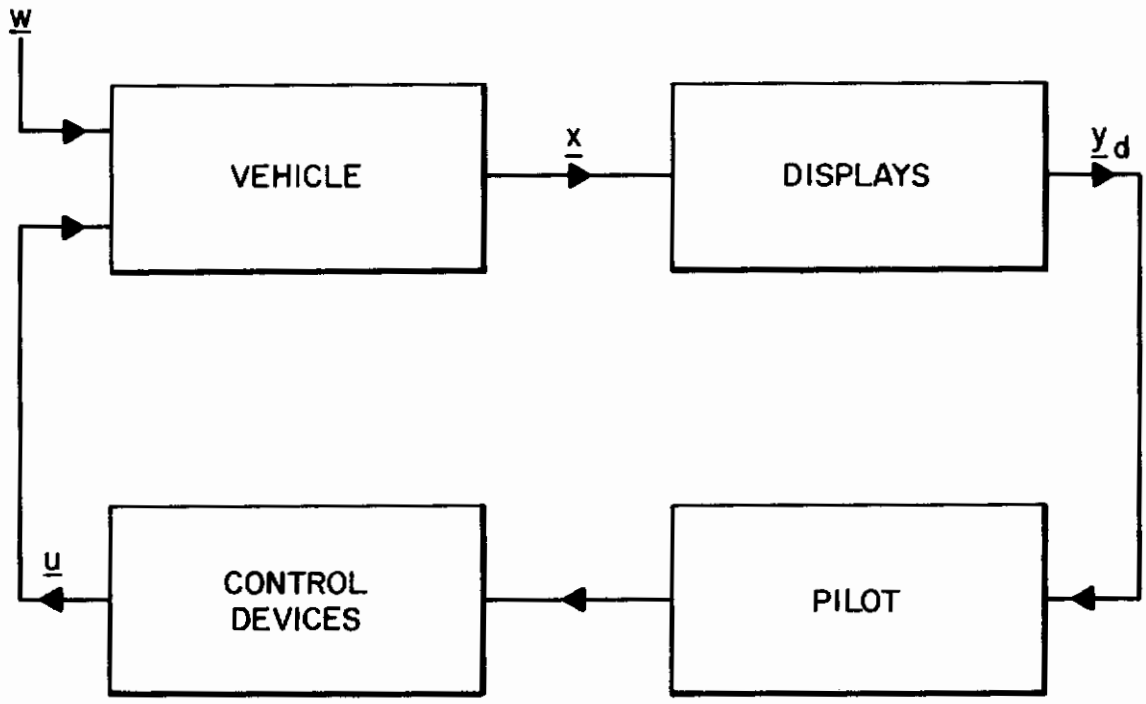

FIG. 1 MANNED - VEHICLE SYSTEM

A set of displays provides the pilot with information about the state of the system. In general, these displays present some transformation of $\underline{x}(t)$, but we will consider only displays of the system state such that the information displayed, represented by the vector $\underline{y}_d(t)$, is equal to $\underline{x}(t)$. The pilot also has control devices that he manipulates to produce control inputs to the vehicle. These inputs are represented by the vector $\underline{u}(t)$. We will consider only ideal control devices such that they may be treated as an integral part of the pilot.

We want to develop analytic procedures for predicting:

(1) What information should be displayed to the pilot,
(2) What control characteristics will be exhibited by the pilot,
(3) How the pilot will allocate his visual attention among the displays.

We take as our starting point existing models for the human operator as a controller and as an instrument monitor. These models, most of which were derived from studies of simple systems, are discussed in Section A of this chapter. To extrapolate from these models to the analysis procedures appropriate to complex systems, we build upon a framework provided by modern control theory. Fundamental to the application of this theory to manual control systems is the assumption that the human controller behaves in an optimal or near optimal manner. The basis for this assumption is discussed in Section B. In the next section we state some results from modern (optimal) control theory that are needed for the analysis method. Finally, in Section D we present the analysis method and discuss its use.

A. HUMAN OPERATOR CHARACTERISTICS

1. Control Behavior

In simple compensatory systems the human controller's characteristics can be represented by a linear describing function and a remnant noise added to its output as shown in Fig. 2a.[1,3†] McRuer et al[4] have shown that the describing function can be partitioned into: (1) a relatively invariant set of dynamics representing the neuromuscular system and certain perceptual, central-processing and neuromuscular time delays; and (2) a highly adjustable equalizer. Moreover, the invariant dynamics can be approximated over a reasonably wide range of frequencies by a simple time delay, e^{-Ts}. Thus we have for the describing function of the invariant dynamics

$$H_I(s) \triangleq e^{-Ts} \tag{2.1}$$

where T is the delay. In general, T will be a function of the plant dynamics. It varies from about T=0.2 sec when the plant is K/s to about T=0.4 sec when the plant is K/s^2. The describing function of the equalizer portion, $H_e(s)$, is typically of the form

$$H_e(s) \triangleq (K_0 + K_1 s + \ldots) \tag{2.2}$$

---

†The control device has been integrated with the pilot and no longer appears as a separate entity. The displayed variables were assumed equal to the state variables, and therefore the pilot's input may be taken to be $\underline{x}$ instead of $\underline{y}_d$.

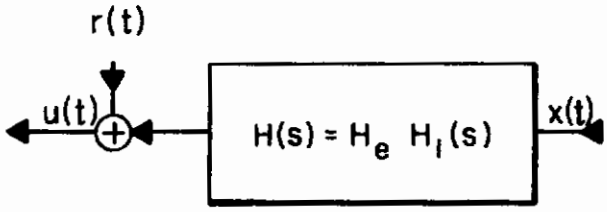

a. CONVENTION DESCRIBING FUNCTION MODEL

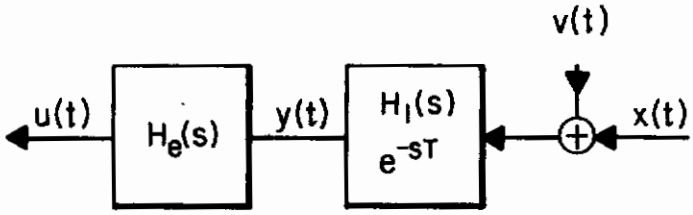

b. OBSERVATION NOISE REPRESENTATION

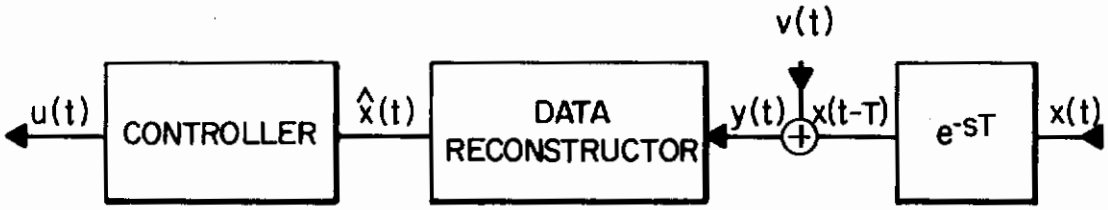

c. ELABORATION SHOWING CONTROLLER AND DATA RECONSTRUCTOR

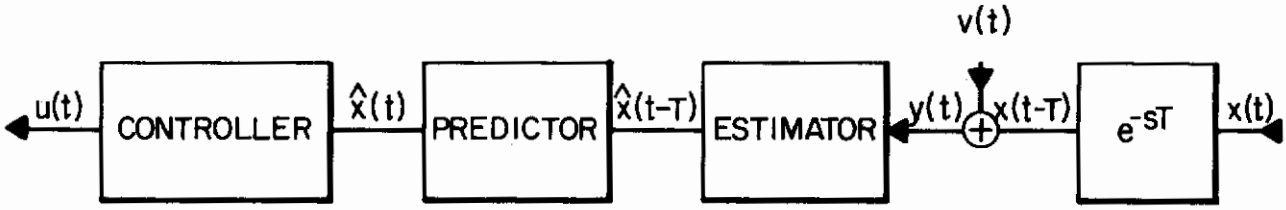

d. FURTHER ELABORATION SHOWING PREDICTOR AND ESTIMATOR

FIG. 2 DEVELOPMENT OF A MODEL FOR THE PILOT FOR SINGLE VARIABLE CONTROL

if the plant is at least of first order. Thus the human controller's describing function, H(s), can be approximated by

$$H(s) \triangleq H_e(s)\, H_I(s)$$

$$\triangleq (K_0 + K_1 s + \ldots)e^{-Ts} \quad . \tag{2.3}$$

If the display system has only a single indicator, such as the error dot on a simple compensatory display, the equalizer will usually not make substantial use of higher than first derivative information. This indicates that the human controller extracts good displacement and good velocity information from a display but is less able to extract information about higher derivative or integrals. Of course, if the display system has several indicators which present explicitly several state variables, such as the displacement, velocity, and acceleration of the vehicle output, the human controller can presumably operate on all of these variables and their first derivatives in his equalizer. In this case the higher order terms of $H_e(s)$ may be important.

The remnant may also be referred to the human controller's input as shown in Fig. 2b. This implies that the remnant is associated with perception. To distinguish this representation from the usual one, we use the term "observation noise" for the remnant when it is referred to the input and represent it by v(t).

In Fig. 2b we have also separated the invariant dynamics $H_I(s)$ from the equalizer dynamics $H_e(s)$. Such a separation suggests the elaboration of the equalizer into a data reconstruction and controller elements shown in Fig. 2c. The data reconstructor operates on y(t-T), the output of $H_I(s)$, which is a delayed and noisy version of x(t), the displayed information. It develops an estimate of the current state of the vehicle. This estimate is

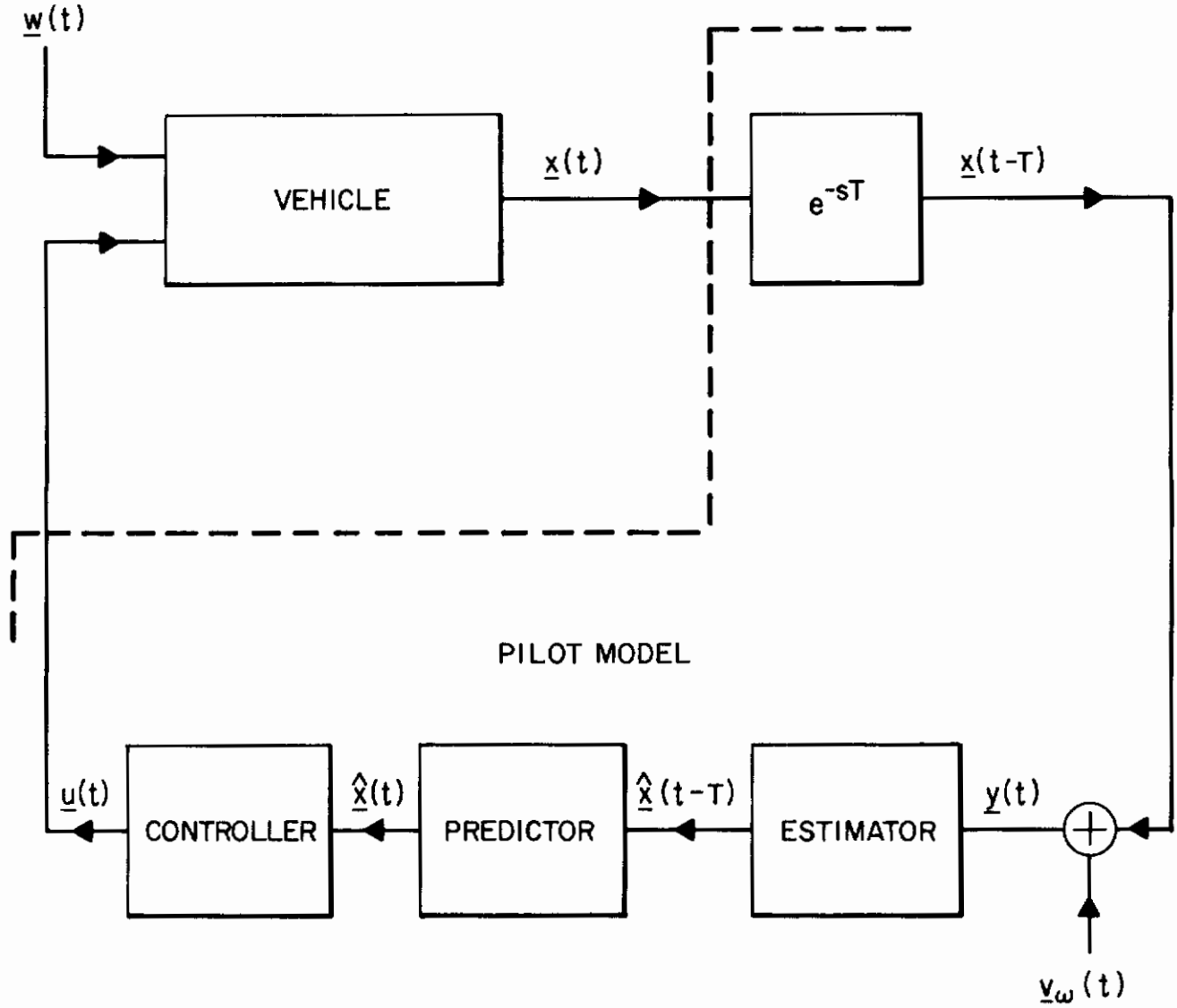

FIG. 3 MULTIVARIABLE MODEL

designated $\hat{x}(t)$ in Fig. 2c. The controller operates on this estimate and produces the control input to the system, u(t). Note that we have interchanged $H_I(s)$ and v(t) which is legitimate since $H_I(s)$ is a delay.

The data reconstructor must perform estimation and prediction functions as is shown explicitly in Fig. 2d. The estimator counters the effects of the noise and develops an estimate of the delayed system state, $\hat{x}(t-T)$. The predictor compensates for the delay and produces an estimate of the current state, $\hat{x}(t)$.

A typical aircraft instrument panel is composed of a set of instruments, some of which may have more than one indicator. The human controller scans these instruments, and at any one time one of the instruments will be in the foveal part of his visual field, and others will fall in the peripheral part of the visual field. Levison and Elkind[7] have shown that when two instruments are to be viewed, the information obtained from peripheral viewing is important for control purposes. They observed that the observation noise for peripheral viewing of an instrument will, in general, be larger than for foveal viewing.

We may use this result to extend the model of Fig. 2 into the multivariable model shown in Fig. 3. The effects of visual scanning are represented in this model by the vector observation noise $\underline{v}_\omega(t)$ whose characteristics are a function of the sampling strategy ω. If the observation noise is a gaussian white noise process, (a reasonable initial assumption if the noise is wideband with respect to the system bandwidth) we may represent its characteristics by the observation noise covariance matrix $\underline{V}_\omega$. $\underline{V}_\omega$ depends upon the sampling strategy and will be a function of time as the human controller attends first to one and then to another display.

Given $\underline{V}_\omega$, a statement of objective of the control task in terms of a cost functional, and other information about the system's

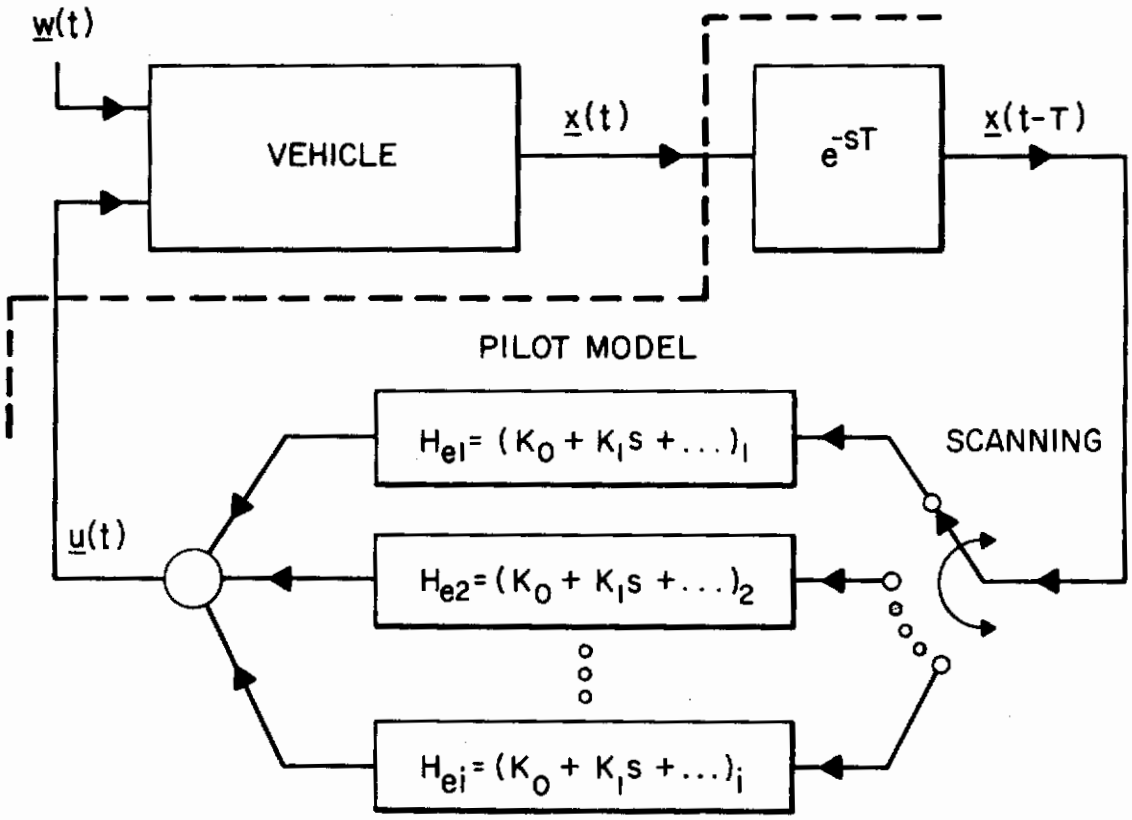

A. SWITCHING MODEL

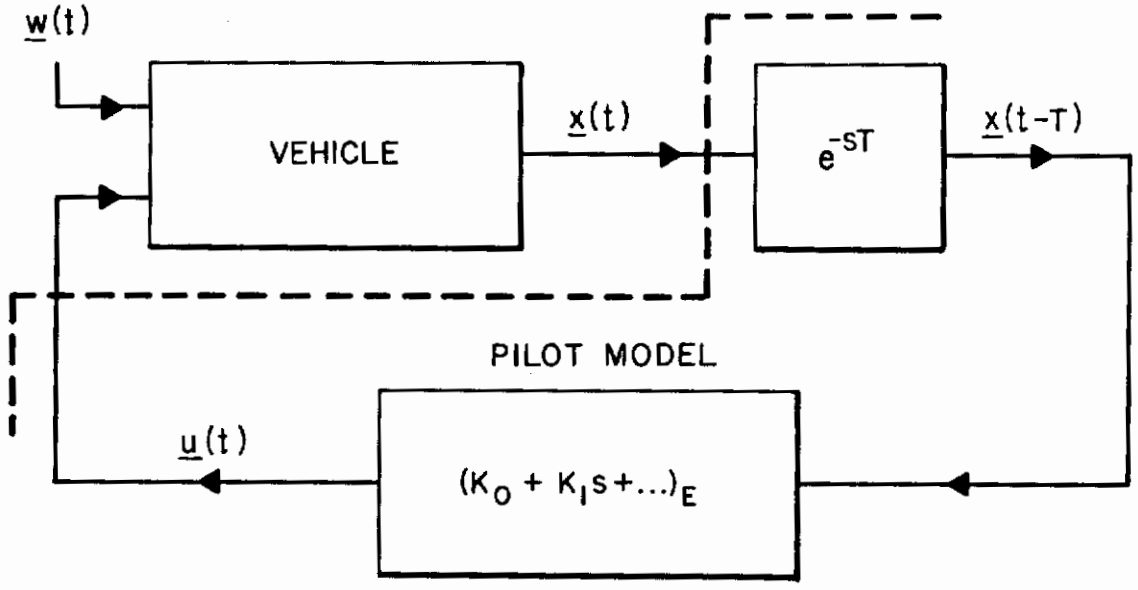

B. EQUIVALENT GAIN MODEL

FIG. 4 SIMPLE MULTIVARIABLE DESCRIBING FUNCTION MODELS

characteristics, we can in principle compute the optimal scanning strategy and also the characteristics of the optimal estimator, predictor and controller. Baron and Kleinman[27] have performed this computation for a very restricted class of problems, but the computations involved are formidable. To avoid these computational complexities, we have chosen for the present to pursue a considerably simpler approach suggested by Levison and Elkind[7] in their study of two-axis tracking.

They found that the describing functions obtained when an instrument is viewed peripherally resemble those obtained when it is viewed foveally. The principal difference between the two is that the gain for peripheral viewing is less than that for foveal viewing. For example, in one of their experiments, the describing function gain was about 7 dB lower when the display was located 30° from the center of the visual field than when it was in the fovea. This decrease in gain is to be expected since an increase in observation noise will force a decrease in gain if good performance is to be maintained. Thus, we may view the lower gains associated with peripheral tracking as resulting from higher observation noise.

Because the foveal and peripheral describing functions are similar in shape and differ primarily in their gain, it is possible to represent the effects of visual scanning by a switching of gains. When a display is viewed foveally, the gains for the quantities presented on it will be high. When the eyes move away from this display, the gains associated with it are switched to lower values. This approach suggests the switching model shown in Fig. 4a in which different equalizers, $H_{e1}(s)$, are switched into operation as the controller views different displays. For this model the controller's describing function will be of the form:

$$H_i(s) \triangleq (K_0 + K_1 s + \ldots)_i e^{-Ts} \quad . \qquad (2.4)$$

The subscript i indicates that the describing function H(s) and the gains K_0, K_1, are appropriate for viewing of the i^{th} display.

If we average over a period of time during which the controller scans all displays, we can replace the several equalizers in Fig. 4a by one equivalent equalizer as in Fig. 4b. The describing function in this model, which we call the equivalent describing function, is:

$$H_E(s) \triangleq (K_0 + K_1 s + \ldots)_E e^{-Ts} \quad . \qquad (2.5)$$

$H_E(s)$ is a weighted average of the $H_i(s)$. The weighting depends upon the fraction of time that each display is fixated, and if the fraction of time that a display is fixated changes, the equivalent gains associated with the variables on that display will also change. The more time spent on a display, the higher will be the equivalent gains for those variables. Thus, we have a simple relation between scanning behavior and control behavior.

Note that the observation noise does not appear explicitly in the models of Fig. 4. The effects of observation noise are implicit in the values of the gains that are used for foveal and peripheral viewing.

Equations (2.4) and (2.5) can also be written in vector notation. For the general case in which the controller generates several control outputs we can write

$$\underline{u}(t) \triangleq -\underline{L}_{Hi}\, \underline{x}(t-T)$$

$$\triangleq -\underline{L}_{HE}\, \underline{x}(t-T) \qquad (2.6)$$

where $\underline{u}(t)$ is the vector of control outputs, $\underline{x}(t)$ is the state vector of the vehicle and $\underline{L}_{Hi}$ and $\underline{L}_{HE}$ are gains matrices representing the human controller's equalizer and contains rows that are $(K_0, K_1, K_2, \ldots)_i$ and $(K_0, K_1, K_2, \ldots)_E$ respectively.† $\underline{L}_{Hi}$ and $\underline{L}_{HE}$ are the control laws that approximate the equalizer behavior of the human controller. $\underline{L}_{Hi}$ is appropriate for viewing the i^{th} display and $\underline{L}_{HE}$ is the appropriate equivalent control law when there is visual scanning of all of the displays.

2. Instrument Monitoring Behavior

Senders[2] proposed a model for instrument monitoring based on information theoretic ideas,[28] that should be useful for predicting the approximate sampling behavior of the human operator. The basic assumptions of Sender's model are (1) that the human operator samples the signals presented on the instruments periodically and attempts to reconstruct the waveforms of these signals, and (2) that the human operator is effectively single-channelled, capable of attending to only one signal at a time. Using these concepts, Senders derived expressions for the frequency and duration of samples of an instrument given the power spectrum of the input and the precision required in reading. The expression obtained by Senders for the duration of a sample of the i^{th} display is

$$D_i = \frac{K}{2} \log_2 \frac{P_i}{E_i} + C \quad . \tag{2.7}$$

†The minus sign is used to indicate that the human controller's responses are directed so as to null $\underline{x}(t)$.

The expression for the sampling frequency is

$$F_i = 2W_i \quad . \tag{2.8}$$

The time per unit time allocated to the ith instrument is the product of sampling frequency and duration:

$$A_i = KW_i \log_2 \frac{P_i}{E_i} + 2W_iC \quad . \tag{2.9}$$

In these relations the subscript i refers to the i^{th} instrument; P_i is the variance of the signal being monitored; E_i is the variance of the permissable error in reading the instrument; K is the time per bit of information that the human operator spends in acquiring and processing information; C, in units of time per sample, accounts for movement time and the minimum fixation time; and W_i is the bandwidth in cps of the signal.

Although Senders was concerned with instrument monitoring rather than with control, the first of his basic assumptions, namely that the human operator samples the signals so as to reconstruct them, is consistent with the control model of Fig. 2. His single channel assumption is at variance with our observations that peripheral vision is also used for control, and is equivalent to assuming that the peripheral observation noise is so high as to make peripherally obtained information useless. If the peripheral noise were very high, the operator would have to rely entirely on foveal information and would probably be forced to sample somewhat more frequently than if the peripheral channel were useful. Nonetheless, Sender's model should give approximately correct for scanning behavior especially in situations in which peripheral vision plays a small role.

To use the model we must determine W_i, the signal bandwidths, P_i/E_i, the required relative readout accuracy. Methods for estimating these quantities are presented in Section D of this chapter.

B. THE ASSUMPTION OF OPTIMALITY

The human controller is self adaptive and if motivated and given good information about his performance, will attempt to change his characteristics so as to perform better. It is reasonable, therefore, to assume that a highly-trained human controller will act in a near optimal manner, subject to certain internal constraints that limit the range of his behavior and also subject to the extent to which he understands the objective of the control task.

Given the self-optimizing tendency of the human controller it is productive to look to optimal control theory as a basis for models of human controller behavior. This is not a new idea. During the late 1940's and early 1950's attempts were made by Phillips[8] and Elkind[9] and others, to use Wiener[10] optimization theory to derive models of the human controller and for predicting human behavior. More recently, with the development of modern optimal control theory there has been a resurgence of interest in optimal control models for the human controller. Roig[11] and Leonard[12] compared the mean-squared error performance of the human operator with that of various optimal controllers and found that the human controller tended to behave in a near optimal manner. Obermayer and Muckler[13] examined existing manual control data and attempted to solve the inverse problem, that is, to find the cost functional that the human controller minimized in these manual control situations. In a paper just published, Wolkovitch[14] determined the relative weighting of quadratic error and control in the pilot's cost functional by solving a limited form of the inverse problem. He assumed that these two were the only components in the cost functional. Using data from previous experiments with pure gain dynamics, he found that the human operator behaved approximately in an optimal manner with stick movement making only a small contribution to the cost.

In a pilot study performed by Miller,[15] the effects of changes in the cost functional on tracking performance was demonstrated. In a recent pilot study Burchfiel, Elkind and Miller[16] found that the human operator's tradeoff between error and control movement when the relative weighting of these quantities in the cost functional was varied followed very closely the tradeoff curve for the optimal controller. The differences between the human controller's and the optimal controller's operating points could be accounted for by the introduction of a subjective weighting.

Although our understanding of the optimization behavior of the human is far from complete, the results of these earlier studies make plausible the assumption that the human controller acts in a near optimal manner subject to certain inherent limitations. When we invoke this assumption, it may be necessary to introduce a subjective cost functional in order to account for the controller's behavior. We would, of course, prefer that the subjective cost functionals for most tasks of interest did not differ greatly from the objective ones used for training and experimental purposes. There is some indication that this is the case at least for quadratic cost functions with relatively simple dynamics.[16] For more complex and realistic control situations it should be possible to select cost functionals that are "natural" from the subject's point of view. If such a natural objective cost functional is used in an experiment, we would hope and expect that the difference between it and the subjective cost functional would be of small consequence. For the present, however, we must rely on plausibility arguments for the near equivalence of subjective and natural objective cost functionals since there exists essentially no data on this issue.

To ascertain whether a cost functional is natural or not may require simulator experiments, discussion with controllers who are experienced in the task being studied, studies of controller behavior in similar real control situations, or some combination

of all of these. In the research discussed in this report we used simulator experiments and discussions with the subjects, who were experienced pilots, to establish a natural performance functional.

Given the assumption that the human controller acts in a near optimal manner, and given a model for the human controller of the form of Eq. (2.6), the plant dynamics, and the cost functional that is to be minimized, we can in principle proceed to solve the optimization problem and predict the human controller's characteristics. Finding the optimal controller is relatively straightforward for the case in which the plant dynamics are linear and the cost functional is quadratic in the state and control vectors. We recognize that not all flight control problems can be adequately represented in this linear-quadratic framework, but a great many can be. The analytic simplification that results from linear dynamics and quadratic cost are great and justify extensive consideration of problems of this type. In this study we consider *only* such problems.

C. SOME RESULTS FROM OPTIMAL CONTROL THEORY

We are given a linear plant disturbed by noise, a quadratic cost functional, and a model for the human controller that contains a time delay. We develop expressions for the optimal state regulator and for the sensitivity of cost to changes in regulator gains. The first of these results will be useful for predicting the control characteristics of the piloted vehicle system. The second will play a role in determining the quantities to be displayed and in predicting scanning patterns.

The material in this section is a summary of results that are derived in Appendices A and B. The reader should refer to these appendices for a detailed discussion of these results.

1. Optimal Regulator Problem - Noise Input

a. No Time Delay

We first consider a time-invariant linear system of the form

$$\dot{\underline{x}}(t) = \underline{A}\,\underline{x}(t) + \underline{B}\,\underline{u}(t) + \underline{w}(t) \qquad (2.10)$$

where $\underline{w}(t)$ is a zero-mean, gaussian vector white noise process with covariance matrix

$$\text{cov}[\underline{w}(t)] = E[\underline{w}(t)\,\underline{w}'(\tau)] = \underline{W}\delta(t-\tau) \quad . \qquad (2.11)$$

For this case we consider the "averaged" cost functional

$$J[\underline{u}(\cdot)] = E\left[\lim_{t_1\to\infty} \frac{1}{t_1} \int_0^{t_1} (\underline{x}'\underline{Q}\,\underline{x} + \underline{u}'\underline{R}\,\underline{u})\, dt\right] \qquad (2.12)$$

or, assuming the validity of interchanging E and lim, the cost functional

$$J[\underline{u}(\cdot)] = \lim_{t_1 \to \infty} E\left[\frac{1}{t_1} \int_0^{t_1} (\underline{x}'\underline{Q}\,\underline{x} + \underline{u}'\underline{R}\,\underline{u})\, dt\right] \quad . \qquad (2.13)$$

In the above $\underline{x}$ is the state vector ($\underline{x}'$ is its transpose), $\underline{u}$ is the control vector, and $u(\cdot)$ represents the entire control function. $\underline{A}$ and $\underline{B}$ are matrices representing the system dynamics and the effects of control in the system. The symmetric matrices $\underline{Q}$ and $\underline{R}$ are, respectively, positive semi-definite and positive definite matrices that establish the relative cost weighting between errors in the state and control movements.

It is assumed that the system of Eq. (2.10) is completely controllable.† Then it is well known[6,19] that the (linear) feedback control which minimizes the cost J is given by

$$\underline{u}^*(\cdot) = -\underline{R}^{-1}\underline{B}'\underline{K}\,\underline{x}$$

$$= -\underline{L}^*\,\underline{x} \qquad (2.14)$$

where the constant matrix $\underline{K}$ is the unique positive definite solution of the algebraic Riccati Equation,

$$\underline{0} = \underline{K}\,\underline{A} + \underline{A}'\underline{K} + \underline{Q} - \underline{K}\,\underline{B}\,\underline{R}^{-1}\underline{B}'\underline{K} \quad . \qquad (2.15)$$

---

†The general equations of motion for aircraft generally are not completely controllable, but the simple linearized equations such as used in this study usually are.

The matrix $\underline{L}^*$ is called the optimal feedback gain matrix. Moreover the optimal trajectory $\underline{x}^*(\cdot)$ is generated by the differential equation

$$\dot{\underline{x}}^* = (\underline{A}-\underline{B}\ \underline{R}^{-1}\underline{B}'\underline{K})\ \underline{x}^* + \underline{w}$$

$$= \overline{\underline{A}}\ \underline{x}^* + \underline{w} \quad , \tag{2.16}$$

and the matrix $\overline{\underline{A}}$ has eigenvalues with negative real parts [i.e., Eq. (2.16) is stable.]

The minimum value of the cost, Eq. (2.13), is

$$J^* = J[\underline{u}^*(\cdot)] = \mathrm{tr}[\underline{K}\ \underline{W}] \tag{2.17}$$

where $\mathrm{tr}(\cdot)$ is the trace of the matrix argument, i.e., the sum of the diagonal terms of $\underline{K}\ \underline{W}$.

If the human controller had no time delay, we would use $\underline{L}^*$ as a prediction of $\underline{L}_{HE}$, his equalizer characteristics. J^* would then be our prediction of the cost that the human controller would incur in regulating the system state $\underline{x}(t)$ with disturbance input $\underline{w}$. As we shall see, the optimal gain matrix and cost obtained with time delay are closely related to the $\underline{L}^*$ and J^* obtained without time delay.

Before considering the time delay problem we investigate the sensitivity of the optimal cost Eq. (2.17) to changes in feedback gains. The sensitivity will be important in our analysis of displays.

Suppose that we do not use the optimal control $\underline{u}^* = -\underline{L}^*\underline{x}$, but instead use the (non-optimal) control law

$$\underline{u}_G = -\underline{G}\ \underline{x} \tag{2.18}$$

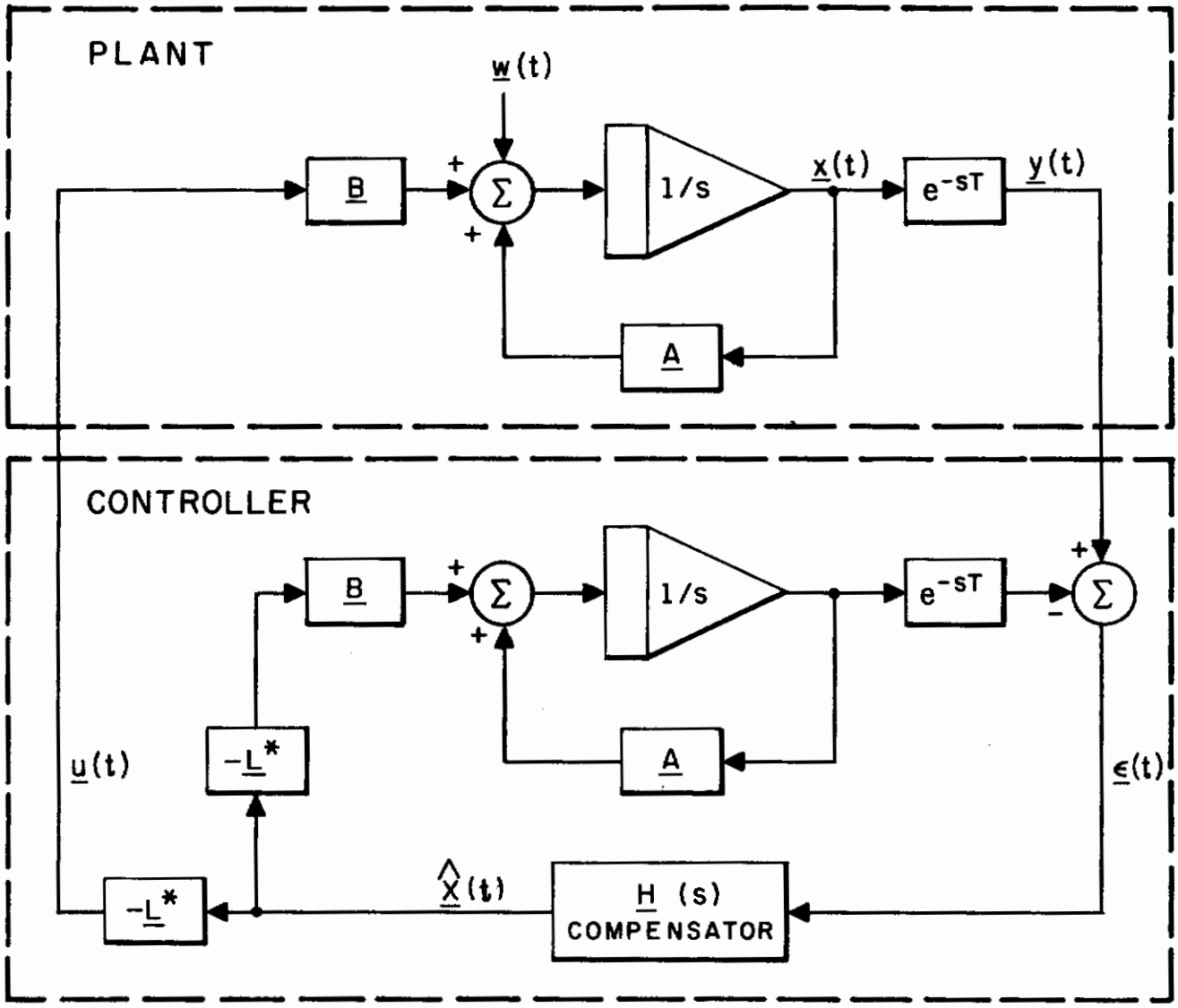

FIG. 5 OPTIMAL CONTROLLER REALIZATION AND PLANT

where $\underline{G}$ is such that $\underline{A}-\underline{B}\ \underline{G}$ has eigenvalues with negative real parts. It is then possible to show[17] (also see Appendix B) that the resulting cost increase is

$$\Delta J(\underline{G}) = J(\underline{u}_{\underline{G}}) - J(\underline{u}^*) = \mathrm{tr}[\underline{S}_{\underline{G}}\ \underline{W}] \tag{2.19}$$

where

$$\underline{S}_{\underline{G}} = \int_0^\infty e^{(\underline{A}-\underline{B}\ \underline{G})'\tau}(\underline{G}-\underline{L}^*)'\underline{R}(\underline{G}-\underline{L}^*)e^{(\underline{A}-\underline{B}\ \underline{G})\tau}d\tau \quad . \tag{2.20}$$

We call $\underline{S}_{\underline{G}}$ the sensitivity matrix of J with respect to $\underline{G}$.

b. Time Delay

Let us now consider, within our control-theoretic framework, the effect of the time delay which is introduced by the human controller. The system equations and quadratic cost functional are again given by Eqs. (2.10) and (2.12) respectively. However, we now suppose that the system output $\underline{y}(t)$ is the delayed state.

$$\underline{y}(t) = \underline{x}(t-T) \tag{2.21}$$

where $T>0$ is a fixed time delay. Thus, a feedback compensator can operate only on $\underline{x}(t-T)$. Consequently, we seek an optimal realizable feedback controller of the form

$$\underline{u}^*(t) = \underline{G}[\underline{y}(t)] \tag{2.22}$$

such that $\underline{u}^*(\cdot)$ minimizes the cost J of Eq. (2.12).

It is shown in Appendix A that the control of Eq. (2.22) can be generated by the time-invariant, linear system shown in Fig. 5. In this figure, we consider the time delay to be an intrinsic part

of the plant being controlled (and of the model plant). The controller consists of a model of the plant and a compensator whose transfer matrix is

$$\underline{H}(s) = (s\underline{I} - \underline{\bar{A}})^{-1} e^{\underline{A}T} (s\underline{I} - \underline{A}) \quad . \tag{2.23}$$

The compensator acts on the difference between the plant's output and the model's output. The overall "closed-loop" behavior of the controller is characterized by the transfer matrix

$$\underline{G^*}(s) = \frac{\underline{u}(s)}{\underline{y}(s)} = -\underline{L}^* \, \underline{H}(s)[\underline{I}-\underline{Z}(s)\underline{L}^*\underline{H}(s)]^{-1} \tag{2.24}$$

where

$$\underline{Z}(s) = \frac{\underline{y}(s)}{\underline{u}(s)} = (s\underline{I}-\underline{A})^{-1}\underline{B} \, e^{-sT}$$

is the transfer matrix of the plant augmented by the time delay.

It is possible to show that the compensator output, $\underline{\hat{x}}(t)$, is the least mean squares prediction of $\underline{x}(t)$ based on the available data $\underline{y}(\tau)$, $\tau \leq t$. Thus,

$$\underline{\hat{x}}(t) = E\{\underline{x}(t) | \underline{y}(\tau), \, \tau \leq t\} \quad . \tag{2.25}$$

The optimal control input to the system is then

$$\underline{u}^*(t) = -\underline{L}^* \, \underline{\hat{x}}(t) \quad . \tag{2.26}$$

This result is intuitively appealing. The optimal control law was $\underline{u}^* = -\underline{L}^*\underline{x}$ when there was no delay and $x(t)$ was available to the controller. Equation (2.26) is the best approximation to this control law given the information available to the controller.

The optimal controller of Fig. 5 has a structure similar to that of the multivariable model of the human operator of Fig. 3. The compensator and plant model together constitute a predictor of system state. Since there is no observation noise in the model of Fig. 5, there is no need for an estimator. The matrix L^* in Fig. 5 corresponds to the controller in Fig. 3.

For the time delay case the optimal cost J^* is given by

$$J[\underline{u}^*(\cdot)] = \mathrm{tr}\left[\underline{K}\, e^{\underline{A}'T}\, \underline{W}\, e^{\underline{A}T}\right] + \mathrm{tr}\left[\underline{Q} \int_0^T e^{\underline{A}\tau}\, \underline{W}\, e^{\underline{A}'\tau}\, d\tau\right] \quad . \qquad (2.27)$$

The first term in Eq. (2.27) represents the cost arising from the disturbance $\underline{w}(t)$. The second term comes from the fact that we cannot obtain $\underline{x}(t)$ exactly. This term is related to the error between $\underline{x}(t)$ and the optimal prediction $\underline{\hat{x}}(t)$ and is monotonic in the time delay T as expected (see Appendix A).

D. ANALYSIS METHOD

In this section we use the results of the previous discussion to develop a method for determining the quantities that should be displayed, for predicting the control characteristics of the human operator, and for predicting his instrument-scanning behavior.

1. Quantities to be Displayed

The fractional cost increase, $\Delta J(G)/J^*$, will be used to determine which of the state variables should be displayed. This problem is approached by noting how $\Delta J(G)/J^*$ depends upon the gain associated with a particular state variable. If $\Delta J(G)/J^*$ is not very sensitive to changes in certain gains, then we postulate that it is not very important to display the variables associated with these gains.

How one chooses a proper set of state variables in the first place is an important and non-trivial question with which we have not dealt. In this study we have used a standard body reference coordinate system and the set of state variables normally associated with the linearized equations of motion in such a system to represent the dynamics of the vehicle. Transformation of such a coordinate system to obtain a different set of state variables is, of course, possible. Whether such a new set of variables will be better may depend upon cost sensitivity as well as upon other factors that we do not yet know how to quantify.

The justification for using the sensitivity of cost to gain changes lies in the earlier assumption that the human operator's equivalent gain matrix, Eq. (2.6), was a function of how he allocated his attention among the displays. Presumably, the more important a variable to the system performance, the greater will be

the time allocated to fixating that variable. The greater the allocation of time, the closer the gain will be to the optimum. Thus, the sensitivity of cost to changes in gain provides a direct measure of the importance of a variable to system performance.

In order to compare the cost sensitivities associated with each state variable, we define, for i=1,2, ..., n

$$\underline{G}_i(D) = \underline{L}^* \underline{\Lambda}_i(D) \tag{2.28}$$

where $\underline{\Lambda}_i(D)$ is a diagonal matrix, all of whose elements are unity expect the i^{th} which is

$$\lambda_i^{ii}(D) = D$$

where $0<D<1$. Thus, the gain matrix $\underline{G}_i(D)$ corresponds to reducing the gains on just state i to D of their optimal values. We now let $\Delta J_i(D)$ denote the cost increase associated with the gains $\underline{G}_i(D)$. [$\Delta J_i(D)$ is calculated from Eq. (2.19).] Finally, we define for i=1,2, ..., n,

$$s_i(D) = \frac{\Delta J_i(D)}{J^*} \tag{2.29}$$

as the sensitivity coefficient associated with ith state variable. Note that s_i as a function of the parameter D.

In the vicinity of the optimum, ΔJ is approximately a quadratic function of the difference between the optimal gains and the actual gains, as may be seen from Eq. (2.20). We divide the sensitivity coefficients by $(1-D)^2$ to obtain the normalize sensitivity coefficients

$$s_i^o(D) = \frac{s_i(D)}{(1-D)^2} = \frac{\Delta J_i(D)/J^*}{(1-D)^2} \quad . \tag{2.30}$$

The normalized coefficients will also be a function of D, but will be more invariant than the unnormalized coefficients.

In order to determine display requirements for a particular task, we compute the normalized coefficients $s_i^o(D)$. The greater s_i^o for a given D, the more important it is to know accurately the state variable x_i. In this manner it is possible to establish an ordering of states in accordance with their accuracy requirements. Thus, we determine those states most important for display to the pilot.

When deciding what displays to provide, we will want to take advantage of the human operator's apparent ability to derive both displacement and velocity information from a single indicator. Thus we need not show every important state variable explicitly.

2. Control Characteristics

The optimal controller of Fig. 5 is a standard against which the human operator's characteristics may be compared. But this controller uses the entire past of its input $\underline{y}(t)$ to produce $\underline{u}(t)$. Our model for the human operator, Eq. (2.6) does not allow operations on the past of $\underline{y}(t)$, only operations on the present of $\underline{y}(t)$ are allowed. Note that $\underline{y}(t)$ is equal to the delayed system state $\underline{x}(t-T)$.

In order to relate the human operator model to the optimal controller of Fig. 5 we must approximate $\underline{G}^*(s)$ of Eq. (2.24) by an equivalent gain matrix. We can do this in one of two ways.

The first method is to compute a set of cross-correlated gains

$$\underline{L}_c = E\left[\underline{u}(t)\ \underline{y}^t(t)\right] \cdot \{\mathrm{cov}[\underline{y}(t)]\}^{-1} \quad . \tag{2.31}$$

In Appendix A we show that

$$\underline{L}_c = -\underline{L}^* e^{\bar{\underline{A}}T}\left[\int_0^T e^{\bar{\underline{A}}(t-T)}\ \underline{A}T\ e^{\underline{A}^t t}\ \underline{W} e^{\underline{A}^t t}\, dt + \underline{\Sigma}_{\hat{x}}\right]\left[\int_0^T e^{\underline{A}t}\ \underline{W}\ e^{\underline{A}^t t}\, dt + \underline{\Sigma}_{\hat{x}}\right]^{-1} \tag{2.32}$$

where

$$\underline{\Sigma}_{\hat{x}} = \int_0^\infty e^{\bar{\underline{A}}t}\ e^{\underline{A}T}\ \underline{W}\ e^{\underline{A}^T T}\ e^{\underline{A}^t t}\, dt$$

is the covariance matrix of the predicted state $\hat{\underline{x}}(t)$.

A second approach is based on constraining the nature of the prediction process. We require the estimate $\hat{\underline{x}}(t)$ to be obtained from a linear operation on only the current value of $\underline{y}(t)$. Thus the prediction process is amnesic, and in such a case, $\hat{\underline{x}}(t)$ would be obtained from $\underline{y}(t)$ by a simple prediction through system dynamics with the result

$$\hat{\underline{x}}(t) = e^{\bar{\underline{A}}T}\ \underline{y}(t) = e^{(\underline{A} - \underline{B}\ \underline{L}^*)T}\ \underline{y}(t) \quad . \tag{2.33}$$

It is possible to show that Eq. (2.30) is an unbiased estimate of $\underline{x}(t)$ and that it is the minimum variance estimate of $\underline{x}(t)$ when $\hat{\underline{x}}(t)$ is constrained to be of the form

$$\hat{\underline{x}}(t) = \underline{G} \cdot \underline{y}(t) \quad . \tag{2.34}$$

Under the assumption of Eq. (2.33) the control input to the plant is given by

$$\underline{u}^* = -\underline{L}_s \, \underline{y}(t)$$

where the simple estimator control gains $\underline{L}_s$ are

$$\underline{L}_s = \underline{L}^* \, e^{(\underline{A}-\underline{B}\,\underline{L}^*)T} \quad . \tag{2.35}$$

The control law Eq. (2.35) corresponds with our human operator model Eq. (2.6). Therefore, the equivalent human operator gains predicted by the above analysis method are $\underline{L}_{HE}=\underline{L}_s$ (or if we use the cross-correlated gain model, $\underline{L}_{HE}=\underline{L}_c$).

If the human operator does in fact operate only on the presence of $\underline{y}(t)$, we would expect $\underline{L}_s$ to be a good predictor of his equivalent gains, $\underline{L}_{HE}$. If, however, he uses some information about the past, as is not unreasonable, his equivalent gains may tend toward $\underline{L}_c$. Thus we expect that his actual equivalent gains will be between $\underline{L}_c$ and $\underline{L}_s$.

Recall that $\underline{G}^*(s)$ was derived without giving any consideration either to scanning or to observation noise. For simplicity of analysis, we have neglected both of these factors in making predictions of the human operator's control characteristics. Actually neglecting the observation noise probably introduces larger errors than neglecting scanning. If the scanning frequency is considerably higher than the natural frequencies of the vehicle (and if observation noise is neglected), little error in prediction of closed-loop performance will result if we replace the gains associated with foveal and peripheral viewing with a single set of equivalent gains.

3. Scanning Characteristics

From Eq. (2.8) the predicted sampling frequency for a displayed variable, F_i, is $2W_i$ samples per second. W_i is some measure of the bandwidth of the signal that is displayed. Several different measures of bandwidth might be used.

The effective bandwidth defined by Blackman and Tukey[24] is a measure that has been found useful for certain problems of manual control,[3] although its utility for scanning predictions has not been established. The effective bandwidth is given by the expression

$$W_{ei} = \frac{\left| \int_0^\infty S_i(f)df \right|^2}{\int_0^\infty S_i^2(f)df} \qquad (2.36)$$

where $S_i(f)$ is the power density spectrum of the i^{th} displayed variable. Another measure of bandwidth that might be useful is the half-power frequency which may be defined as the frequency at which the power density spectrum falls below and remains below one-half its maximum value. Which of these measures is best remains to be determined.

The expression for the fixation time given earlier is

$$D_i = \frac{K}{2} \log_2 \frac{P_i}{E_i} + C \quad . \qquad (2.37)$$

The ratio P_i/E_i is the required readout accuracy.

It is difficult to know how to estimate this ratio in a control task. A possible approach is provided by the sensitivities of cost to gain changes. If the cost sensitivity to a change in

a gain is large, then this gain must be maintained close to its optimal value and the instrument must be read accurately.

We have not been able to establish rigorously an equivalence between readout accuracy and sensitivity. However, it will be noted that the quantity $[1 + s_i^o(D)]$ behaves approximately in the correct way. For the limiting case of $s_i^o(D)$ equal to zero, the cost does not depend upon the i^{th} gain and this variable may be ignored. Thus both $[1 + s_i^o(D)]$ and P_i/E_i will be unity, and zero bits of information will be derived from the instrument on which this variable is displayed. If the sensitivity is very high, $[1 + s_i^o(D)]$ will be large. For this case the readout accuracy must also be high and P_i/E_i will therefore be large. Finally, P_i/E_i and $[1 + s_i^o(D)]$ are dimensionally compatible, being ratios of quantities that are quadratic in the state variables.

If we accept these heuristic justifications, we have the following expression for the duration of fixation

$$D_i = \frac{K'}{2} \log_2[1+s_i^o(D)] + C \quad , \tag{2.38}$$

where C is the time for a minimum length fixation and includes movement time. A reasonable value for C is 0.2 sec. K' is a constant having dimensions of seconds/bit whose value must be determined experimentally.

The time per unit time allocated to the i^{th} variable is just

$$A_i = F_i D_i \quad . \tag{2.39}$$

If several variables are displayed on a single indicator, we must combine the sampling frequencies and fixation times in some reasonable way. The simplest way of treating this problem is to

assume that all variables are sampled independently. In this case the time allocated to display k is

$$A_k = \sum_{i \epsilon k} F_i D_i \quad . \tag{2.40}$$

Another approach is suggested if the bandwidths of all the variables on an indicator are approximately the same. In this case, a simplification results if we assume that all of the variables on the instrument are sampled once per fixation of that instrument. The duration of the fixation will be

$$D_k = \frac{K'}{2} \sum_{i \epsilon k} \{\log_2[1+s_i^o(D)] + C\} \quad . \tag{2.41}$$

The summation may or may not be made to include C depending upon whether or not we believe there is a minimum fixation time associated with each indicator on an instrument.

CHAPTER III

APPLICATION OF THE ANALYSIS METHOD

In this chapter we demonstrate the application of the analysis method. Since the goal of our research is the development of an analytic procedure for the design of aircraft instrument panels and the prediction of pilot behavior, it is important that we deal with a "real" vehicle and a realistically complex control task. On the other hand we must not, at least at the start, choose a control situation whose inherent complexity would make experimental evaluation of our theoretical work overly difficult. We chose to work with longitudinal control in hovering flight of the XV-5A lift fan vehicle.[18] The principal reasons for this choice, the simplified linearized equations of motion of the XV-5A, and the particular longitudinal dynamics with which we worked are discussed in Section A. In Section B we apply the methods described in the previous chapter to this longitudinal hovering problem. The display requirements are established and predictions are made of the pilot's gain matrix and allocation of visual attention.

A. SELECTION OF VEHICLE AND CONTROL TASKS

1. Description of the XV-5A

The XV-5A is a lift fan vehicle. It has a fan in each wing which is the principal source of lift in hover. Louvres on these fans control the direction and magnitude of the thrust vector. The pilot controls the louvre position to produce yawing and rolling moments to control lift. There is also a nose fan that is used primarily for control of pitch. Doors on this fan control the magnitude and direction of the nose fan thrust. The pilot has a control of the nose fan door position and can thereby control the pitching moment. In normal operation longitudinal position is controlled by establishing a pitch angle and relying upon the horizontal component of the wing fan thrust vector to provide longitudinal acceleration. This was the mode of control used in our experiments.

2. Reasons for the Selection

There were two principal reasons for the selection of the XV-5A. The XV-5A is a real V/STOL vehicle that exhibits many features of the class of V/STOL vehicles which are not conventional helicopters. Secondly, considerable aerodynamic and other needed data were readily available to us for the XV-5A in reports by the Ryan Company.[18]

We sought a control task for the XV-5A in the fan mode which would be sufficiently realistic and which, at the same time, would be amenable both to theoretical analysis and experimental treatment. Maintenance of a hovering flight condition in the presence of such disturbances as wind gusts is indeed a realistic task. Moreover, the linearized equations of motion about the hovering

equilibrium condition are easily simulated and are readily analyzed. Also considerable data relative to the hovering mode were available for the XV-5A.[18]

We will deal with control of displacement along the longitudinal axis when altitude and lateral position variations are surpressed. This problem is a realistic one and yet is simple. Several displays are required and the control task is not easy. The analysis of the model for human control and scanning behavior in this task involves all of the essential elements of the general problem of aircraft control and while still being tractable. Thus this task provides a satisfactory testing ground for the model.

3. Equations of Motion

We assume a right-hand coordinate system coinciding with the principal axes of the vehicle and centered at the center of gravity of the vehicle as illustrated in Fig. 6.

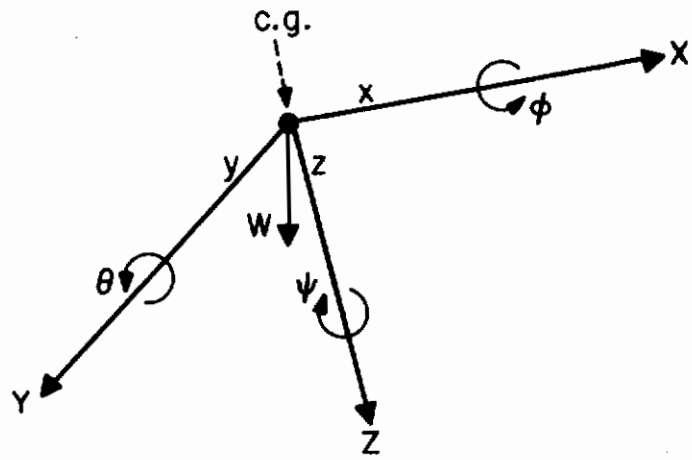

FIG. 6 COORDINATE SYSTEM FOR EQUATIONS OF MOTION

From the pilot's viewpoint, X points forward, Y right, and Z downward. At the steady state operating point the wings are level (ϕ_o=0), the heading reference is defined to be along the initial X-axis (ψ_o=0) and the inclination of the principal X-axis to the horizontal (θ_o) is assumed small.

The complete linearized equations of motion for the XV-5A are in Appendix F. In this section we give the equations for the simplified problem that we investigated experimentally: control of x position in hovering flight. Vertical and lateral motion was suppressed and no control over these quantities was provided the subjects in the experiments.

The equations of motion for the simplified problem are[18]

$$\begin{bmatrix} \dot{u} \\ \dot{x} \\ \dot{q} \\ \dot{\theta} \end{bmatrix} = \begin{bmatrix} X_u & 0 & 0 & -\bar{g} \\ 1 & 0 & 0 & 0 \\ M_u & 0 & M_q & 0 \\ 0 & 0 & 1 & 0 \end{bmatrix} \begin{bmatrix} u \\ x \\ q \\ \theta \end{bmatrix} + \begin{bmatrix} 0 \\ 0 \\ M_{NF} \\ 0 \end{bmatrix} \delta_\theta \qquad (3.1)$$

where:

u	incremental translational velocity along X axis of the aircraft
x	increment displacement of aircraft along its X axis
q	angular velocity about the Y axis (pitch rote)
θ	pitch angle at operating point θ=0
δ_θ	deflection of control of noise fan thruster doors, i.e., pitching moment control
X	force along X axis
M	moment about Y axis

m	mass; 28.5 slugs
I_y	moment of inertia about Y-axis; 15,139 slug-ft^2
$\bar{g}$	g/157.3, gravitational constant (converted); .561 ft/deg-sec
X_u	$\frac{1}{m}\frac{\partial x}{\partial u}$, drag damping; -.11 sec^{-1}
M_u	$\frac{1}{I_y}\frac{\partial M}{\partial u}$, velocity stability; .51 deg/ft-sec
M_q	$\frac{1}{I_y}\frac{\partial M}{\partial q}$, pitch damping; -.0704 sec^{-1}
M_{NF}	pitching moment control coefficient; 2.66 sec^{-2}

In our experiments, we introduced a disturbance analogous to windgusts by passing white noise through a linear filter of the form $1/(s+\alpha)$ and adding the resulting noise signal to $\dot{u}$. This, in effect, adds an additional state to the system. More precisely, letting $w_1(t)$ be a white noise process and setting

$$u_w(s) = w_1(s)/(s+\alpha)$$

so that,

$$\dot{u}_w(t) + \alpha u_w(t) = w_1(t) \quad ,$$

the equations of the disturbed system become

$$\begin{bmatrix} \ddot{u} \\ \dot{u} \\ \dot{x} \\ \dot{q} \\ \dot{\theta} \end{bmatrix} = \begin{bmatrix} X_u-\alpha & \alpha X_u & 0 & -\bar{g} & -\alpha\bar{g} \\ 1 & 0 & 0 & 0 & 0 \\ 0 & 1 & 0 & 0 & 0 \\ 0 & M_u & 0 & M_q & 0 \\ 0 & 0 & 0 & 1 & 0 \end{bmatrix} \begin{bmatrix} \dot{u} \\ u \\ x \\ q \\ \theta \end{bmatrix} + \begin{bmatrix} 0 \\ 0 \\ 0 \\ M_{NF} \\ 0 \end{bmatrix} \delta_\theta + \begin{bmatrix} 1 \\ 0 \\ 0 \\ 0 \\ 0 \end{bmatrix} w_1 \quad . \tag{3.2}$$

Two gust break frequencies were used in the experiments, α= .24 and α=8 radians/sec. For α=.24 the equations of motion are

$$\begin{bmatrix} \ddot{u} \\ \dot{u} \\ \dot{x} \\ \dot{q} \\ \dot{\theta} \end{bmatrix} = \begin{bmatrix} -.351 & -.0266 & 0 & -.561 & -.135 \\ 1 & 0 & 0 & 0 & 0 \\ 0 & 1 & 0 & 0 & 0 \\ 0 & .510 & 0 & -.07 & 0 \\ 0 & 0 & 0 & 1 & 0 \end{bmatrix} \begin{bmatrix} \dot{u} \\ u \\ x \\ q \\ \theta \end{bmatrix} + \begin{bmatrix} 0 \\ 0 \\ 0 \\ 2.66 \\ 0 \end{bmatrix} \delta_\theta + \begin{bmatrix} 1 \\ 0 \\ 0 \\ 0 \\ 0 \end{bmatrix} w_1 \quad , \quad \alpha = .24 \tag{3.3}$$

for $\alpha = 8$,

$$\begin{bmatrix} \ddot{u} \\ \dot{u} \\ \dot{x} \\ \dot{q} \\ \dot{\theta} \end{bmatrix} = \begin{bmatrix} -8.11 & -.888 & 0 & -.561 & -4.49 \\ 1 & 0 & 0 & 0 & 0 \\ 0 & 1 & 0 & 0 & 0 \\ 0 & .510 & 0 & -.07 & 0 \\ 0 & 0 & 0 & 1 & 0 \end{bmatrix} \begin{bmatrix} \dot{u} \\ u \\ x \\ q \\ \theta \end{bmatrix} + \begin{bmatrix} 0 \\ 0 \\ 0 \\ 2.66 \\ 0 \end{bmatrix} \delta_\theta + \begin{bmatrix} 1 \\ 0 \\ 0 \\ 0 \\ 0 \end{bmatrix} w_1 \quad , \quad \alpha = 8 \tag{3.4}$$

The transfer matrix relating the states to δ_θ and to w is

$$\begin{bmatrix} \dot{u}\ (s) \\ u\ (s) \\ x\ (s) \\ q\ (s) \\ \theta\ (s) \end{bmatrix} = \underline{T}_{\delta\theta}\ \delta_\theta(s) + \underline{T}_w\ w_1(s) \tag{3.5}$$

where

$$\underline{T}_{\delta\theta} = \begin{bmatrix} -M_{NF}\ s^2(s+\alpha)\bar{g}/D \\ -M_{NF}\ s(s+\alpha)\bar{g}/D \\ -M_{NF}\ (s+\alpha)\bar{g}/D \\ M_{NF}\ s^2\left(s^2+\alpha s-X_u s-\alpha X_u\right)/D \\ +M_{NF}s\ \left(s^2+\alpha s-X_u s-\alpha X_u\right)/D \end{bmatrix} \tag{3.6}$$

$$\underline{T}_{w} = \begin{bmatrix} s^3(s-M_q)/D \\ s^2(s-M_q)/D \\ s(s-M_q)/D \\ s^2M_u/D \\ s\ M_u/D \end{bmatrix} \tag{3.7}$$

and

$$\begin{aligned} D &= s\{s(s-M_q)[s^2+\alpha s-X_u s-\alpha X_u] + (s+\alpha)\bar{g}M_u\} \\ &= s(s+\alpha)\{s(s-M_q)(s-X_u) + \bar{g}\ M_u\} \quad . \end{aligned} \tag{3.8}$$

We observe that the factor $(s+\alpha)$ is common to the numerator and denominator of each element of the $\underline{T}_{\delta\theta}$. Thus, the transfer matrix relating system states to control input is independent of α as it should be since α is a disturbance parameter.

Substituting the appropriate numerical values in Eqs. (3.6), (3.7), and (3.8), we find the transfer matrix $\underline{T}_{\delta\theta}$ in factored form is given by:

$$\underline{T}_{\delta\theta} = \begin{bmatrix} -.149s/D' \\ -.149/D' \\ -.149/sD' \\ .266\ s(s+.11)/D' \\ .266\ (s+.11)/D' \end{bmatrix} \qquad (3.9)$$

and $\underline{T}_w$ is

$$\underline{T}_w = \begin{bmatrix} s^2(s+.07)/(s+\alpha)D' \\ s(s+.07)/(s+\alpha)D' \\ (s+.07)/(s+\alpha)D' \\ .51\ s/(s+\alpha)D' \\ .51\ /(s+\alpha)D' \end{bmatrix} \qquad (3.10)$$

where

$$D' = [s + .721]\ [s-(.27 + .569j)]\ [s-(.27 - .569j)] \quad . \qquad (3.11)$$

B. DISPLAY REQUIREMENTS AND PREDICTED PILOT BEHAVIOR FOR THE XV-5A

In this section numerical results are presented which predict (a) the relative importance of each state variable to the control task, (b) the fractional allocation of time spent viewing each display, and (c) the pilot's gain matrix. Both low and high bandwidth noise cases are considered (α=.24 and α=8.0, respectively).

1. Riccati Equation Computations

The quantity most central to our theoretical analysis via optimization theory is the Riccati equation solution $\underline{K}$. Once $\underline{K}$ is obtained, we can compute the optimal controller gains $\underline{L}^*$, the closed-loop system matrix $(\underline{A}-\underline{B}\ \underline{L}^*)$, and the transition matrix $\exp[(\underline{A}-\underline{B}\ \underline{L}^*)t]$. In the present study, the computation of $\underline{K}$ was accomplished by using the iterative technique discussed in Appendix C for both cases, α=.24 and α=8.0. The requisite $\underline{Q}$ and $\underline{R}$ matrices were

$$\underline{Q} = \text{diag}(0,\ 0,\ 1,\ 0,\ 0)$$

$$R = r = 1.0 \quad .$$

That is, only position (x) and control deflection (δ_θ) contributed to the cost, with equal weight to each. The results of the Riccati equation computations are shown in Tables I and II for α=.24 and α=8.0. The matrix $\overline{A}$ has eigenvalues with negative real parts which indicate closed-loop stability.

TABLE I

Riccati Computations for $\alpha = .24$

$$\underline{A} = \begin{bmatrix} -.351 & -.027 & 0 & -.561 & -.135 \\ 1.0 & 0 & 0 & 0 & 0 \\ 0 & 1.0 & 0 & 0 & 0 \\ 0 & .510 & 0 & -.07 & 0 \\ 0 & 0 & 0 & 1.0 & 0 \end{bmatrix} \qquad \underline{B} = \begin{bmatrix} 0 \\ 0 \\ 0 \\ 2.66 \\ 0 \end{bmatrix}$$

$$\underline{K} = \begin{bmatrix} 2.785 & 3.345 & 1.704 & -.818 & -.196 \\ 3.345 & 4.603 & 2.774 & -.802 & -.193 \\ 1.704 & 2.774 & 2.371 & -.376 & -.089 \\ -.818 & -.802 & -.376 & .383 & .086 \\ -.196 & -.193 & -.089 & .086 & .020 \end{bmatrix}$$

$$\underline{L}^* = \underline{R}^{-1}\ \underline{B}^1\ \underline{K} = [-2.176 \quad -2.133 \quad -1.0 \quad 1.018 \quad .23]$$

$$\overline{\underline{A}} = \underline{A} - \underline{B}\ \underline{L}^* = \begin{bmatrix} -.351 & -.027 & 0 & -.561 & -.135 \\ 1.0 & 0 & 0 & 0 & 0 \\ 0 & 1.0 & 0 & 0 & 0 \\ 5.788 & 6.184 & 2.66 & -2.78 & -.612 \\ 0 & 0 & 0 & 1.0 & 0 \end{bmatrix}$$

TABLE II

Riccati Computations for $\alpha = 8.0$

$$\underline{A} = \begin{bmatrix} -8.11 & -.888 & 0 & -.561 & -4.49 \\ 1 & 0 & 0 & 0 & 0 \\ 0 & 1 & 0 & 0 & 0 \\ 0 & .510 & 0 & -.07 & 0 \\ 0 & 0 & 0 & 1 & 0 \end{bmatrix} \qquad \underline{B} = \begin{bmatrix} 0 \\ 0 \\ 0 \\ 2.66 \\ 0 \end{bmatrix}$$

$$\underline{K} = \begin{bmatrix} .054 & .463 & .294 & -.087 & -.194 \\ .463 & 4.0 & 2.617 & -.72 & -1.64 \\ .294 & 2.617 & 2.37 & -.376 & -.88 \\ -.087 & -.72 & -.376 & .383 & .50 \\ -.194 & -1.64 & -.88 & .50 & .88 \end{bmatrix}$$

$$L^* = [-.23 \quad -1.918 \quad -1.0 \quad 1.018 \quad 1.321]$$

$$\overline{A} = \begin{bmatrix} -8.11 & -.888 & 0 & -.561 & -4.49 \\ 1 & 0 & 0 & 0 & 0 \\ 0 & 1 & 0 & 0 & 0 \\ .614 & 5.61 & 2.66 & -2.78 & -3.514 \\ 0 & 0 & 0 & 1 & 0 \end{bmatrix}$$

2. Calculation of Sensitivities – No Time Delay

In this section the normalized sensitivity coefficients $s_i^o(D)$ are presented for each of the five state variables. Recall that $s_i^o(D)$ is defined as the fractional increase in cost when the gain on state i is reduced to D of its optimal value, normalized with respect to $(1-D)^2$. The $s_i^o(D)$ serve to indicate the relative importance of each state variable to the control task.

The cost increases were calculated as described in Appendix B from the sensitivity matrices $\underline{S}_G$ corresponding to each gain change. The $s_i^o(D)$ were computed from the cost increases by Eq. (2.30),

$$s_i^o(D) = \frac{\Delta J(D)/J^*}{(1-D)^2}$$

and are given in Table III for several values of D. For the control problem we are considering, input driving noise was added to only the first state equation so that the noise covariance matrix $\underline{W}$ used in the computation of $\underline{S}_G$ is merely

$$\underline{W} = \text{diag}(w_{11}, 0, 0, 0, 0) \quad .$$

The results in Table III indicate that the gains on $\dot{u}$, u, and q have the greatest influence on system performance for $\alpha=.24$. For $\alpha=8.0$, the gains on u, q, and θ have the greatest influence.

We assume that the human controller can obtain good information about displacement and first derivative of a displayed variable but little information about higher derivatives or about integrals of a displayed variable. For the case of $\alpha=.24$, displays of x, u, and θ would allow the pilot to obtain the information

TABLE III

Normalized Sensitivity Coefficients, $s_i^o(D)$

α rad/sec	D	$\dot{u}$	u	x	q	θ
.24	.7	3.3	1.5	.47	2.4	.18
	.6	5.3	1.9	.50	2.9	.25
	.5	21.8	2.5	.63	4.1	.24
8.0	.7	.08	1.8	.72	1.6	4.2
	.6	.081	2.0	.79	2.0	8.6
	.5	.08	2.6	.90	2.9	∞

about u, $\dot{u}$, and q that he requires for good control. For α=8.0, displays of θ and x should be sufficient for him to obtain the θ, q, and u information that the sensitivity analysis indicates is important.†

†Note that $\dot{u}$, u, and q correspond to $\ddot{x}$, $\dot{x}$, and $\dot{\theta}$, respectively.

3. Prediction of Pilot Gains

The optimal control model for the human operator consists of an assumed time delay followed by a predictor and a set of gains. In order to compare this theoretically derived model with the experimental model of the human operator, it is necessary to determine an equivalent "gain matrix" for the prediction process. Once accomplished, an equivalent set of gains which describe the pilot's overall behavior can be calculated.

In Chapter II we suggested two approaches. The first replaces the predictor (which consists of dynamical elements) by a set of cross-correlated gains which depend upon the nature of the input driving noise. The second approach approximates the prediction process by a simple prediction through the closed-loop system dynamics. This approach yields an unbiased (nonminimum variance) prediction of the system state. The control gains obtained via this latter approach are called the simple predictor controller gains.

The simple predictor controller gains are given by Eq. (2.36) and are easy to calculate. The cross-correlated gains [Eq. (2.33)], on the other hand, are more difficult to obtain. Their calculation is tedious, but straightforward.

Both of these sets of gains are dependent upon the equivalent human time delay. This time delay, an unknown parameter, was to be determined experimentally. Its value was expected to be between .2 and .5 sec. Consequently, both sets of equivalent gains were computed for various time delays between T=.2 and T=.5 sec. The results appear in Table IV (cross-correlated gains) and Table V (simple predictor gains).

TABLE IV

Cross-Correlated Gains, $\underline{L}_c$

α = .24

Delay T sec	Gain on:				
	$\dot{u}$	u	x	q	θ
0	-2.176	-2.133	-1.000	1.018	.230
.2	-1.569	-1.576	- .604	.931	.167
.3	-1.334	-1.332	- .417	.889	.115
.4	-1.142	-1.070	- .216	.831	.039
.45	-1.056	- .936	- .109	.796	-.009
.5	- .980	- .801	.001	.759	-.063

α = 8.0

Delay T sec	Gain on:				
	$\dot{u}$	u	x	q	θ
0	- .231	-1.918	-1.0	1.018	1.32
.45	- .302	- .402	- .147	.571	.287
.5	- .310	- .328	- .099	.551	.214

TABLE V

Simple Predictor Gains, $\underline{L}_S = \underline{L}^* e^{\overline{A}T}$

$\alpha = .24$

Delay T sec	Gain on:				
	$\dot{u}$	u	x	q	θ
0	-2.176	-2.133	-1.00	1.018	.230
.2	-1.354	-1.177	- .528	.762	.169
.3	-1.003	- .782	- .341	.648	.142
.4	- .690	- .438	- .183	.543	.116
.48	- .466	- .198	- .076	.465	.098
.5	- .413	- .143	- .052	.447	.094

$\alpha = 8.0$

Delay T sec	Gain on:				
	$\dot{u}$	u	x	q	θ
0	- .231	-1.918	-1.00	1.018	1.321
.2	- .127	-1.041	- .528	.762	.857
.3	- .084	- .680	- .341	.648	.657
.4	- .047	- .367	- .183	.543	.477
.45	- .032	- .228	- .114	.493	.395
.48	- .021	- .149	- .076	.465	.348
.5	- .015	- .099	- .052	.447	.317

4. Prediction of Display Attention

The sensitivity coefficients and the pilot's gain matrix can be used to predict allocation of display attention. It is necessary to assume in this analysis that the time delay does not affect the sensitivity coefficients significantly since they were computed only for T=0. The prediction of display attention accomplished by using Eqs. (2.39) and (2.40).

In order to use these relations we must compute the state variable bandwidths F_i and the normalized sensitivity coefficients $s_i^o(D)$, and we must have values for the constant K' and C.

The sensitivity coefficients are in Table III. The constants K' and C are as yet undetermined, and their values will have to be determined from comparisons between theoretical and experimental results. For the present, the analysis will have to be performed with several different values for these constants. The bandwidths can be determined from the power density spectra of the state variables.

The power spectra of the state variables depend upon the disturbance excitation and upon the closed-loop dynamics. The closed-loop dynamics depend in turn upon the time delay and upon which approximation to the predictor we use, the correlated gains $\underline{L}_c$ or the simpler predictor gains $\underline{L}_s$.

In Figs. 7 and 8 are the computed power spectra for the two disturbance conditions, α=.24 and α=8, respectively. In this computation we assumed that the delay T was 0.5 second. This was the value of delay that we found to be best in our experiments.

The effective bandwidths, W_{ei} computed from these power spectra using Eq. (2.37) are in Table VI. Also shown are the half power bandwidths $W_{1/2}$ obtained from the power spectra plots of Figs. 7 and 8.

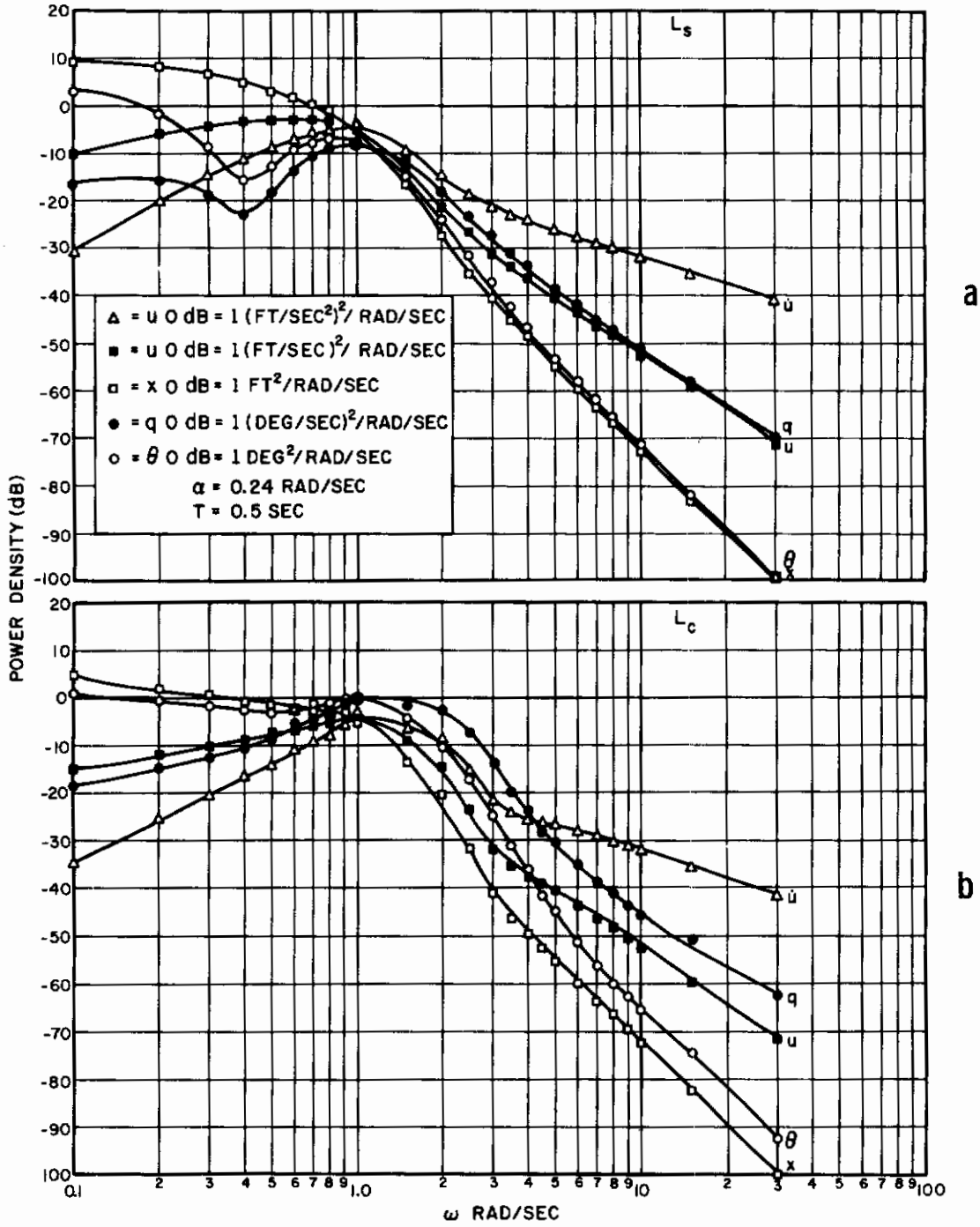

FIG. 7 COMPUTED POWER DENSITY SPECTRA OF STATE VARIABLES FOR (a) $\underline{L}_s$ AND (b) $\underline{L}_c$ GAINS WHEN α = 0.24 RAD/SEC

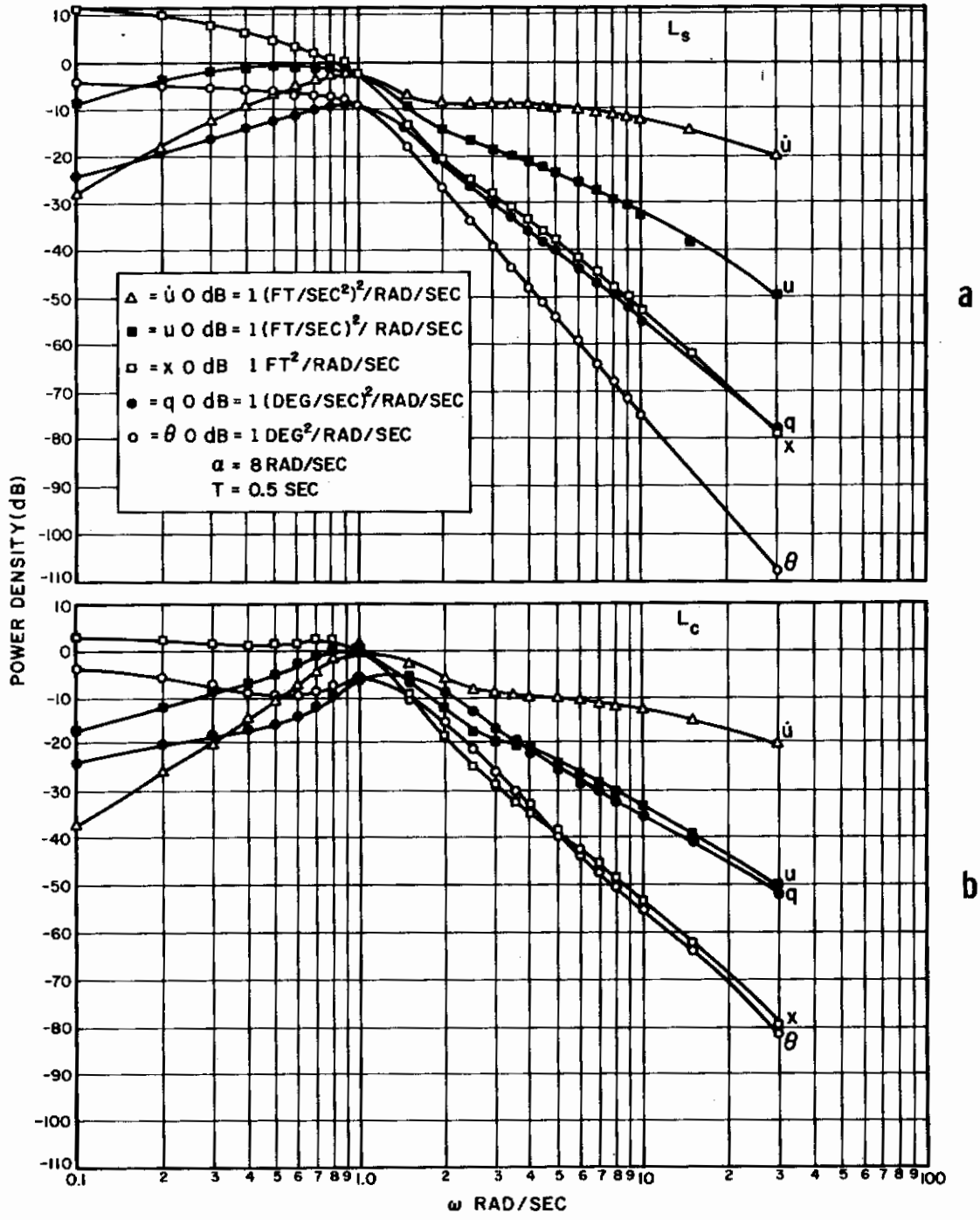

FIG. 8 COMPUTED POWER DENSITY SPECTRA OF STATE VARIABLES FOR (a) $\underline{L}_s$ AND (b) $\underline{L}_c$ GAINS WHEN α = 8 RAD/SEC

We used these bandwidth measures to predict the allocation of attention for the display configuration that we investigated experimentally. There were two displays in this configuration. On one, x and, in some cases, u were presented, and on the other θ was presented. We assumed that x, u, and $\dot{u}$ information were obtained from the x display and θ and q information from the θ display.

The predicted allocation of attention results for several values of the constants C and K' are in Table VII. For these computations we used the sensitivity coefficients for D=0.7. We have treated each of the displayed variables as independent and have attributed the same minimum fixation time C to each.

Only the results for the W_{ie} bandwidth measure are in Table VII. The results for the $W_{1/2}$ bandwidth measure did not differ much from those shown. However, the results for the W_{ie} bandwidths corresponding to both the $\underline{L}_s$ and $\underline{L}_c$ gains are given to provide a comparison between the two approaches to the characterizing of the human operator's control behavior.

In Table VII we give values of A_x and A_θ, the predicted allocation of time per unit time to the x and the θ displays, and fraction of time spent on the x display f_x. The A_x, A_θ values do not necessarily add to unity, which they should if the task consumed all of the controller's visual attention without overloading him. To obtain the fractional attention scores we assumed that the controller allocates all of his attention in exactly the same ratio as given by A_x and A_θ. Note that the sum of the times, A_x+A_θ, is approximately unity most consistently for K'=.5 bits/sec and C=.05 sec.

The most important result shown in Table VII is that the fraction of time allocated to the x-display is consistently less with the α=8.0 rad/sec disturbance than it is with the α=.24 rad/sec disturbance. Also, whereas the amount of time allocated to

TABLE VI

State Variable Bandwidths (CPS)

			$\dot{u}$	u	x	q	θ
W_{EFF}	α=.24	L_s	.23	.19	.093	.20	.058
		L_c	.27	.23	.016	.32	.19
	α=8	L_s	2.0	.22	.093	.21	.18
		L_c	1.1	.21	.20	.24	.41
$W_{1/2}$	α=.24	L_s	.24	.17	.020	.24	.19
		L_c	.29	.22	.032	.33	.27
	α=8	L_s	.22	.18	.048	.22	.013
		L_c	.29	.21	.17	.32	.24

TABLE VII

Allocation of Attention

Disturbance Break Freq. rad/sec	Gain Measure		K'=.5 sec/bit		K=1 sec/bit	
			C=0 sec	C=.05 sec	C=0 sec	C=1 sec
α=.24	$\underline{L}_s$	$A_x \frac{sec}{sec}$	.39	.44	.79	.89
		$A_\theta \frac{sec}{sec}$	.18	.21	.37	.42
		f_x	.68	.68	.68	.68
	$\underline{L}_c$	$A_x \frac{sec}{sec}$	.31	.54	.62	1.1
		$A_\theta \frac{sec}{sec}$	.36	.40	.72	.80
		f_x	.59	.58	.59	.58
α=8.0	$\underline{L}_s$	$A_x \frac{sec}{sec}$	.44	.49	.88	.98
		$A_\theta \frac{sec}{sec}$	.31	.36	.61	.71
		f_x	.46	.58	.46	.58
	$\underline{L}_c$	$A_x \frac{sec}{sec}$	.30	.45	.59	.89
		$A_\theta \frac{sec}{sec}$	.65	.72	1.31	1.4
		f_x	.31	.38	.31	.38

the x-display (A_x) is approximately the same for the two disturbance break frequencies, the time allocated to the θ display (A_θ) is very much greater when α=8.0 than when α=.24. These results are to be expected from the results in Table III when shown that for $\dot{u}$ the sensitivity is less and for θ it is greater with α=8.0 than with α=.24.

5. Calculation of Optimal Costs

The minimum cost, $J(u^*)$, for the case of a system with time delay which is disturbed by white noise is given by Eq. (2.35). For the V/STOL problem being considered, noise was effectively added to only the first state equation so that w_{11} is the only non-zero element in the disturbance covariance matrix $\underline{W}$. The noise disturbance was filtered by a low-pass filter of the form $1/(s+\alpha)$. The variance of the output of this filter is given by the expression

$$E = \frac{w_{11}}{2\pi} \cdot \int_{-\infty}^{\infty} \frac{d\omega}{\omega^2+\alpha^2} \quad .$$

Hence,

$$w_{11} = 2\alpha E$$

where E was chosen to be .82 $(ft/sec^2)^2$ for α=.24 and 3.8 for α=8.0. Table VIII lists the minimum costs for several values of the time delay T.

TABLE VIII

Optimal Costs

Delay T sec	Cost	
	α=.24	α=8.0
0	1.09	3.27
.3	1.77	4.29
.4	2.05	4.64
.45	2.19	4.82
.5	2.35	5.0

CHAPTER IV

EXPERIMENTAL VALIDATION

Two experiments were performed to test the validity of the predictions derived from the analysis procedures. The importance of an explicit display of rate-of-change of vehicle position was investigated in the first experiment under both low- and high-bandwidth simulated windgust conditions. The effects of changes in display gain were explored in the second experiment. The XV-5A longitudinal, hovering flight conditions described in Chapter III were simulated, and the disturbance inputs described in that chapter were used.

The apparatus and procedures used in Experiment 1 are described in Section A, the analysis procedures are described in Section B, and the experimental results are presented in Section C. The variations in experimental procedure that were adopted for Experiment 2 are described along with the presentation of the results of that experiment.

A. DESCRIPTION OF APPARATUS AND PROCEDURES

1. The Basic Task

The pilot was required to maintain the ground-reference position of a simulated XV-5A operating in the hovering mode (fan mode). A block diagram of the flight-control system is shown in Fig. 9.

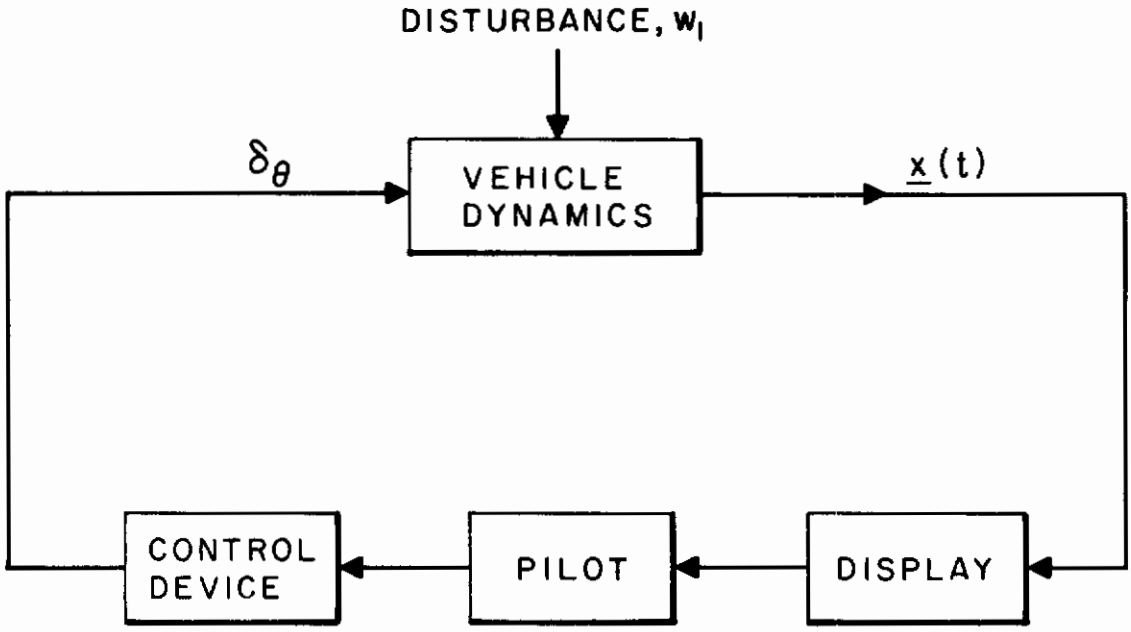

FIG. 9 BLOCK DIAGRAM OF SIMULATED FLIGHT CONTROL SYSTEM

The pilot was shown a subset of the vector state $\underline{x}$ of the vehicle. He controlled the angular (pitch) acceleration of the vehicle by manipulating a control stick whose displacement δ_θ determined the position of the (simulated) nose-fan louvres. The vehicle was disturbed by a gustlike disturbance which acted as a longitudinal acceleration of the vehicle.

Figure 10 shows the analog computer simulation of the vehicle dynamics investigated in this program. (The equations of motion of the XV-5A in hover were derived in Chapter III.) Only pitch and longitudinal position variables were simulated. The vehicle dynamics were simulated on a Goodyear Aircraft GEDA L3 analog computer; scoring and recording operations were performed on an Electronics Associates, Inc. TR-48 analog computer. A Digital Equipment Company PDP-1B digital computer was used to generate the disturbance function and to record the results.

2. Control and Display Apparatus

The control and display apparatus was located in a subject booth that was isolated both acoustically and visually. A photograph of the subject booth is shown in Figure 11. The displayed variables were presented to the subject by two cathode-ray tubes, each of which was 12 cm in diameter. An overlaid reticle provided a rectangular array of grid lines separated by 0.2 in. The distance between the subject's eyes and the plane of the displays was fixed at 28 in. The two display tubes subtended a visual angle of 20° and were placed symmetrically about the median plane. A chin rest was provided to minimize head motions. An electrophotometer was used to assure that there were no left/right differences between either the display or the scope background intensities. Intensity levels were consistent throughout the experimental program.

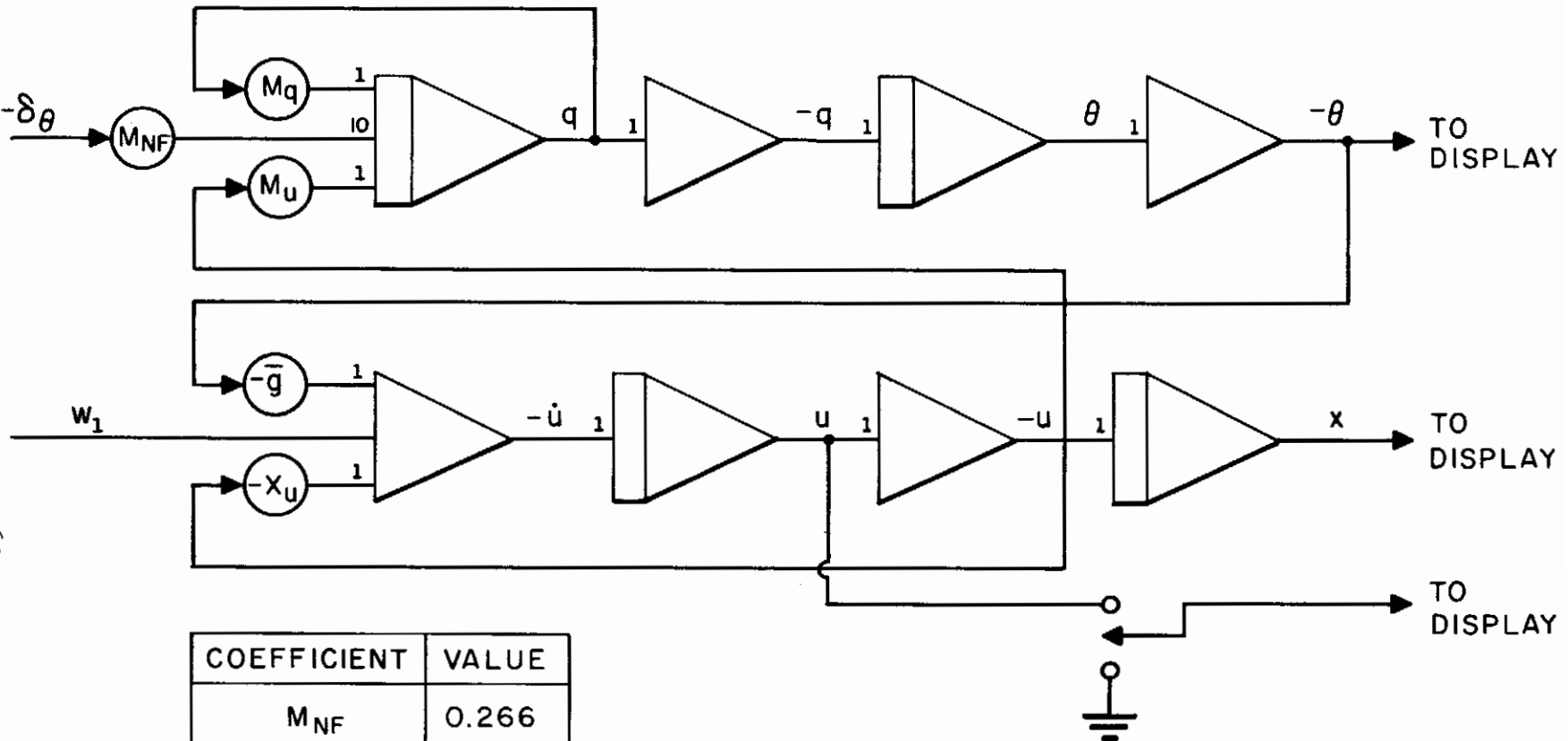

COEFFICIENT	VALUE
M_{NF}	0.266
M_q	0.070
M_u	0.510
$-\bar{g}$	0.561
$-X_u$	0.111

FIG.10 ANALOG SIMULATION OF THE RELATION BETWEEN PITCH AND POSITION OF THE XV-5A IN HOVER

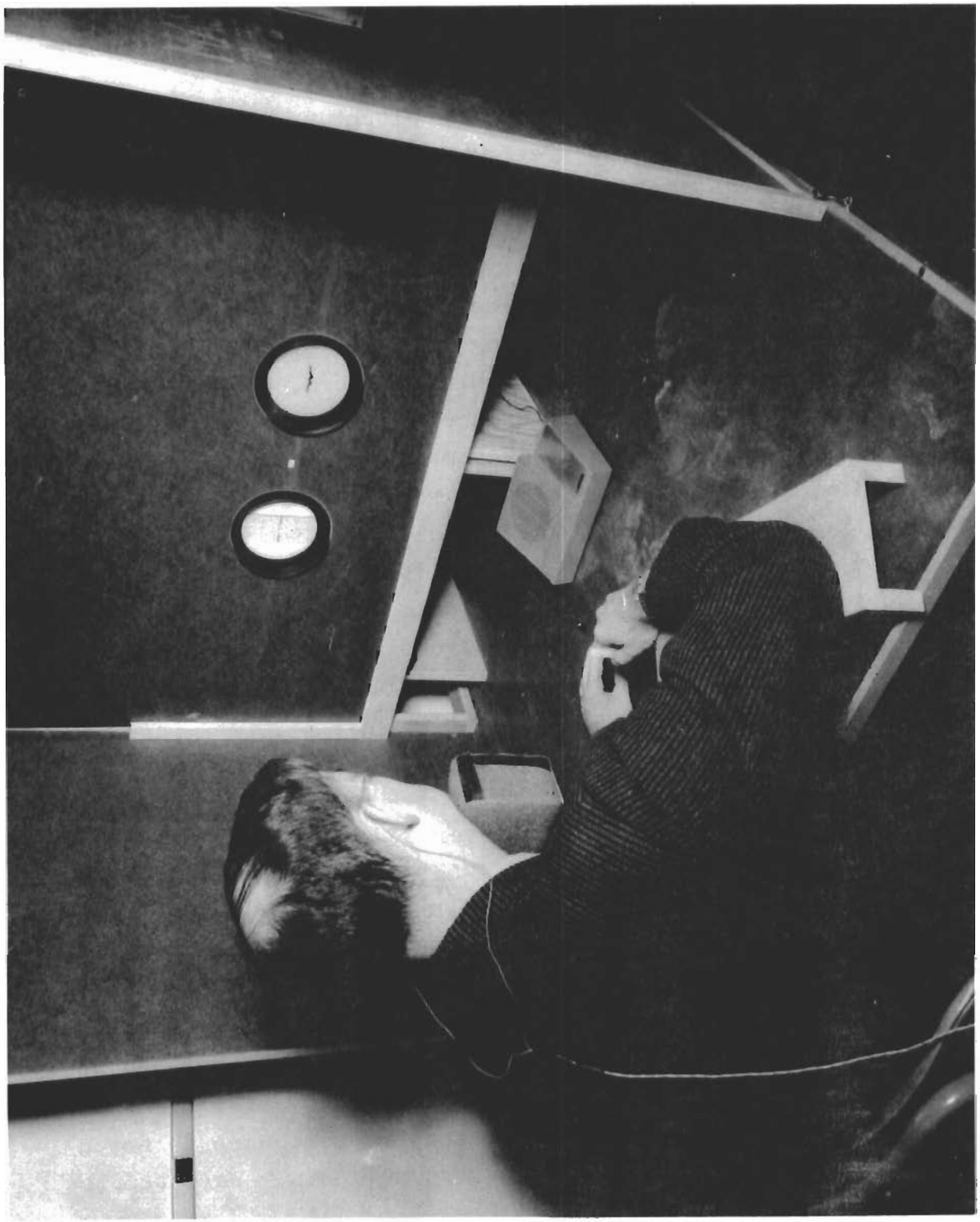

FIG. 11 SUBJECT BOOTH

An artificial horizon was presented on one display tube as a horizontal bar 3 in. wide. A sketch of an airplane bisected the face of the display vertically and served as pitch reference. The pitch display gain was set so that the pitch indicator was deflected 0.2° of visual arc per degree of vehicle pitch. This setting corresponded to a deflection of 0.1 in. per degree of pitch.

The position of the vehicle, with respect to ground reference, was indicated on the second display by the vertical position of a horizontal bar, which was 2 in. wide. Ground reference was indicated by a horizontal line bisecting the face of the display vertically. The display gain was fixed at about 0.08° of visual arc (.04 in.) per foot of vehicle displacement. In addition, the rate of vehicle translation could be presented explicitly as the vertical position of a dot. Indication of rate, when presented, appeared on the same display as the vehicle position. The gain of the display was 0.2° of visual arc per ft/sec of vehicle translation. During training and formal experimentation, the positions of the pitch and position displays were alternated at regular intervals so that the results would not reflect left-right biases in the subject's scanning behavior.

The subject manipulated a flexible control stick that was attached to a force-sensitive hand control (Measurement Systems Hand Control, Model 435). The stick was vertical and mounted directly in front of the subject as shown in Fig. 11. The stick-control combination provided an omnidirectional spring restraint with a restoring force of about 1.25 lbs per inch of deflection of the tip of the stick. One pound of force applied to the control stick toward the subject's body simulated an increase in the opening of the nose-fan louvres of 3° and thereby produced a pitch acceleration of about $8°/sec^2$ in the nose-up direction.

The display and control gains that were used were selected after informal experiments with the test subjects. We attempted

to find gains that resulted in a natural control task insofar as the subjects were concerned.

3. Measurement of Eye Movements

Eye movements were monitored via electro-oculographic techniques.[20] Voltages proportional to the horizontal deflection of the eyes were detected via Beckman biopotential skin electrodes and preamplified by an Electro Instruments Model A20B DC Amplifier.

4. Disturbance Input

A disturbance input, consisting of the sum of 17 sinusoids, was provided via a multichannel FM magnetic tape system during training and was generated by the PDP-1B digital computer during data-taking sessions. The component sinusoids were spaced at approximately equal intervals on a logarithmic frequency scale, and their magnitudes were chosen to approximate a continuous power spectral density function of the form

$$S_{w_1}(\omega) = \frac{w_{11}}{\omega^2 + \alpha^2} \qquad (4.1)$$

where α is the break frequency in rad/sec. Break frequencies of 0.24 and 8.0 rad/sec were used. Figure 12 shows the discrete experimental forcing function along with the approximate continuous spectral-density function for α=0.24.

The mean-squared disturbance levels, given in terms of simulated vehicle accelerations, were 0.82 and 3.80 $(ft/sec^2)^2$ for the low- and high-bandwidths, respectively. The levels were adjusted to make the performance scores approximately equal with the two inputs for the "rate-on" display configuration.

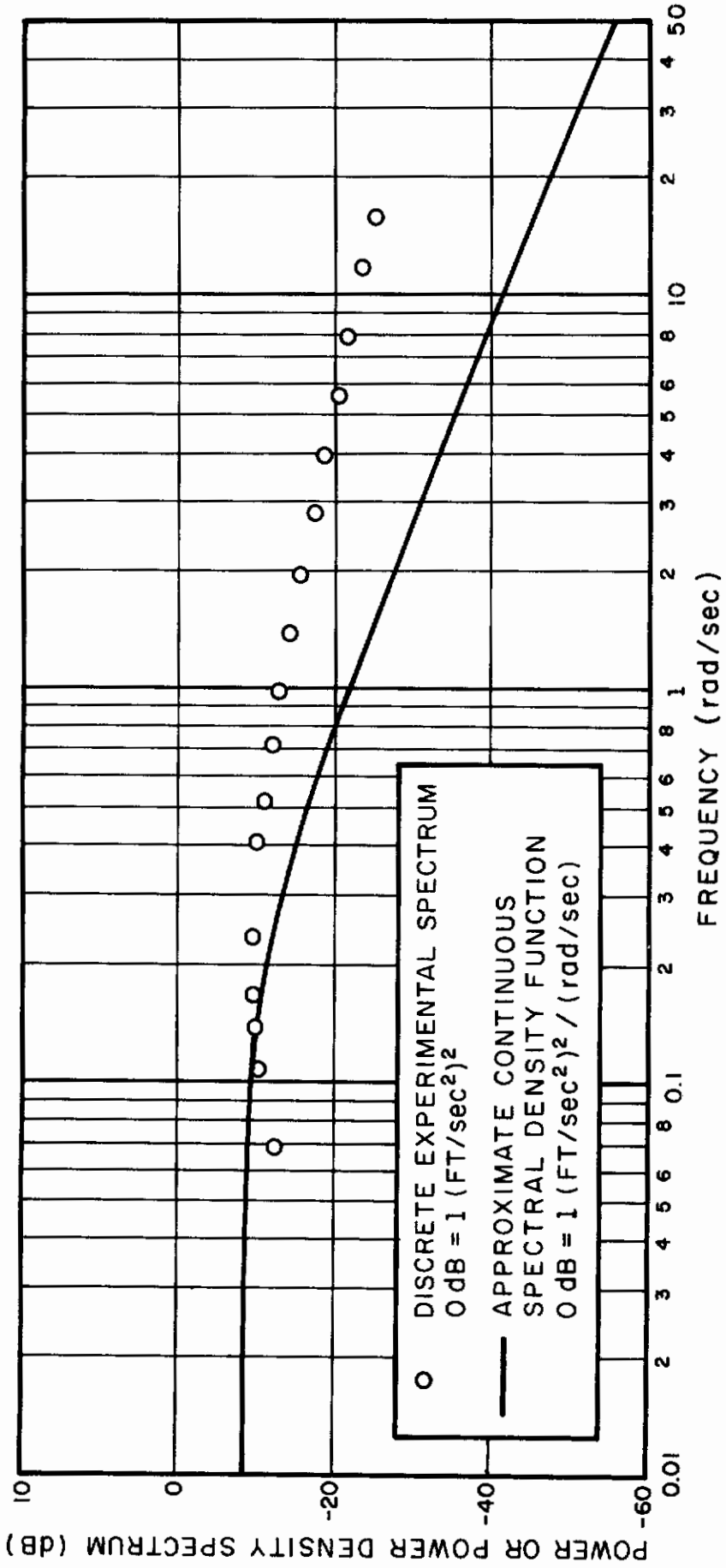

FIG. 12 POWER SPECTRUM OF THE DISCRETE EXPERIMENTAL FORCING FUNCTION AND POWER SPECTRAL DENSITY FUNCTION OF THE APPROXIMATE CONTINUOUS FUNCTION.

In order to assure orthogonality among the component sinusoids, an integral number of cycles of each component was contained in the measurement interval which was 180 sec. Thus, each component was a harmonic of the fundamental frequency.

$$\omega_o = 2\pi/180 = .035 \text{ rad/sec}$$

5. Instructions and Knowledge of Performance

The subjects were instructed to minimize a performance score which was defined as the sum of the mean-squared vehicle positional error and the mean-squared control deflection. After each training run the subject was informed of his total score and of the component error and deflection scores. Performance scores were not announced to the subject after each data-taking run, but the subject was allowed to observe his scores after each session of three trials.

The performance functional thus gave equal weighting to system error and control input. After various weightings were tried early in the training phase, this one was chosen because it seemed most natural to the subjects.

6. Training and Data-Taking Procedures

All training and experimental trials lasted four minutes and were presented in sessions of three trials each with a fifteen-minute rest between sessions. All performance measures were obtained from three-minute record lengths beginning 30 seconds after the onset of the forcing function. The subjects received an average of 90 training runs (equivalent to 6 hours of tracking)

before the first experiment was performed and an additional 36 training runs were provided between Experiments 1 and 2. The training period was sufficient for the subjects to reach an apparently stable performance level.

7. Subjects

Three subjects, all of them Naval or Naval Reserve helicopter pilots with instrument ratings, participated in the experimental program. One of the subjects was on active duty with the Navy as a flight training officer. The remaining two subjects were active in the Naval Reserve. The subjects had flight experience that ranged from 1800 to 2800 hours of flight time in fixed wing and helicopter aircraft.

B. ANALYSIS TECHNIQUES

1. Total Performance Measure

A total performance measure, given by

$$J = \frac{1}{T} \int_0^T [x^2(t) + \delta_\theta^2(t)]\, dt \qquad (4.2)$$

was computed for the middle three minutes of each experimental trial. This measure served as the primary indicator of the quality of system performance.

2. Eye-Movement Statistics

The mean observation time and the fraction of foveal attention allocated to each display were computed for each trial.† Transition times were disregarded in the computation of these statistics; the subject was considered to be fixating either the pitch or the position display at any instant of time.

3. Linear Model of the Human Controller

Regression analysis[21] was performed on the PDP-1B to find the best fit to the observed data of a linear model having the form

---

†We use the term "foveal attention" as a convenient designation of fixation of gaze. No other connotation of the word "attention" is implied.

$$\underline{u} \doteq -\underline{H}_i \, \underline{x}(t-T) \quad , \tag{4.3}$$

where $\underline{u}$ is the pilot's response, $\underline{x}$ is the vector state of the vehicle, $\underline{H}_i$ is the pilot's gain matrix when viewing the i^{th} display, and T is the pilot's effective time delay, which is assumed to be the same with respect to all state variables.

The only control response available to the pilot in these experiments was δ_θ, a scalar. The vehicle state variables used in this analysis were vehicle position (x), rate of vehicle translation (u), acceleration of vehicle translation ($\dot{u}$), pitch (θ), and pitch rate (q). Thus we can write Eq. (4.3) as

$$\delta_\theta \doteq -\underline{K}_i \, \underline{x}(t-T) \tag{4.4}$$

where the pilot's gain vector K_i is $(K_x, K_u, K_{\dot{u}}, K_\theta, K_q)_i$, a row vector. The components of this vector relate the incremental control deflection(degrees of nose-fan louvre) to an incremental change in the corresponding state variable. The display gain and gain of the control device are thus included in the measurement of the pilot's gain.

Three gain vectors were computed per experimental trial: (1) $\underline{K}_p$, which represents the subject's strategy when the position display was fixated,† (2) $\underline{K}_\theta$, which represents his strategy when the pitch display was fixated, and (3) $\underline{K}_E$, a weighted average of (1) and (2) which was computed from

$$\underline{K}_E = f_\theta \, \underline{K}_\theta + f_x \, \underline{K}_x \quad . \tag{4.5}$$

---

†Synchronization of the regression analysis with the record of eye position allowed us to selectively analyze only those points corresponding to fixation of the position (or pitch) display.

f_θ and f_x represent the fraction of the total run time that the pitch and position displays, respectively, were fixated.

A full set of five human controller gains was computed for fixation of each display. We interpret the gains on the acceleration rate, and position variables to be "foveal" gains and the gains on pitch and pitch rate to be "peripheral" gains for the gain matrix obtained during fixation of the position display. The reverse interpretation applies for the gain matrix obtained during fixation of the pitch display. A residual, which indicates the fraction of control movement not accounted for by the linear model, was computed for each gain vector.

The computation of the gain vectors and associated residuals was performed using the Signal Analyzer system of Grignetti, Payne, and Elkind.[22] This system was modified to use the state variables as the independent variables in the regression analysis. The computation procedure was calibrated and checked for accuracy by using the modified signal analysis system to measure the characteristics of controller that were simulated on the analog computer and whose characteristics were therefore known. The results of these calibration tests, discussed in Appendix D, are considered satisfactory.

4. Power Spectra

Power spectra of the position and pitch variables and of the control movements are given for selected experimental trials. The computational procedure, based on the Cooley-Tukey[23] method of computing transforms, was imbedded in the Signal Analyzer system. In order to be able to extract the "remnant", power-measurement frequencies and forcing-function frequencies were made to coincide.

5. Fractional Remnant Power

The "fractional remnant power" is defined as the fraction of the power in a signal that does not appear at the forcing frequencies.[29] This measure is an indication of the extent to which the pilot is not a time-invariant, noiseless, linear controller. Fractional remnant power measurements were obtained for the middle three minutes of selected experimental trials. The pilot's scanning behavior was considered in this computation; one measure was obtained per trial.

6. Effective Signal Bandwidth

Effective bandwidths were computed for selected signals using Eq. (2.37) as suggested by Blackman and Tukey.[24]

C. EXPERIMENTAL RESULTS

1. Experiment 1

The object of this experiment was to investigate the effect on the controller's performance of an explicit display of vehicle velocity. In all runs, the vehicle positional error was indicated by the displacement of a bar. In half the runs, the velocity was also indicated by the displacement of a dot on the same display. The dot was clamped at zero displacement for the remainder of the runs. Pitch of the vehicle was presented on another display as the displacement of a bar (pitch rate was not explicitly displayed), and the pitch display gain was 0.2° of display deflection per degree of pitch. The disturbance cutoff frequencies were 0.24 and 8.0 rad/sec. Each subject tracked three runs for each bandwidth, rate condition.

Performance measures, mean observation times, and fractional allocation of attention, averaged across subjects, are shown in Table IX.

The average results for each subject for each experimental condition are shown in Appendix E (Tables E-1 and E-2). Each ratio shown in Table IX is the average of the ratios for each subject, not the ratio of the grand averages. Table IX shows that for the low-bandwidth input the total performance measure obtained in the absence of the rate display was, on the average, 70° greater (indicating poorer performance) than the score obtained when the rate display was presented. This difference was significant at the 0.01 level.† There was no significant effect of the rate display on performance for the high-bandwidth disturbance. The mean-squared error portion

†The sign test was used to test for statistical significance.[30]

TABLE IX

Effect of Explicit Display of Vehicle Velocity on Performance Score, Mean Observation Time, and Fractional Allocation of Attention

		α, Disturbance Break Frequency (rad/sec)	
		0.24	8.0
Total Performance Score	J_u†	21	27
	$J_{\not u}$‡	37	27
	$J_{\not u}/J_u$	1.70**	1.03
Mean-Squared Positional Error $(\text{feet})^2$	$\overline{x_u^2}$	18	23
	$\overline{x_{\not u}^2}$	33	24
	$\overline{x_{\not u}^2}/\overline{x_u^2}$	1.83**	1.06
Mean-Squared Control Deflection (degrees^2)	$\overline{\delta_u^2}$	3.3	3.6
	$\overline{\delta_{\not u}^2}$	3.2	3.1
	$\overline{\delta_{\not u}^2}/\overline{\delta_u^2}$	1.21	0.94
Mean Scan Period (seconds)	T_u	2.04	1.95
	$T_{\not u}$	1.85	1.61
	$T_{\not u}/T_u$	0.91	0.83**
Mean Observation Time on Position Display (seconds)	T_{xu}	1.43	1.30
	$T_{x\not u}$	1.17	0.95
	$T_{x\not u}/T_{xu}$	0.82	0.73**
Mean Observation Time on Pitch Display (seconds)	$T_{\theta u}$	.61	.65
	$T_{\theta \not u}$	.67	.66
	$T_{\theta \not u}/T_{\theta u}$	1.10	1.01
Fraction of Attention Devoted to Position Display	f_{xu}	.69	.65
	$f_{x\not u}$	.62	.59
	$f_{xu}-f_{x\not u}$	.07	.06

†Subscript u indicates explicit presentation of rate.

‡Subscript $\not u$ indicates no explicit presentation of rate.

*Significant at the 0.05 level.

**Significant at the 0.01 level.

of the score varied in about the same way as the total score. The control score was affected to a lesser degree by the rate presentation and the variations were not statistically significant.

Although the mean observation time on the pitch display was consistently less than the time on the position display, the *fraction* of total attention devoted to the pitch display increased by about 7% (for either input) upon removal of the rate display. The way in which this shift of attention occurred was different for the two inputs. When tracking the low-bandwidth input, the subjects decreased the mean observation time on the position display by about 18% and increased the time attending to the pitch display by 10%. When tracking the high-bandwidth input, the subjects decreased mean observation time on the position display by 27% and did not materially change the time spent on the pitch display. The mean scan period (sum of the mean observation times on the position and pitch displays) decreased upon removal of the rate display when tracking either input, although the change was greater for the high-bandwidth input.

Average pilot gain vectors are shown in Table X, and gains for the individual subjects are given in Table E-3 (see Appendix E). Three vector gains are shown for each experimental condition: (1) gains associated with fixation of the position display, (2) gains associated with fixation of the pitch display, and (3) the average of (1) and (2) weighted by the fraction of attention spent on each display. The residuals, also shown in Table X, were generally less than 0.30 and lie in the range of residual values that are commonly associated with human controller describing functions.[21]

Because of the time involved in obtaining the gain vectors, we were not able to analyze all the experimental runs. Instead,

TABLE X

EFFECT OF RATE DISPLAY ON AVERAGE PILOT GAINS

Display Related Gains

Experimental Conditions		Display Fixated											
		POSITION						PITCH					
		Gain on:						Gain on:					
α (rad/sec)	Rate Display	$\dot{u}$	u	x	q	θ	Residual	$\dot{u}$	u	x	q	θ	Residual
0.24	ON	-.557	-.302	-.076	.635	.046	.270	.031	-.202	-.113	.580	.376	.222
	OFF	-.272	-.240	-.098	.487	.184	.282	-.052	-.165	-.114	.548	.324	.160
8.0	ON	-.134	-.231	-.114	.471	.270	.321	-.017	-.113	-.056	.540	.232	.153
	OFF	-.037	-.320	-.105	.584	.291	.332	.017	-.161	-.097	.570	.314	.170

Weighted Average Gains

Experimental Conditions		Gain on:				
α (rad/sec)	Rate Display	$\dot{u}$	u	x	q	θ
0.24	ON	-.416	-.273	-.081	.616	.119
	OFF	-.195	-.207	-.098	.505	.227
8.0	ON	-.095	-.192	-.094	.501	.254
	OFF	-.018	-.257	-.105	.584	.302

Average of Three Subjects

T = 0.5 sec.

we analyzed one run per subject per experimental condition. The runs chosen for analysis were those that had associated performance scores that were closest to the grand average for each experimental condition. Thus, the individual runs are not necessarily representative of the individual subjects, but rather of the subjects as a group.

A time delay of about 0.5 sec, on the average, yielded the smallest residual and was considered to represent the controller's equivalent time delay. Since there were no consistent differences between subjects or between experimental conditions, a time delay of 0.5 sec was used for all computations of the gain vectors. This time delay is compatible with other results for complex manual control systems. For example, with K/s^2 dynamics, (a situation which also requires the subject to provide lead), McRuer et al[4] found that the asymptotic value of the time delay approached 0.5 sec as the bandwidth of the input approached zero. They considered inputs that, in effect, perturbed the plant output. If we were to refer our disturbances to the plant output, the bandwidth would be very low because of the filtering effects of the plant dynamics. Thus, comparison with McRuer's asymptotic values of time delay is appropriate.

Consider now the average gains for the case in which $\alpha=.24$. Without the u display, the gain on $\dot{u}$, $K_{\dot{u}}$, decreased to less than half of the value we obtained when u was displayed. The gain on u, K_u, decreased by only 25% with the removal of the u display. Without the u display, the pilot would have to extract the second derivative of x(t) from the x display in order to obtain $\dot{u}$ information. He could still obtain u information by taking the first derivative of x(t). One of our initial assumptions was that second derivative information would be difficult for the pilot to obtain, although first derivative information would be readily available to him. The large decrease of $K_{\dot{u}}$, and

the relatively smaller decrease in K_u, observed with the removal of the u display, supports this assumption.

The gain K_θ nearly doubled when the $\dot{u}$ display was removed (α=.24). The longitudinal acceleration of the vehicle ($\dot{u}$) depends very strongly upon the pitch angle, and thus information about θ is a reasonable substitute for information about $\dot{u}$. Hence, we would expect K_θ to increase upon removal of the u display. The increase in K_θ is also consistent with the differences in visual scanning that were observed with and without the u display (Table IX). Without the u display the subjects increased their mean observation time of the pitch display, decreased their mean observation time of the position display, and increased the fraction of attention devoted to the pitch display. Thus we see evidence of the direct relation between gain associated with a variable (θ) and the time that the variable is viewed foveally. The gains on the other state variables were not affected substantially by the presence or absence of the u display.

For the high-bandwidth disturbance (α=8.0), $\dot{u}$ information is not very important for control, because the disturbance results in rapid, large random fluxuations in $\dot{u}(t)$. We see that $K_{\dot{u}}$ is small with and without the $\dot{u}$ display, and the other gains do not change in an important way when the u display is removed.

Now consider the gains vectors associated with fixation on the position and on the pitch displays. When the subject fixates on the position display, $\dot{u}$, u, and x are viewed foveally; and the gains on the first two of these variables are much larger in magnitude than when the subject fixates in the pitch display and these quantities are viewed peripherally. K_x is small for both foveal and peripheral viewing, and the differences are probably not important. The differences between the "foveal" and "peripheral" gains are consistent with our assumptions that the magnitude of

each component of the gain vector is related directly to the subject's ability to obtain information about the corresponding state variable and that foveal viewing gives better information (and therefore higher gain) than does peripheral viewing.

The measurements of K_q and K_θ are ambiguous. For the α=.24 condition, the measured values of K_θ when the pitch display was fixated (foveal viewing) were higher than the corresponding values of K_θ when the position display was fixated (peripheral viewing). This is the expected result. For the α=8.0 condition, the differences between the K_θ gains were small and probably not significant. However, the foveal and peripheral values of K_q for both α=.24 and α=8.0 differed by less than 10% to 15%, and the direction of the change was not consistent. This indicates, perhaps, that the subjects could obtain pitch rate information about equally well, foveally or peripherally. In this experiment, the pitch rate was obtained from the velocity of the pitch bar. The pitch bar was highly visible peripherally, and peripheral vision is well suited to perception of movement. Thus, there is reason to expect that the subjects could obtain fairly good q information peripherally. Another explanation is that the measured values of the gains associated with fixation on the pitch display may be erroneously low. The average observation time on the pitch display was between 0.6 and 0.7 sec. The time delay used in the measurement, 0.5 sec., was just slightly less than the observation time. The near equality of the fixation and delay time tends to make the pitch display gain measurements more susceptible to errors than the position display measurements because of variations in the pilot's time delay and the possible use of an incorrect value of the time delay in our measurement procedure.

Equivalent power density spectra of $x(t)$, $\theta(t)$, and $\delta_\theta(t)$ for Subject JM are shown in Fig. 13 for α=.24 and in Fig. 14

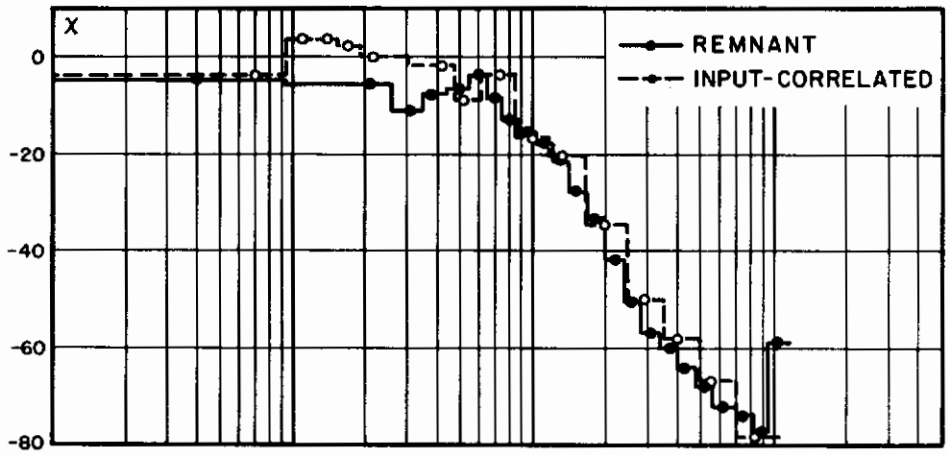

FIG. 13a POWER DENSITY SPECTRUM OF x(t) FOR α = .24 SUBJ JM (0dB = 1 FT^2/RAD/SEC)

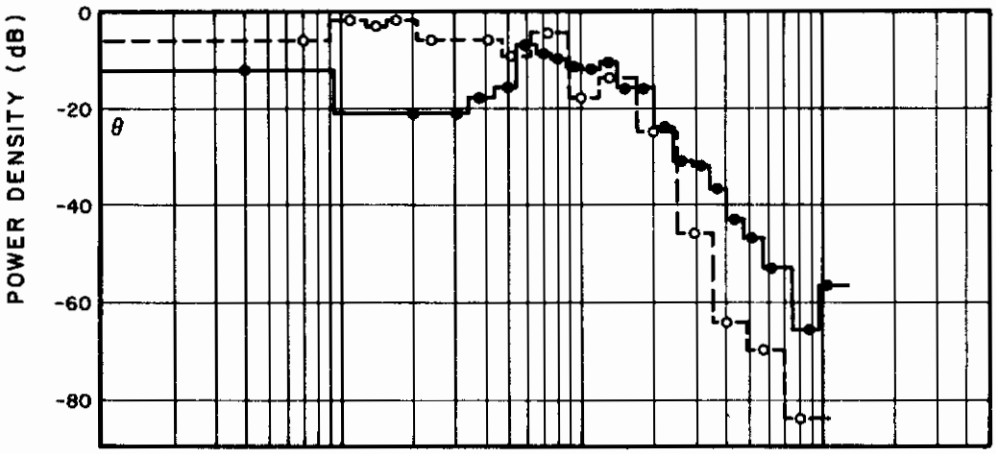

FIG. 13b POWER DENSITY SPECTRUM OF θ(t) FOR α = .24 SUBJ JM (0dB = 1 DEG^2/RAD/SEC)

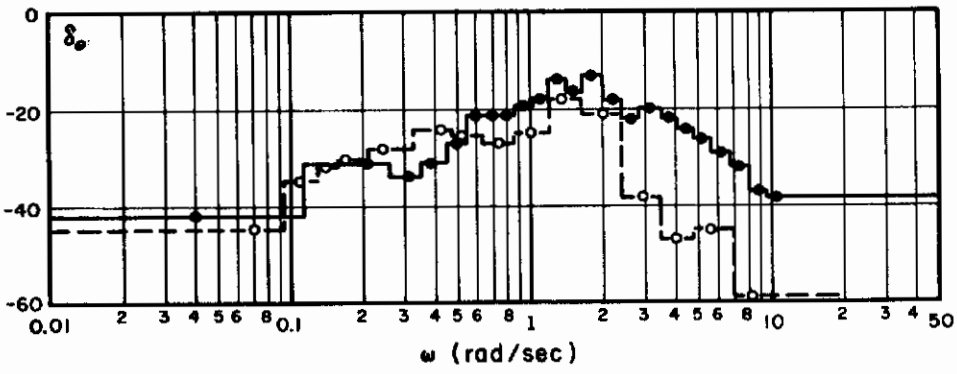

FIG. 13c POWER DENSITY SPECTRUM OF δ_θ(t) FOR α = .24 SUBJ JM (0dB = 1 DEG^2/RAD/SEC)

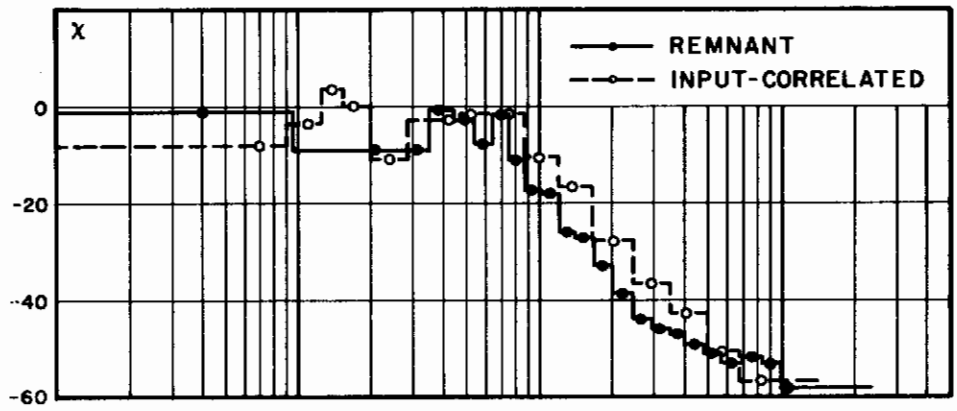

FIG.14a POWER DENSITY SPECTRUM OF x(t) FOR α = 8.0 SUBJ JM (0dB=1 FT^2/RAD/SEC)

FIG 14b POWER DENSITY SPECTRUM OF θ(t) FOR α = 8.0 SUBJECT JM (0dB=1 DEG^2/RAD/SEC)

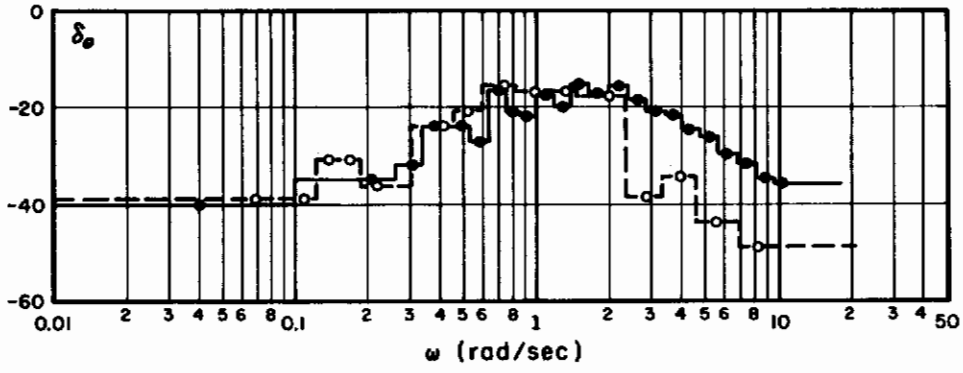

FIG.14c POWER DENSITY SPECTRUM OF δ_θ(t) FOR α = 8.0 SUBJ JM (0dB=1 DEG^2/RAD/SEC)

for α=8.0. The spectra of the portion of these signals that is correlated with the disturbance input and the portion that is remnant are shown separately in these figures. The power spectra were obtained by dividing the power spectra obtained from Fourier analysis by the frequency interval between adjacent points on the spectra. For the input-correlated portion of the signal the interval between adjacent components of the input disturbance was used. For the remnant portion, the power in third-octave frequency bands was obtained first, and then the power density in these third-octave bands was computed by dividing the power in each band by the appropriate bandwidth. Third-octave bands were used to smooth the remnant spectra and average out the point-to-point variability in the remnant.

The differences between the remnant and input-correlated portions of the spectral densities are similar for both high- and low-bandwidth inputs. The control (δ_θ) remnant and input-correlated spectra do not differ consistently at frequencies below 2 rad/sec, but the remnant clearly dominates the input-correlated component at higher frequencies. Since most of the control power is contained in the higher frequencies, the control power is largely remnant power. The relation between remnant and input-correlated pitch power (θ) shows the following trend: (1) the input-correlated power dominates at frequencies below 0.5 rad/sec, (2) the input-correlated and remnant power densities are similar between 0.5 and about 2 rad/sec, and (3) the remnant dominates at higher frequencies. For x(t), the input-correlated power is about 6 to 10 dB greater than the remnant at frequencies above 1 rad/sec for only α=8.0. There is no consistent difference between the remnant and input-correlated power densities for α=0.24 at frequencies above 0.5 rad/sec, although at frequencies below 0.5 rad/sec, the input-correlated component appears to dominate the remnant.

Measurements of fractional remnant power for position, pitch, and control movement variables are given for Subject JM in Table XI. The increase in fractional remnant power upon removal of the rate display observed for all variables indicates that removal of the display caused the pilot to be either more noisy, more time-varying, more non-linear, or a combination of these effects. The fractional remnant power did not apparently vary much with the disturbance bandwidth.

Note that the remnant power in Table XI is about one third of the power of $x(t)$, about one half of $\theta(t)$, and about three fourths of $\delta_\theta(t)$. This is consistent with the spectral densities shown in Figs. 13 and 14. Furthermore the remnant in δ_θ is much larger than the residuals in δ_θ (Table X). The residual is the portion of δ_θ that is not accounted for by the model for the pilot of Eq. (4.4) (a set of gains and a time delay) operating on the state variables. The remnant, on the other hand, is the portion of δ_θ that is not correlated with the input disturbance. Since the model that we have used to derive the pilot's gains operates on all of each of the state variables (not just the part that is correlated with the disturbances) we would expect the residuals to be smaller than the remnant.

In Table XII are the effective bandwidths of the state variables. These were computed from the power spectra and were obtained for Subject JM only. The signal bandwidths generally increased with removal of the rate display. The bandwidths also increased with an increase in the disturbance bandwidth. The magnitude of the increase – generally less than 50% – was not nearly so great as the increase in input bandwidth (a factor of about 33). The relative insensitivity of the bandwidths of the state variables to changes in input bandwidth correlates with the small effect of input bandwidth on scanning behavior.

TABLE XI

Effect of Rate Display on Fractional Remnant Power

Experimental Conditions		Fractional Remnant of:		
α (rad/sec)	Rate Display	x	θ	δ_θ
0.24	ON	.293	.342	.773
	OFF	.335	.526	.792
8.0	ON	.307	.339	.635
	OFF	.396	.497	.767

Subject JM

TABLE XII

Effect of Rate Display on Effective Bandwidth

α (rad/sec)	Rate Display	Bandwidth (rad/sec)				
		$\dot{u}$	u	x	q	θ
0.24	ON	.48	.20	.12	.47	.26
	OFF	.80	.23	.17	.26	.26
8.0	ON	1.29	.22	.17	.52	.26
	OFF	.58	.26	.27	.37	.30

Subject JM

In Table XIII, the mean-square of the state variables and of δ_θ are given for Subject JM. The mean-square of nearly all state variables increased upon removal of the u display. The values for α=.24 were generally lower than those for α=8.0.

TABLE XIII

Effect of Rate Display on Mean-Squared Signal Levels

α (rad/sec)	Rate Display	$\overline{\dot{u}^2}$ $(ft/sec^2)^2$	$\overline{u^2}$ $(ft/sec)^2$	$\overline{x^2}$ ft^2	$\overline{q^2}$ $(deg/sec)^2$	$\overline{\theta^2}$ $(deg)^2$	$\overline{\delta_\theta^2}$ $(deg)^2$
0.24	ON	2.24	3.56	18.5	6.74	9.00	2.47
	OFF	4.80	6.70	25.3	12.6	16.2	2.87
8.0	ON	6.38	5.66	19.3	7.32	8.69	2.58
	OFF	9.03	7.33	14.6	17.9	16.8	5.39

Subject JM

2. Experiment 2

The object of this experiment was to investigate the effect on the controller's performance of changes in the pitch display gain. Two values of display gain were employed: a "high" gain of 0.2 degrees of display deflection per degree of vehicle pitch, and a "low" gain of 0.1 degree/degree. The high gain was the one used in Experiment 1. Half the runs were conducted with an explicit display of the vehicle velocity; the rate display was inoperative for the remainder of the runs. Each subject tracked three runs under each gain, rate-display condition. The conditions were presented in a balanced order. The low-bandwidth disturbance input (α=0.24 rad/sec) was used throughout this experiment.

Average performance measures, mean observation times, and attentional allocation are shown in Table XIV. The performance of the individual subjects is in Tables E4 and E5. Since the effects of pitch gain were similar with and without the presentation of the rate display, the results have been averaged across the rate-display condition so that computations of statistical significance might be based on as large a data base as possible.

The average total performance score was 27% greater (performance was poorer) when the lower pitch gain was used. This performance difference was significant at the 0.05 level, and arose primarily through a doubling of the control-deflection score (significant at the 0.01 level).[†] There was no significant change in the error score.

The effects of display gain on performance score varied among the subjects. Subjects JM and RW both showed differences of 40% or more, whereas the effect was reversed for Subject WW, who achieved a lower score with the lower display gain. The performance scores of Subject WW in this experiment appear to be anamolous, because his high-gain score was greater than it was for

---

[†]The sign test was used to test for significance.

TABLE XIV

Effect of Pitch Display Gain on Performance Score, Mean Observation Time, and Fractional Allocation of Attention

Total Performance Score	$^{\dagger}J_H$	26
	$^{\ddagger}J_L$	32
	J_L/J_H	1.27*
Mean-Squared Positional Error (feet^2)	$\overline{x_H^2}$	23
	$\overline{x_L^2}$	25
	$\overline{x_L^2}/\overline{x_H^2}$	1.10
Mean-Squared Control Deflection (degrees^2)	$\overline{\delta_H^2}$	2.9
	$\overline{\delta_L^2}$	6.9
	$\overline{\delta_L^2}/\overline{\delta_H^2}$	2.13**
Mean Scan Period (seconds)	T_H	1.59
	T_L	1.57
	T_L/T_H	0.97
Mean Observation Time on Position Display (seconds)	T_{xH}	.98
	T_{xL}	.87
	T_{xL}/T_{xH}	.91*
Mean Observation Time on Pitch Display (seconds)	$T_{\theta H}$	.61
	$T_{\theta L}$	.70
	$T_{\theta L}/T_{\theta H}$	1.17***
Fraction of Attention Devoted to Pitch Display	f_{xH}	.62
	f_{xL}	.55
	$f_{xL}-f_{xH}$	.07***

†H denotes high pitch gain (0.2 deg. display deflection/degree pitch)

‡L denotes low pitch gain (0.1 deg. display deflection/degree pitch)

*Significant at 0.05 level.

**Significant at 0.01 level.

***Significant at 0.001 level.

the same conditions in Experiment 1. (The other subjects showed a decrease in score on this condition of between 20 and 35% between the first and second experiments.) One would expect an improvement in tracking ability of this kind because the subjects had more experience with the control task by the time Experiment 2 was run than they did when Experiment 1 was run.

The effects of pitch gain on scanning behavior were consistent for the three subjects. There was no significant change in total scanning period, which was about 1.6 seconds. The scanning pattern, however, was significantly altered. When the pitch gain was decreased, the subjects spent 0.1 second per scan less on the X display and a similar amount more on the pitch display. They thereby decreased the fraction of attention devoted to the x display from 0.62 for the high-gain condition to 0.55 for the low-gain condition.

Average pilot gain matrices are shown in Table XV, and Table E6 shows the gains for the individual subjects. The effective time delay used in the computation was again 0.5 seconds.

Because of the small effect of pitch gain on the controller's gain matrix, the increase in performance score accompanying the decrease in display gain must have been due primarily to an increase in controller's remnant. Table XV shows that a reduction in display gain caused (1) a substantial increase in control-deflection fractional remnant when the rate display was present, and a small increase when it was not and (2) a substantial increase in the fractional remnant of the pitch and position signals with and without the rate display. This increase in remnant is consistent with the notion that the importance of visual threshold effects — and thus the relative contribution of the noisy and nonlinear components of the controller's response — increases as the display gain is reduced.

TABLE XV

EFFECT OF PITCH DISPLAY GAIN ON AVERAGE PILOT GAINS

Display Related Gain

Experimental Conditions		Display						Fixated					
		POSITION						PITCH					
Display Gain (deg/deg)	Rate Display	Gain on:						Gain on:					
		$\dot{u}$	u	x	q	θ	Residual	$\dot{u}$	u	x	q	θ	Residual
0.2	ON	-.431	-.273	-.105	.601	.102	.245	-.081	-.206	-.100	.564	.277	.207
	OFF	-.225	-.330	-.128	.691	.235	.337	.063	-.200	-.103	.634	.301	.195
0.1	ON	-.379	-.418	-.118	.543	.157	.203	-.040	-.272	-.153	.523	.309	.139
	OFF	-.237	-.242	-.159	.480	.221	.216	-.009	-.230	-.137	.500	.315	.196

Weighted Average Gains

Experimental Conditions		Weighted Average				
Display Gain (deg/deg)	Rate Display	Gain on:				
		$\dot{u}$	u	x	q	θ
0.2	ON	-.297	-.243	-.102	.587	.169
	OFF	-.100	-.275	-.115	.668	.261
0.1	ON	-.244	-.356	-.132	.533	.218
	OFF	-.119	-.235	-.147	.491	.270

TABLE XVI

Effect of Pitch Display Gain on

Fractional Remnant Power

Experimental Conditions		Fractional Remnant of:		
Pitch Gain	Rate Display	x	θ	δ_θ
0.2	ON	.153	.237	.693
	OFF	.146	.225	.723
0.1	ON	.443	.732	.901
	OFF	.413	.473	.757

Subject JM

CHAPTER V

DISCUSSION OF ANALYSIS PROCEDURE AND EXPERIMENTAL RESULTS

The objectives of the analysis procedures were (1) to determine what quantities should be displayed (2) to predict how the human controller will allocate his visual attention and (3) to predict the human operator's control characteristics. In this chapter we first examine how well the analysis procedure satisfies these objectives by comparing the experimental results with those predicted by the procedure. Then we use the results of this comparison to reevaluate the analysis procedure and to indicate its principal deficiencies. Finally, we discuss ways of improving the procedure and suggest areas where further development is required.

A. COMPARISON OF THEORETICAL AND EXPERIMENTAL RESULTS

1. Selection of Displays

Our approach to the display selection problem was to examine the cost sensitivities and to choose for display those state variables for which the cost was highly sensitive to changes in the associated gains. Analysis of the XV-5A indicated that when the input disturbance had low bandwidth (α=.24 rad/sec), the cost was most sensitive to the gains on $\dot{u}$, q, and u in that order. The sensitivities to the gains on x and θ were small. For the high bandwidth input the cost was most sensitive to the gain on θ, then to $\dot{x}$ and q. The sensitivity to changes of gain on x and $\dot{u}$ was small and very small, respectively. Since we assumed that

displacement and velocity information, but not higher derivatives or integrals, can be obtained from a single display, we predicted that for α=.24 x, u, and θ displays would be required. For α=8.0 we predicted that only x and θ displays would be necessary.

Experiment 1 provides a partial test of this method for selecting the quantities to be displayed. For α=.24, the performance scores without the u display were 1.7 times those obtained with the u display. For α=8.0 the scores were approximately the same with and without the u display. For the α=8.0 case we predicted that a u display would not be necessary since both x and u information could be obtained from the x display and $\dot{u}$ information was not important. The fact that the score was not materially different with and without the u display confirms this prediction. Similarly, the considerably larger score observed without the u display when α=.24 confirms our prediction of the importance of $\dot{u}$ information and therefore the importance of a u display.

2. Control Characteristics

In Table XVII are the predicted and measured human operator gains for those runs of Experiment 1 in which the u display was on. The predicted gains are from Tables IV and V and are respectively the cross-correlation and the simple predictor gains.

The agreement between the measured and simple predictor gains in Table XVII is good. Consider the α=.24 results. The three most important gains from the point of view of cost sensitivity are, in order of decreasing sensitivity, $K_{\dot{u}}$, K_q, and K_u. The ratios of the measured to the simple predictor gains for these three gains are 1.01, 1.4, 1.9. Thus for the most sensitive gain the simple predictor and measured values are about equal and for the two next most sensitive gains the simple predictor and measured values are within a factor or two of each other. Even for the two least sensitive gains, K_x and K_θ, the agreement between the measured and simple predictor values is good, the ratios being 1.6 and 1.3 respectively.

TABLE XVII

Comparison of Predicted

and Measured Gains

α (rad/sec)		Gain on:				
		$\dot{u}$	u	x	q	θ
.24	Simple Predictor	-.413	-.143	-.052	.447	.094
	Cross Correlation	-.980	-.801	.001	.759	-.063
	Human Controller	-.416	-.273	-.081	.616	.119
8.0	Simple Predictor	-.015	-.099	-.052	.447	.317
	Cross Correlation	-.310	-.328	-.099	.551	.214
	Human Controller	-.095	-.192	-.094	.501	.254

For α=8.0, we also have good agreement between the measured and simple predictor gains. For two of the three most sensitive gains (K_θ and K_q) the measured and simple predictor values are within 20% of each other. For the third most sensitive gain K_x, the measured value is 1.9 times the simple predictor value. It is only for the least sensitive gain, $K_{\dot{u}}$ that we see a very large ratio between measured and simple predictor results (a ratio of almost 6). But variations of this gain have a negligible effect on the system cost and there is little reason to expect close correspondence between human behavior and the theoretical optimal behavior.

The cross-correlation gains do not agree nearly as well with the measured gains as did the simple predictor gains for the α=.24 disturbance, although for the α=8 disturbance the cross-correlation gains provide the better match to the measured results. For α=.24, the ratios of the measured to cross-correlation gains for the three most sensitive gains, $K_{\dot{u}}$, K_q, and K_u, are .43, .81 and .34, respectively. For α=8, the ratios of measured to cross-correlation gains for K_θ, K_q, and K_x, the most sensitive gains, are 1.19, .91, and .99.

It is interesting to note that, with two unimportant exceptions, the human controller gains fall between the simple predictor gains and the cross-correlation gains. Recall that the cross-correlation gains are the equivalent gains of an optimal controller that employs an optimal predictor to derive $\underline{\hat{x}}(t)$ from the delayed state $\underline{y}(t)$. This predictor operates on the entire past of $\underline{y}(t)$. If the human controller's characteristics were the same as this optimal controller, the multiple regression measurement technique that we used would give us the cross-correlation gains. If the human controller acted in a suboptimal manner in the sense that he used the simple predictor, which operates only on the present value of $\underline{y}(t)$ to estimate $\underline{\hat{x}}(t)$, the multiple regression measurement technique would give the so-called simple predictor gains.

The fact that the measured human controller gains lie between the simple predictor gains and the cross-correlation gains implies that the human controller's characteristics lie between those of the optimal predictor operating on the entire past of $\underline{y}(t)$ and the simple predictor operating on only the present of $\underline{y}(t)$. The fact that his gains are generally somewhat closer to the simple predictor than to the cross-correlation gains implies that the simple predictor is a better model of his behavior than the optimal predictor.

The simple predictor model gives a remarkably good approximation to the human controller's characteristics. The differences between the model gains and the measured gains were found to be less than 6 dB (a factor of two) for all of the important gains. This level of agreement is comparable with that normally obtained using describing function techniques in which comparisons are made between the parameters of analytic describing function models and parameters obtained from measured human controller describing functions.

3. Allocation of Display Attention

The prediction of the fractional allocation of visual attention made in Chapter III was based upon the normalized sensitivity coefficients and the predicted signal bandwidths in accordance with Eqs. (2.39) and (2.40). For the calculation of the predicted allocation of attention we used the sensitivity coefficients for D equal to 0.7. (1-D is the fractional change in gain relative to the optimal.) This turns out to be a fairly reasonable choice for D. We see from Table III that the sensitivity coefficients are relatively invariant to D for values near D=0.7. Moreover, we would expect the human operator to choose his gains such that at the operating point of the system, the sensitivities to gain changes were well behaved. For α=8 this appears to be the case since the measured values of the three most important gains are within 20% of the cross-correlation gains. For α=.24, however, two of the three most important gains are less than half of the cross-correlation gains. We assume that the human operator has chosen his gains so that the gain sensitivities about the operating point is much less than the very high sensitivities about the optimum point observed in Table III when D is small. If this is the case, taking D=0.7 is reasonable.

The predicted power density spectra of x(t) and θ(t) (Figs. 7 and 8) agree very well with the measured spectra of the input correlated portions of these signals (Figs. 13 and 14). The agreement is somewhat better for the spectra computed with the cross-correlated gains $\underline{L}_c$ than with the simple predictor gains $\underline{L}_s$. The predicted effective bandwidths (Table VI) agree reasonably well with the measured effective bandwidths (Table XII). The $\underline{L}_c$ effective bandwidths are in all cases within a factor of two of the measured effective bandwidths for condition in which there was an explicit display of u(t). Comparison with the measured bandwidths for the condition in which there is no display of u(t) is not appropriate, since the pilot will have difficulty obtaining $\dot{u}(t)$ information which is important for control.

Now let us compare the predictions and measurements of the fractional allocation of attention, Tables VII and IX respectively. We note that the predicted values of f_x, the fraction of attention allocated to the position display, depends to a great extent upon the values that are assumed for the constants K' and C and upon the choice of gains, $\underline{L}_c$ or $\underline{L}_s$. If we use the $\underline{L}_s$ gains with K'=0.5 sec/bit and C=.05 sec, we obtain good agreement for α=.24 rad/sec between the predicted f_x and the f_x observed when there was an explicit presentation of u(t). For α=8 rad/sec, we predicted a decrease in f_x from .68 to .58, whereas we observed a decrease from .69 to .65.

For most other choices of the gains or constants the agreement between predicted and measured allocation of attention for the two disturbance inputs, α=.24 and α=8, is less good. We have at present no basis for choosing the constants of the visual attention model except by matching observed performance. The fact that the predictions depend heavily upon the values assumed is a major limitation of the analysis method.

It should be noted that the analysis method does not provide a mechanism for taking into account effects such as a change in display gain (as in Experiment 2) or not presenting all of the information required for control (as in Experiment 1). This is another limitation of the model.

4. Performance Scores

Table VIII shows that the performance scores of the optimal controller were predicted to be 2.35 and 5.0 for α=.24 and α=8, respectively. The corresponding measured scores from Experiment 1 were 21 and 27 with the rate display (Table IX). Thus the predicted scores are only between 10 and 20% of the measured scores.

There are two reasons for the difference between human controller and optimal controller scores. First the model for the human controller does not include a source of remnant. Table XI shows that for subject JM about a third of the power in x(t) and three quarters of the power in $\delta_\theta(t)$ consists of remnant. Since most of the score results from x(t), about 1/3 of the human controller scores result from a factor that is not taken into account by the present optimal controller model.

The second source of disagreement is that the human controller's gains are much lower than the optimal controller's (cross correlation) gains. Because the human controller's gains are lower than the optimal, we would expect his scores to be higher than the optimal controller's scores. The sensitivity coefficients of Table III provide an indication of how much larger we would expect the scores to be. For example, if with α=.24 the human controller changed his gain on $\dot{u}$ by 50%, he would cause an increase

in the score by a factor of about five.† The human controller's gain on $\dot{u}$ was in fact somewhat less than one half of the cross-correlation gain for this case.

Note, however, that the sensitivity results in Table III were derived under the assumption that only one gain at a time is changed from the optimal. However all of the human controller's gains differed materially from the optimal. Thus we must be careful in our use of the sensitivity coefficients of Table III to estimate the increase in cost resulting from nonoptimal human controller gains. It seems reasonable to conclude, however, that the departure of the human controller's gains from optimum is responsible for much of the difference between the optimal and the human controller's scores.

---

†Recall that the normalized sensitivity coefficients are equal to $\frac{\Delta J/J^*}{(1-D)^2}$. For D=.5, we must divide the entries in Table III by 4 to find the fractional increase in cost.

B. EVALUATION OF ANALYSIS PROCEDURE

The validation experiments, although far from being an exhaustive test, provide sufficient information to judge, at least in a preliminary way, the adequacy and correctness of the basic assumptions of the analysis procedure, the predictions made from it, the structure of the human controller model used in it, and the implementation of the method. The fundamental assumption upon which the procedure rests, namely that the human controller acts as a near-optimal controller subject to certain inherent limitations, appears to be a useful concept. It is certainly one that is well worth exploiting in the further development of the procedure. The state space representation of the human controller's control characteristics appears to be a very powerful and yet simple way of handling multivariable systems. By using it we avoid many of the problems encountered in the describing function approach in which we must arbitrarily and somewhat artificially specify the inner and outer loops. Moreover, we avoid the considerable difficulty that is encountered when we try to measure the human controller's characteristics in these various loops.

The results obtained from application of the method range from good to poor. We were able to achieve reasonably good predictions of the human controller's control characteristics. His gains were close to those predicted under the assumption that he acts like a simple predictor of the system state and an optimal controller acting on the predicted state. The sensitivity method of selecting the information that should be displayed seems reasonable, is quantitative, and gave rational results.

The procedure for predicting the allocation of visual attention gave results that were sensitive to the choice of constants and gains. The procedure does not take into account factors such

as display gain or the absence of some information. The assumption that visual attention is simply related to the logarithm of the sensitivity coefficients cannot be completely justified from theoretical considerations, although it did give approximately correct results.

There are also certain structural deficiencies in the analysis procedure and in the model for the human controller upon which it rests. The model does not include remnant and the optimization techniques employed in predicting human behavior therefore cannot take into account this important component of the human controller's response. In addition the representation of the perceptual processes is weak. We have no way within the existing framework of representing the effects of differences of display design such as display gain or of viewing displays peripherally instead of foveally. Although a simple representation of the human controller in terms of a pure delay and an equalizer composed of a set of gains operating on the state variables appears to give meaningful results, some improvement in the accuracy of the analysis could no doubt be achieved by elaborating upon this representation.

Finally, there is a major implementation deficiency in the procedure. The treatment of sensitivity, which allows only one gain to vary at a time, is not adequate since almost all of the human controller's gains differ substantially from the optimal (cross-correlation) gains. The simple sensitivity analysis used in the present method does not account for the fact that the sensitivity about some nonoptimal operating point may be different from the sensitivity around the optimal operating point.

C. SUGGESTED IMPROVEMENTS TO ANALYSIS PROCEDURE

The two most important improvements that should be made to the analysis procedure are (1) the inclusion of a perceptual noise to account for human controller remnant and for perceptual factors such as scale changes and peripheral viewing; and (2) the addition of a relatively sophisticated visual sampling model which includes eye movement dynamics and elements of perception such as minimum fixation and accommodation times. In addition the sensitivity analysis should be improved to allow for simultaneous changes of several controller gains and for suboptimal operating points.

By adding the remnant to the model it should be possible to consider within the framework of the analysis procedure many issues that are directly related to the detailed design of the display instruments. We should also be able to make more accurate predictions of the pilot's control characteristics which depend heavily upon the remnant. The use of a sophisticated sampling model should lead to more accurate prediction of the allocation of visual attention and also permit prediction of scanning patterns. Such information would be useful for instrument panel design. An attempt to extend the analysis procedures along these lines is being made. Initial results, which look very promising, are discussed by Baron and Kleinman.[27]

APPENDIX A

OPTIMAL CONTROL OF A LINEAR SYSTEM WITH TIME DELAY AND QUADRATIC COST FUNCTIONAL

A. PROBLEM FORMULATION

We assume the (time-invariant) linear system characterized by

$$\dot{\underline{x}}(t) = \underline{A}\,\underline{x}(t) + \underline{B}\,\underline{u}(t) + \underline{w}(t) \qquad (A.1)$$

where $\underline{x}(t)$ and $\underline{u}(t)$ are the state and control vectors, respectively, and $\underline{w}(t)$ is a gaussian, white-noise input disturbance having zero mean and covariance matrix $\underline{W}$, i.e.

$$\text{cov}[\underline{w}(t)] = E[\underline{w}(t)\underline{w}'(\tau)] = \underline{W}\delta(t-\tau) \quad . \qquad (A.2)$$

We assume further that the system output, $\underline{y}(t)$, is the delayed replica of the state $\underline{x}(t)$, i.e.,

$$\underline{y}(t) = \underline{x}(t-T) \quad , \quad T>0 \qquad (A.3)$$

or put in frequency domain terms we require $\underline{y}(s)=e^{-sT}\underline{x}(s)$.

We wish to construct a feedback controller of the form

$$\underline{u}^*_T[\underline{y}(t),\, t] = H^*[\underline{y}(t),\, t] \quad , \qquad (A.4)$$

such that (1) $H^*(\cdot,\cdot)$ is realizable – i.e., if $\underline{x}(t)\equiv\underline{0}$ for $t\varepsilon(-\infty,t_0)$ – then $H^*[\underline{y}(t),t]\equiv\underline{0}$ for $t\varepsilon(-\infty,t_0+T)$, and (2) $H^*[\underline{y}(t),t]$ absolutely minimizes the cost functional

$$J[\underline{u}(\cdot)] = E_{\underline{w}(\cdot)}\left\{ \lim_{t_1 \to \infty} \frac{1}{t_1} \int_0^{t_1} [\underline{x}'(t)\ \underline{Q}\ \underline{x}(t) + \underline{u}'(t)\ \underline{R}\ \underline{u}(t)]dt \right\} . \tag{A.5}$$

Under these conditions, we call $\underline{u}_T^*(\cdot)$ the optimal control. It has been shown[19] that if T=0, i.e., $\underline{y}(t)=\underline{x}(t)$, the optimal control $\underline{u}_o^*(\cdot)$ is merely

$$\underline{u}_o^*[\underline{y}(t)] = -\underline{R}^{-1}\underline{B}'\underline{K}\ \underline{y}(t) = -\underline{L}^*\underline{y}(t) \quad , \tag{A.6}$$

where $\underline{K}$ is the unique positive-definite solution of the algebraic equation

$$\underline{0} = \underline{K}\ \underline{A} + \underline{A}'\underline{K} + \underline{Q} - \underline{K}\ \underline{B}\ \underline{R}^{-1}\underline{B}'\underline{K} \quad . \tag{A.7}$$

The object of this appendix is to modify the above solution in order to obtain the optimal control law Eq. (A.4) for the case T>0. In the sequel we shall approach this problem by first considering the case when $\underline{w}(t)$ is simply an impulse applied to the system at $t=t_0$, i.e.

$$\underline{w}(t) = \underline{x}_0\delta(t-t_0) \quad .$$

Hence, $\underline{x}(t)\equiv\underline{0}$ for $t\in(-\infty,t_0)$ and $\underline{x}(t_0)=\underline{x}_0$. The cost functional we shall minimize is

$$\hat{J}[\underline{u}(\cdot)] = \int_{t_0}^{\infty} [\underline{x}'(t)\ \underline{Q}\ \underline{x}(t) + \underline{u}'(t)\ \underline{R}\ \underline{u}(t)]dt \quad . \tag{A.8}$$

We first solve this basically simpler problem for completeness

and to give the reader a clearer understanding of the behavior of linear regulator systems operating with inherent time-delays. We then extend the solution for the noiseless case to cover the situation first discussed in which $\underline{w}(t)$ is a noise disturbance.

B. NO NOISE SOLUTION

In the absence of a time delay, the optimal control is

$$\underline{u}_0^*[\underline{y}(t),t] = -\underline{L}^*\underline{y}(t) = -\underline{L}^*\underline{x}(t) \quad ; \quad t \geq t_0 \quad . \tag{A.9}$$

Furthermore, in the absence of noise, the feedback control Eq. (A.9) is identical to the open-loop control

$$\begin{aligned} \underline{u}_0^*(t) &= -\underline{L}^* \, e^{(\underline{A}-\underline{B}\,\underline{R}^{-1}\underline{B}'\underline{K})\,(t-t_0)}\,\underline{x}_0 \quad ; \quad t \geq t_0 \\ &= -\underline{L}^* \, e^{\overline{\underline{A}}(t-t_0)}\,\underline{x}_0 \quad . \end{aligned} \tag{A.10}$$

Let us now consider the case $T>0$. We note that the control Eq. (A.10) must minimize $\hat{J}[\underline{u}(\cdot)]$. However, this control is *unrealizable* since $\underline{u}_0^*(t) \neq \underline{0}$ for $t \varepsilon (t_0, t_0+T)$.

The realizability condition (1) requires $\underline{u}_T^*[\underline{y}(t),t]$ to be zero for $t \varepsilon (t_0, t_0+T)$ irrespective of $\underline{x}_0$. This in turn implies that the value of

$$\int_{t_0}^{t_0+T} \underline{x}'(t)\,\underline{Q}\,\underline{x}(t)\,dt$$

cannot be altered by control action. Therefore, the task of minimizing $\hat{J}[\underline{u}(\cdot)]$ is equivalent to minimizing

$$\hat{J}[\underline{u}(\cdot)] = \int_{t_0+T}^{\infty} [\underline{x}'(t)\underline{Q}\ \underline{x}(t) + \underline{u}'(t)\underline{R}\ \underline{u}(t)]dt \quad . \tag{A.11}$$

The *open-loop* control which minimizes Eq. (A.11) is given by

$$\underline{u}_T^*(t) = -\underline{L}^*\ e^{\overline{\underline{A}}[t-(t_0+T)]}\ \underline{x}(t_0+T) \text{ for } t \geq t_0+T$$

$$= 0 \text{ for } t<t_0+T \quad . \tag{A.12}$$

In order to construct a (realizable) controller $H^*[\underline{y}(t),t]$ which generates the control Eq. (A.12) we note, since $H^*[\underline{y}(t),t] \equiv 0$ for $t \in (t_0, t_0+T)$, that

$$\underline{x}(t_0+T) = e^{\underline{A}T}\ \underline{x}_0 = e^{\underline{A}T}\ \underline{y}(t_0+T) \quad . \tag{A.13}$$

Indeed, we can now construct an optimal realizable controller as follows. At time t_0+T we obtain $\underline{x}(t_0+T)$ from the system output $\underline{y}(t_0+T)$ using Eq. (A.13), and then implement the control Eq. (A.12) for $t \geq t_0+T$. However this procedure generates an open-loop control, whereas we seek a closed-loop control.

C. OPTIMAL FEEDBACK CONTROL — NO NOISE CASE

To construct a feedback control law which minimizes $\hat{J}$, we must find an operator $H^*[\underline{y}(t),t]$ such that

$$H^*[\underline{y}(t),t] = -\underline{L}^* \, e^{\overline{\underline{A}}(t-t_0+T)} \, e^{\underline{A}T} \, \underline{y}(t_0+T) \text{ for } t \geq t_0+T \quad . \qquad (A.14)$$

We shall show that such an $H^*[\underline{y}(t),t]$ may be realized by a *linear* feedback law

$$H^*[\underline{y}(t),t] = \underline{G}^*(t) \, \underline{y}(t) \text{ for } t \geq t_0+T \quad . \qquad (A.15)$$

To do so, we first note that since $H^*[\underline{y}(t),t]$ must be identically zero for $t<t_0+T$, the effect of control is not "seen" in $\underline{y}(t)$ until $t>t_0+2T$, and so

$$\underline{y}(t) = \underline{x}(t-T) = e^{\underline{A}[t-(t_0+T)]} \, \underline{x}_0 \text{ for } t_0+T \leq t \leq t_0+2T \quad . \qquad (A.16)$$

But, since $\underline{y}(t_0+T) = \underline{x}_0$, we have

$$\underline{y}(t_0+T) = e^{-\underline{A}[t-(t_0+T)]} \, \underline{y}(t) \qquad t_0+T \leq t \leq t_0+2T \quad . \qquad (A.17)$$

Therefore, substituting Eq. (A.17) into Eq. (A.14) we see that over the interval (t_0+T, t_0+2T) the linear feedback law

$$H^*[\underline{y}(t),t] = -\underline{L}^* \, e^{\overline{\underline{A}}[t-(t_0+T)]} \, e^{\underline{A}T} \, e^{-\underline{A}[t-(t_0+T)]} \, y(t) \qquad (A.18)$$

$$= -\underline{L}^* \, e^{\overline{\underline{A}}(t-t_0-T)} \, e^{-\underline{A}(t-t_0-2T)} \, \underline{y}(t) \quad ,$$

will generate the required control input $\underline{u}_T^*[\underline{y}(t),t]$ given by Eq. (A.12). Therefore, on the interval (t_0+T, t_0+2T) we have

$$\underline{x}(t) = e^{\overline{\underline{A}}(t-t_0-T)} \underline{x}(t_0+T) \qquad (A.19)$$

by virtue of the fact that the control law Eq. (A.18) is optimal over (t_0+T, t_0+2T). Furthermore, over the time interval (t_0+2T, t_0+3T), since

$$\underline{y}(t) = \underline{x}(t-T) = e^{-\overline{\underline{A}}T} \underline{x}(t) \quad ,$$

and since we wish to generate the control law

$$\underline{u}^*(t) = -\underline{L}^*\underline{x}(t)$$

we see that

$$H^*[y(t),t] = -\underline{L}^* e^{\overline{\underline{A}}T} \underline{y}(t)$$

will accomplish the required task. Extending this argument, we see that for $t>t_0+2T$ the control law

$$H^*[\underline{y}(t),t] = -\underline{L}^* e^{\overline{\underline{A}}T} \underline{y}(t) \qquad (A.20)$$

will result in the desired system input

$$\underline{u}_T^*(t) = -\underline{L}^*\underline{x}(t)$$

provided of course that over the interval (t_0+T, t_0+2T) we apply the control Eq. (A.18).

In summary, the linear feedback law

$$H^*[y(t),t] = \begin{cases} \underline{0} & t<t_0+T \\ -\underline{L}^*e^{\overline{\underline{A}}(t-t_0-T)}\, e^{-\underline{A}(t-t_0-2T)}\, \underline{y}(t), & t_0+T\leq t\leq t_0+2T \\ -\underline{L}^*e^{\overline{\underline{A}}T}\, \underline{y}(t) & t>t_0+2T \end{cases} \tag{A.21}$$

is realizable and minimizes the cost functional $\hat{J}[\underline{u}(\cdot)]$.

The optimal controller consists of gains which are time-varying over $(t_0+T,\ t_0+2T)$ and which are *constant* for $t>t_0+2T$. Note that these gains are continuous in t. In the following section it is shown that one can implement the control law Eq. (A.21) by means of a time invariant, linear dynamical system whose input is $\underline{y}(t)$ and whose output is $H^*[t,\underline{y}(t)]$. This is possible because the system Eq. (A.1) is time-invariant and all time variations in $H^*(\cdot,\cdot)$ are exponential and of the form $(t-t_0)$ only.

D. FREQUENCY DOMAIN REALIZATION OF THE OPTIMAL CONTROLLER

In this section we find a (realizable) compensator $\underline{G}^*(s)$ which represents the optimal feedback controller. The optimal control system will then be as shown in Fig. A1. Since $\underline{G}^*(s)$ will be independent of t_0, we shall henceforth assume $t_0=0$ for convenience.

In order to obtain an expression for $\underline{G}^*(s)$, i.e. the matrix transfer function relating $\underline{y}(\cdot)$ to $\underline{u}(\cdot)$ via

$$\underline{u}(s) = \underline{G}^*(s)\ \underline{y}(s) \quad ,$$

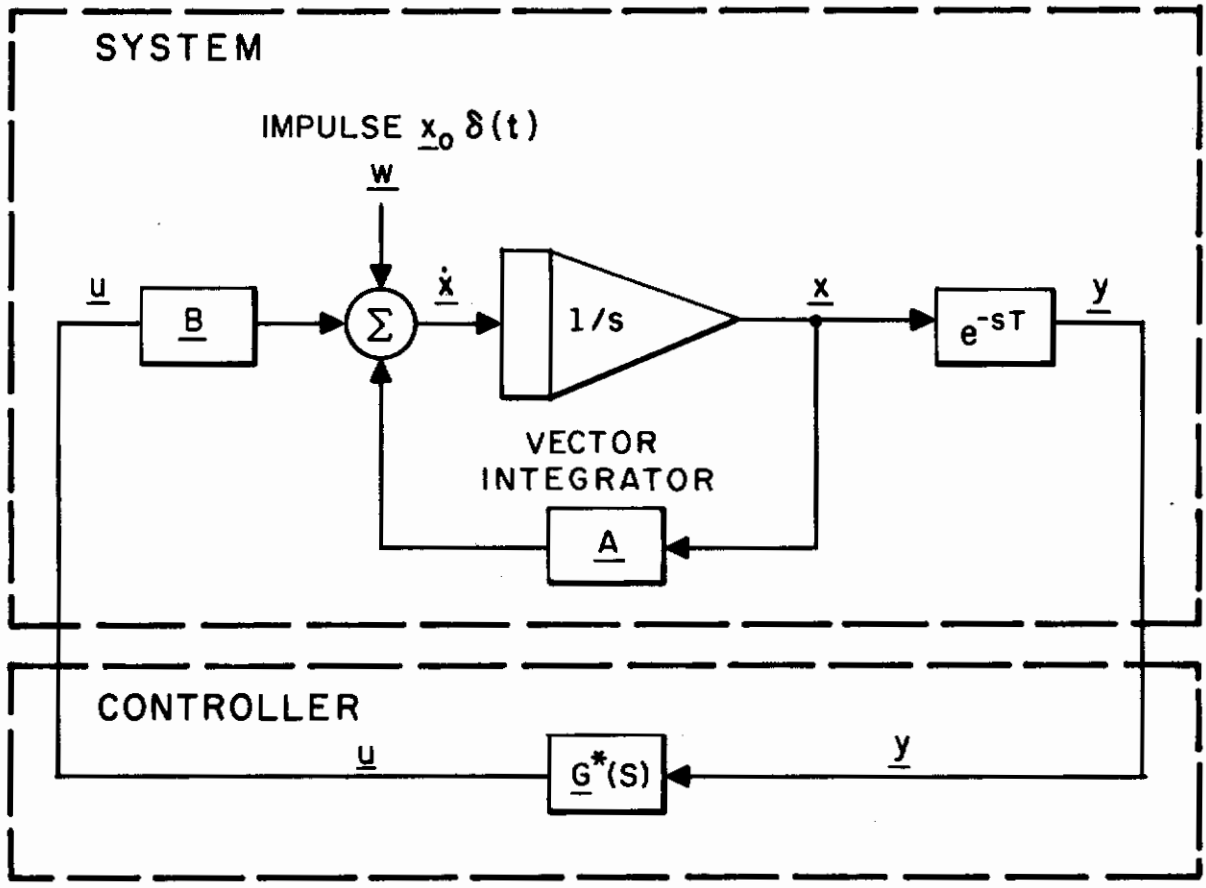

FIG. A1 FEEDBACK REPRESENTATION OF OPTIMAL CONTROLLER

we first find the transfer functions between disturbance input $\underline{w}(\cdot)$ and $\underline{y}(\cdot)$ and $\underline{u}(\cdot)$. These are denoted by $\underline{M}(s)$ and $\underline{N}(s)$ respectively, i.e.

$$\left.\begin{aligned} \underline{y}(s) &= \underline{M}(s)\ \underline{w}(s) \\ \underline{u}(s) &= \underline{N}(s)\ \underline{w}(s) \end{aligned}\right\} \tag{A.22}$$

$\underline{G}^*(s)$ may then be obtained from the equation

$$\underline{G}^*(s) = \underline{N}(s)\ \underline{M}^{-1}(s) \quad . \tag{A.23}$$

$\underline{M}(s)$ and $\underline{N}(s)$ are found as follows. In the developments of section C, $\underline{w}(t)$ was a single impulse. Consequently, M(s) is merely the Laplace transform of the transition (or Green's) function which relates $\underline{w}(t)$ to $\underline{y}(t)$. Let us call this transition matrix $\underline{\Phi}_y(t)$. From the analysis of section C we have ($t_0=0$)

$$\underline{\Phi}_y(t) = \begin{cases} 0 & t<T \\ e^{\underline{A}(t-T)} & T\leq t\leq 2T \\ e^{\underline{\bar{A}}(t-2T)}\, e^{AT} & 2T\leq t \end{cases} \quad . \tag{A.24}$$

Thus,

$$\underline{M}(s) = \int_0^\infty \underline{\Phi}_y(t) e^{-st}\, dt = \int_T^{2T} e^{\underline{A}(t-T)}\, e^{-st}\, dt + \int_{2T}^\infty e^{\underline{\bar{A}}(t-2T)}\, e^{\underline{A}T}\, e^{-st}\, dt$$

$$= \{[\underline{I}-e^{(\underline{A}-s\underline{I})T}](s\underline{I}-\underline{A})^{-1} + (s\underline{I}-\underline{\bar{A}})^{-1}\, e^{(\underline{A}-s\underline{I})T}\}e^{-sT} \quad . \tag{A.25}$$

In similar manner, the Green's function which relates $\underline{w}(t)$ to $\underline{u}(t)$, and which we call $\underline{\Phi}_u(t)$ is merely

$$\underline{\Phi}_u(t) = \begin{cases} 0 & t<T \\ -\underline{L}^* e^{\overline{\underline{A}}(t-T)} \; e^{\underline{A}T} & t \geq T \end{cases} \quad . \tag{A.26}$$

Thus, $\underline{N}(s)$ is

$$\underline{N}(s) = -\underline{L}^*(s\underline{I}-\overline{\underline{A}})^{-1} \; e^{(\underline{A}-s\underline{I})T} \quad . \tag{A.27}$$

If we now write $(s\underline{I}-\underline{A})=(s\underline{I}-\overline{\underline{A}}-\underline{B}\;\underline{R}^{-1}\underline{B}'\underline{K})=(s\underline{I}-\overline{\underline{A}})[\underline{I}-(s\underline{I}-\overline{\underline{A}})^{-1}\underline{B}\;\underline{R}^{-1}\underline{B}'\underline{K}]$ we can obtain an expression for $N(s)\underline{M}^{-1}(s)=\underline{G}^*(s)$ with the aid of the matrix identity

$$(\underline{X}\;\underline{Y}^{-1} + \underline{I})^{-1} = \underline{I} - \underline{X}(\underline{X} + \underline{Y})^{-1} \quad .$$

The result is

$$\underline{G}^*(s) = -\underline{L}^* e^{sT}\left\{\underline{I} - [e^{(s\underline{I}-\underline{A})T} - \underline{I}]\cdot[e^{(s\underline{I}-\underline{A})T} - (s\underline{I}-\overline{\underline{A}})^{-1}\underline{B}\;\underline{L}^*]^{-1}\right\} \quad . \tag{A.28}$$

Note that the term $-\underline{L}^* e^{sT}$ is the optimal *unrealizable* controller. It would be the optimal controller if a pure predictor (e^{sT}) could be mechanized. The total expression for $\underline{G}^*(s)$ represents the optimal *realizable* controller.

Lastly, it is not difficult to show that $\underline{G}^*(s)$ can be synthesized as in Fig. A2 where

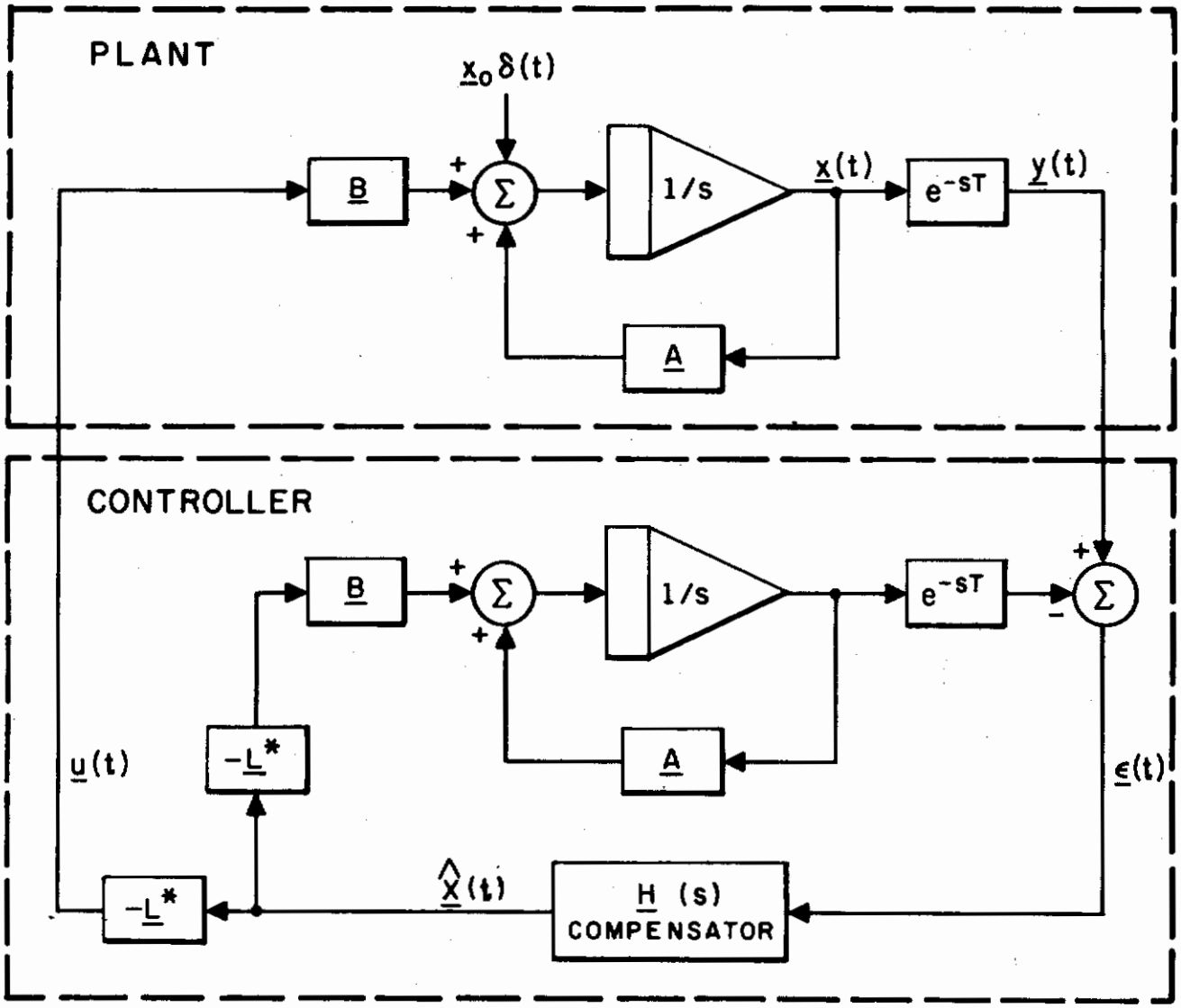

FIG. A2 OPTIMAL CONTROLLER REALIZATION AND PLANT

$$\underline{H}(s) = (s\underline{I}-\underline{\bar{A}})^{-1}\ (s\underline{I}-\underline{A})\ e^{\underline{A}T} \quad . \tag{A.29}$$

This synthesis is appealing from a physical point of view since it shows that the optimal controller constructs, in essence a model of the actual system being controlled. This is characteristic of most joint estimation and control problems. (See Ref. 5)

We shall now investigate the case when $\underline{w}(t)$ is a white-noise and show that the system of Fig. A1 is the optimal system for this case as well.

E. OPTIMAL CONTROL SOLUTION-NOISE CASE

Before we consider the case when $\underline{w}(t)$ is a noise process, let us examine the solution Eq. (A.21) further. We recognize the matrix $\underline{L}^*=\underline{R}^{-1}\underline{B}'\underline{\bar{K}}$ as the optimal gain matrix for the case T=0. What then do the other terms represent? If we define

$$\hat{\underline{x}}(t) = \begin{cases} e^{\underline{\bar{A}}(t-t_0-T)}\ e^{-\underline{A}(t-t_0-2T)}\ \underline{y}(t) & t_0+T\leq t\leq t_0+2T \\ e^{\underline{\bar{A}}T}\ \underline{y}(t) & t>t_0+2T \end{cases} \tag{A.30}$$

we see, retracing the development of section C, that $\hat{\underline{x}}(t)$ must be identical to $\underline{x}(t)$ for $t>t_0+T$, i.e.

$$\hat{\underline{x}}(t) = \underline{x}(t) \text{ for } t\geq t_0+T \quad . \tag{A.31}$$

Therefore, the optimal controller behaves in a very logical manner. Once it receives an input $\underline{y}(t)$, $t\geq t_0+T$ it first reconstructs the *current* state of the system, namely $\underline{x}(t)$ and then applies the optimal control $\underline{u}^*(t)=-\underline{L}^*\hat{\underline{x}}(t)$. Since the process is deterministic, $\hat{\underline{x}}(t)\equiv\underline{x}(t)$.

Let us now investigate the case when $\underline{w}(t)$ is a white-noise, gaussian process and $T>0$. With analogy to the noiseless case, it is reasonable to assume that the optimal controller first constructs the minimal variance estimate $\underline{\hat{x}}(t)$ of the current system state given $\underline{y}(\tau)$, $\tau \leq t$[†] and then applies the control $\underline{u}^*(t) = -\underline{L}^*\underline{\hat{x}}(t)$.[‡] We shall show that the controller $\underline{G}^*(s)$ precisely accomplishes this task. Refer to Fig. A3 where we have written

$$\underline{G}^*(s) = -\underline{R}^{-1}\underline{B}'\underline{K} \cdot \underline{G}_1(s) = -\underline{L}^*\underline{G}_1(s) \quad . \tag{A.32}$$

Let $\underline{\hat{x}}(t)$ denote the output of $\underline{G}_1(s)$, i.e., $\underline{\hat{x}}(s)=\underline{G}_1(s)\,\underline{y}(s)$. We shall show that $\underline{\hat{x}}(t)$ is the best estimate of $\underline{x}(t)$ given the data $\underline{y}(\tau)$, $\tau \leq t$.

The Green's function relating $\underline{\hat{x}}(t)$ to $\underline{w}(t)$ is

$$\underline{\Phi}_{\hat{x}}(t) = \begin{cases} 0 & t<T \\ e^{\overline{\underline{A}}(t-T)}\, e^{\underline{A}T} & t \geq T \end{cases} \quad . \tag{A.33}$$

In order to show that $\underline{\hat{x}}(t)$ is the optimal estimate [in a probability sense] of $\underline{x}(t)$, it is sufficient to show, since $\underline{w}(t)$ is Gaussian, that the "error" $\underline{e}(t)=\underline{x}(t)-\underline{\hat{x}}(t)$ is uncorrelated[31] (since uncorrelated in the Gaussian case implies independent) with $\underline{y}(\tau)$, $\tau \leq t$. The Green's function relating $\underline{e}(t)$ to $\underline{w}(t)$ is merely

---

[†] i.e., $\underline{\hat{x}}(t)=E[\underline{x}(t) \mid \underline{y}(\tau),\ \tau \leq t]$

[‡] It is possible to show that this assumption is indeed true.

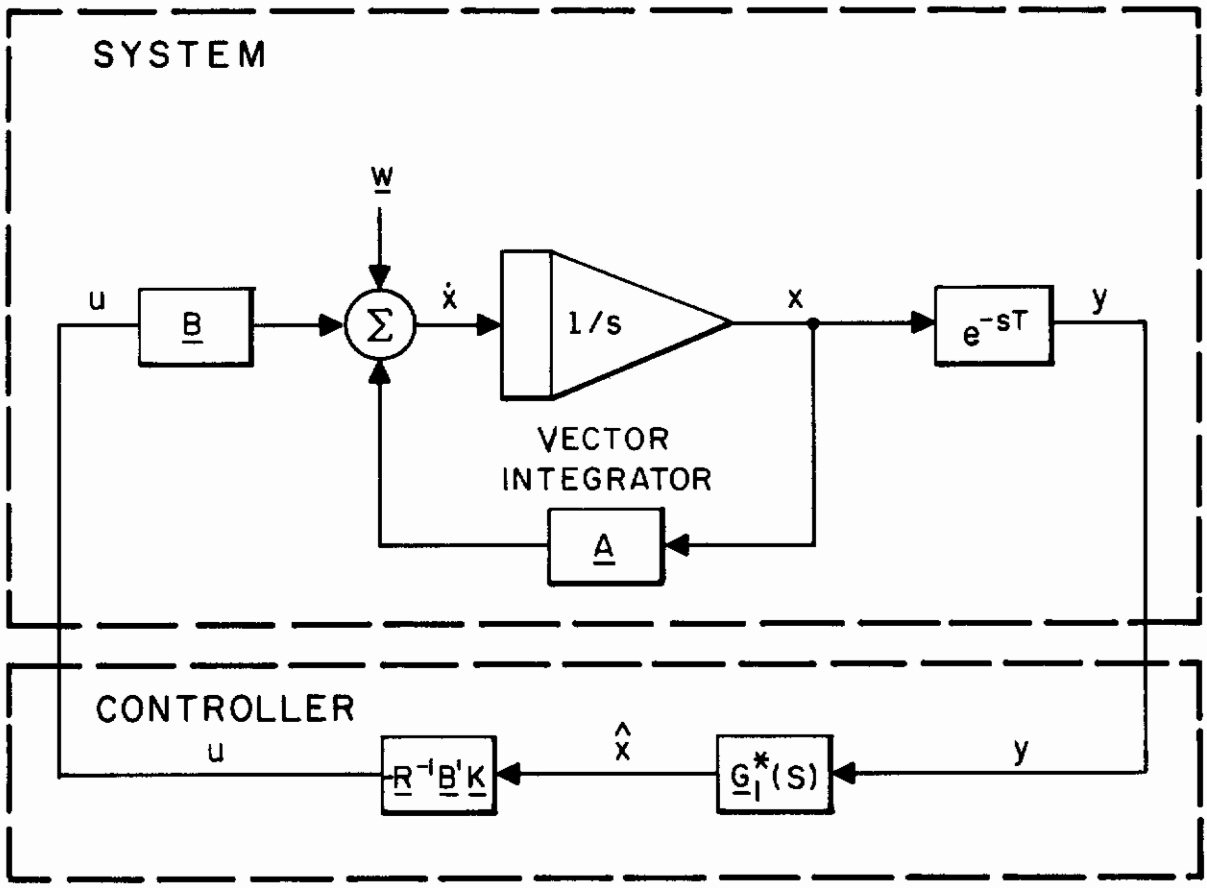

FIG. A3 PREDICTOR - CONTROL REALIZATION OF OPTIMAL SYSTEM

$$\underline{\Phi}_e(t) = \begin{cases} 0 & t<0 \\ e^{\underline{A}t} & 0\leq t\leq T \\ 0 & t>T \end{cases} \quad . \tag{A.34}$$

Hence

$$E[\underline{e}(t)\ \underline{y}'(\tau)] = E\left[\int_{-\infty}^{t}\int_{-\infty}^{t} \underline{\Phi}_e(t-\xi)\underline{w}(\xi)\ \underline{w}'(\sigma)\ \underline{\Phi}_y'(\tau-\sigma)d\xi d\sigma\right] \quad \tau\leq t$$

$$= \int_{-\infty}^{t}\int_{-\infty}^{\tau} \underline{\Phi}_e(t-\xi)\ E[\underline{w}(\xi)\ \underline{w}'(\sigma)]\ \underline{\Phi}_y'(\tau-\sigma)d\xi d\sigma \quad ,$$

but $E[\underline{w}(\xi)\underline{w}'(\sigma)]=\underline{W}\delta(\xi-\sigma)$ so that

$$E[\underline{e}(t)\ \underline{y}'(\tau)] = \int_{-\infty}^{\tau} \underline{\Phi}_e(t-\sigma)\ \underline{W}\ \underline{\Phi}_y'(\tau-\sigma)d\sigma$$

$$= \int_{0}^{\infty} \underline{\Phi}_e(t-\tau+\sigma)\underline{W}\ \underline{\Phi}_y'(\sigma)d\sigma \quad , \quad (t-\tau)\geq 0 \quad .$$

This integral is zero since $\underline{\Phi}_y(\sigma)=\underline{0}$ for $0<\sigma<T$ and $\underline{\Phi}_e(\sigma)=\underline{0}$ elsewhere. Thus, the error $\underline{e}(t)$ is independent of the past history of $\underline{y}(t)$. This implies that $\underline{\hat{x}}(t)$ is the best estimate of $\underline{x}(t)$ and hence our claim is established. We have shown that for the system Eq. (A.1) the feedback controller which minimizes the performance index Eq. (A.5) is a dynamical system with impulse response $\underline{G}^*(s)$ given by Eq. (A.28) and pictures in Fig. A2.

Lastly, we can obtain expressions for the various covariance matrices as

$$\text{cov}[\underline{e}(t)] = E[\underline{e}(t)\underline{e}'(t)] = \int_0^\infty \underline{\Phi}_e(\tau)\ \underline{W}\ \underline{\Phi}_e'(\tau)\ d\tau$$

$$= \int_0^T e^{\underline{A}\tau}\ \underline{W}\ e^{\underline{A}'\tau}\ d\tau \quad , \tag{A.35}$$

$$\text{cov}[\underline{\hat{x}}(t)] = E[\underline{\hat{x}}(t)\ \underline{\hat{x}}'(t)] = \int_0^\infty \underline{\Phi}_{\hat{x}}(\tau)\ \underline{W}\ \underline{\Phi}_{\hat{x}}'(\tau)\ d\tau$$

$$= \int_0^\infty e^{\overline{\underline{A}}\tau}\ e^{\underline{A}T}\ \underline{W}\ e^{\underline{A}'T}\ e^{\overline{\underline{A}}'\tau}\ d\tau \quad , \tag{A.36}$$

$$\text{cov}[\underline{y}(t)] = \text{cov}[\underline{y}(t)\underline{y}'(t)] = \text{cov}[\underline{x}(t)]$$

$$= \text{cov}[\underline{e}(t)] + \text{cov}[\underline{\hat{x}}(t)]$$

$$= \int_0^T e^{\underline{A}\tau}\ \underline{W}\ e^{\underline{A}'\tau}\ d\tau + \int_0^\infty e^{\overline{\underline{A}}\tau}\ e^{\underline{A}T}\ \underline{W}\ e^{\underline{A}'T}\ e^{\overline{\underline{A}}'\tau}\ d\tau \quad . \tag{A.37}$$

F. CALCULATION OF OPTIMAL COST

To compute $J(\underline{u}^*)$ we write

$$J(\underline{u}^*) = \text{tr}\{\underline{Q} \cdot \text{cov}[\underline{x}(t)] + \underline{K}\ \underline{B}\ \underline{R}^{-1}\underline{B}'\underline{K} \cdot \text{cov}[\underline{\hat{x}}(t)]\}$$

$$= \text{tr}\{\underline{Q}+\underline{K}\ \underline{B}\ \underline{R}^{-1}\underline{B}'\underline{K}) \cdot \text{cov}[\underline{\hat{x}}(t)] + \underline{Q} \cdot \text{cov}[\underline{e}(t)]\} \quad . \tag{A.38a}$$

It is possible to write Eq. (A.38a) in a more convenient form by first noting (Eq. A.7) that

$$\underline{Q} + \underline{K}\,\underline{B}\,\underline{R}^{-1}\underline{B}'\underline{K} = -\bar{\underline{A}}'\underline{K} - \underline{K}\,\bar{\underline{A}}$$

and, from Eq. (A.36), that

$$\bar{\underline{A}} \cdot \mathrm{cov}[\underline{\hat{x}}(t)] + \mathrm{cov}[\underline{\hat{x}}(t)] \cdot \bar{\underline{A}}' = \int_0^\infty \frac{d}{d\tau}[e^{\bar{\underline{A}}\tau}\, e^{\underline{A}T}\, \underline{W}\, e^{\underline{A}'T}\, e^{\bar{\underline{A}}'\tau}]d\tau$$

$$= -\, e^{\underline{A}T}\, \underline{W}\, e^{\underline{A}'T} \quad .$$

The last equality following since $e^{\bar{\underline{A}}\tau} \to \underline{0}$ as $\tau \to \infty$. Upon subsituting into Eq. (A.38a) and using the cyclic property of the trace functional we obtain

$$J(\underline{u}^*) = \mathrm{tr}\{\underline{K}\, e^{\underline{A}T}\, \underline{W}\, e^{\underline{A}'T} + \underline{Q} \cdot \mathrm{cov}[\underline{e}(t)]\} \quad . \qquad \text{(A.38b)}$$

The first term in the above expression is the result of the noise disturbance $\underline{w}(t)$. The second term results from the prediction error $\underline{\hat{x}}(t)-\underline{x}(t)$ and increases with increasing time lag.

G. CROSS-CORRELATED GAINS

In the foregoing section we have seen that the optimal controller becomes a linear, time-invariant, dynamical system when a time delay is introduced into the optimal regulator problem. In order to compare this result with the assumed model of the human operator we require an equivalent gain, in some sense, of $\underline{G}^*(s)$. One of the most natural which comes to mind is the cross-correlated gain

$$\underline{L}_1 = E[\underline{u}(t)\underline{y}'(t)] \cdot \{\mathrm{cov}[\underline{y}(t)]\}^{-1} \quad . \qquad \text{(A.39)}$$

The matrix $E[\underline{u}(t)\ \underline{y}'(t)]$ is given by

$$E[\underline{u}(t)\ \underline{y}'(t)] = \int_0^\infty \underline{\Phi}_u(\tau)\ \underline{W}\ \underline{\Phi}_y'(\tau)\ d\tau \quad ,$$

$\underline{\Phi}_u(\tau)$ and $\underline{\Phi}_y(\tau)$ are given by Eqs. (A.26) and (A.24) respectively. Substituting these expressions in the above yields

$$E[\underline{u}(t)\underline{y}'(t)] = -\underline{L}^*\left[\int_T^{2T} e^{\underline{\bar{A}}(\tau-T)}\ e^{\underline{A}T}\ \underline{W}\ e^{\underline{A}'(\tau-T)}\ d\tau + \int_{2T}^\infty e^{\underline{\bar{A}}(\tau-T)}\ e^{\underline{A}T}\ \underline{W}\ \cdot\right.$$

$$\left. e^{\underline{A}'T}\ e^{\underline{\bar{A}}'(\tau-2T)}\ d\tau\right]$$

$$= -\underline{L}^*\left[\int_0^T e^{\underline{\bar{A}}\sigma}\ e^{\underline{A}T}\ \underline{W}\ e^{\underline{A}'\sigma}\ d\sigma + e^{\underline{\bar{A}}T}\int_{2T}^\infty e^{\underline{\bar{A}}(\tau-2T)}\ e^{\underline{A}T}\ \underline{W}\ \cdot\right.$$

$$\left. e^{\underline{A}'T}\ e^{\underline{\bar{A}}'(\tau-2T)}\ d\tau\right]$$

$$= -\underline{L}^*\left\{\int_0^T e^{\underline{\bar{A}}\sigma}\ e^{\underline{A}T}\ \underline{W}\ e^{\underline{A}'\sigma}\ d\sigma + e^{\underline{\bar{A}}T}\ \cdot\ \mathrm{cov}[\underline{\hat{x}}(t)]\right\} \quad . \qquad (A.40)$$

Thus one may compute $\underline{L}_1$ from Eqs. (A.40) and (A.36).

H. SIMPLE ESTIMATION-CONTROLLER

In the preceding sections we showed that the optimal feedback controller $\underline{G}^*(s)$ first estimated the current system state $\underline{x}(t)$.

This estimate was $\underline{\hat{x}}(t)$. The control $\underline{u}= -\underline{L}^*\underline{\hat{x}}(t)$ was then applied. The optimal estimate $\underline{\hat{x}}$ is obtained by operating on the entire past history of $\underline{y}(t)$, that is to say

$$\underline{\hat{x}}(t) = E[\underline{x}(t) \mid \underline{y}(\tau),\ \tau \leq t] \quad . \tag{A.41}$$

Suppose, however, that it is not in fact possible to form an estimate of $\underline{x}(t)$ from $\underline{y}(\tau)$, $\tau \leq t$ but only from the current value $\underline{y}(t)$. This would correspond to an amnesic estimator. Hence, $\underline{\hat{x}}(t)$ would be constrained as

$$\underline{\hat{x}}(t) = E[\underline{x}(t) \mid \underline{y}(t)] \quad , \tag{A.42}$$

and the control input $\underline{u}(t)$ would be $\underline{u}(t)= -\underline{L}^*\underline{\hat{x}}(t)$. In this latter case, $\underline{\hat{x}}(t)$ could be obtained from $\underline{y}(t)=\underline{x}(t-T)$ by a simple prediction through the system dynamics by assuming $\underline{\hat{x}}(t)\approx\underline{x}(t)$. The result of this is (for $t>T$)

$$\underline{\hat{x}}(t) = e^{\overline{\underline{A}}T}\,\underline{y}(t) = e^{(\underline{A}-\underline{B}\ \underline{L}^*)T}\,\underline{y}(t) \tag{A.43}$$

where $e^{\overline{\underline{A}}T} = \underline{\Phi}(t+T,t)$ is the closed-loop state transition matrix. Consequently, the "simple" control input is

$$\underline{u}(t) = -\underline{L}^* e^{(\underline{A}-\underline{B}\ \underline{L}^*)T}\,\underline{y}(t) \quad . \tag{A.44}$$

Relative to the above we note in passing that (a) It can be shown that the estimate $\underline{\hat{x}}(t)$ given by Eq. (A.43) is the only unbiased estimate of $\underline{x}(t)$ for the case when the predictor is constrained to operate solely on the present value of system output $\underline{y}(t)$, (b) The resulting closed-loop system will be stable for

sufficiently small T. Stability questions may be answered analytically by using the results in Ref. 32, (c) The estimate $\underline{\hat{x}}(t)$ is the minimal variance estimate of $\underline{x}(t)$ conditioned on $\{\underline{x}(\tau), \tau \leq t-T\}$ when $\underline{x}(t)$ is generated by

$$\dot{\underline{x}}(t) = (\underline{A}-\underline{B}\ \underline{L}^*)\ \underline{x}(t) + \underline{w}(t) \quad ,$$

i.e., if $\underline{u}(t) = -\underline{L}^*\underline{x}(t)$. This is a standard result for linear prediction problems.[5]

APPENDIX B

SENSITIVITY OF OPTIMAL REGULATOR SOLUTIONS TO CHANGES IN FEEDBACK GAINS

In this appendix we investigate, for an optimal linear regulator system, the cost increase which results from using feedback gains other than the optimal ones. In this manner we investigate the sensitivity of the optimal system with respect to gain changes. We first consider the noise-free problem and then the regulator problem with input driving noise. It is shown that both problems are essentially equivalent as regards their sensitivities. The material presented below is based, in large measure, on the results of Ref. 17, Appendix C.

A. DETERMINISTIC CASE

We first deal with the linear, time-invariant system

$$\dot{\underline{x}}(t) = \underline{A}\,\underline{x}(t) + \underline{B}\,\underline{u}(t) \quad ; \quad \underline{x}(o) = \underline{x}_o \tag{B.1}$$

and the quadratic cost functional

$$J[\underline{x}_o;\underline{u}(\cdot)] = \int_0^\infty [\underline{x}'(t)\,\underline{Q}\,\underline{x}(t) + \underline{u}'(t)\,\underline{R}\,\underline{u}(t)]dt \quad . \tag{B.2}$$

The control $\underline{u}^*(\cdot)$ which minimizes Eq. (B.2) is given by the linear feedback law

$$\underline{u}^*(t) = -\underline{L}^*\underline{x}(t) = -\underline{R}^{-1}\underline{B}'\underline{K}\,\underline{x}(t) \tag{B.3}$$

where $\underline{K}$ is the solution of the algebraic equation

$$\underline{0} = \underline{K}\,\underline{A} + \underline{A}'\underline{K} + \underline{Q} - \underline{K}\,\underline{B}\,\underline{R}^{-1}\underline{B}'\underline{K} \quad . \tag{B.4}$$

The minimum cost is

$$J[\underline{x}_o;\ \underline{u}^*(\cdot)] = J^*(\underline{x}_o) = \underline{x}_o'\ \underline{K}\ \underline{x}_o \quad . \tag{B.5}$$

Let us now suppose that instead of applying the feedback law $\underline{u}^*=-\underline{L}^*\underline{x}$, we apply the control input $\underline{u}_G=-\underline{G}\ \underline{x}$ to the system Eq. (B.1). Clearly $\underline{u}_G(\cdot)$ is non-optimal for $\underline{G}\neq\underline{L}^*$ and so

$$\Delta J(\underline{x}_o) = J[\underline{x}_o;\ \underline{u}_G(\cdot)] - J[\underline{x}_o;\ \underline{u}^*(\cdot)] > 0 \quad . \tag{B.6}$$

We wish to derive an expression for the cost difference Eq. (B.6). To do this we first note that $J[\underline{x}_o;\ \underline{u}_G(\cdot)]$ can be written as

$$J[\underline{x}_o;\ \underline{u}_G(\cdot)] = \underline{x}_o'\ \underline{V}_G\ \underline{x}_o \tag{B.7}$$

where

$$\underline{V}_G = \int_0^\infty e^{(\underline{A}-\underline{B}\ \underline{G})'t}\ [\underline{Q}+\underline{G}'\underline{R}\ \underline{G}]\ e^{(\underline{A}-\underline{B}\ \underline{G})t}\ dt \quad . \tag{B.8}$$

We call the matrix $\underline{V}_G$ the *cost matrix* associated with the gain matrix $\underline{G}$. Note that if $\underline{G}$ is such that $(\underline{A}-\underline{B}\ \underline{G})$ has eigenvalues with negative real parts then $\underline{V}_G$ is the (unique) solution of

$$\underline{0} = (\underline{A}-\underline{B}\ \underline{G})'\underline{V}_G + \underline{V}_G(\underline{A}-\underline{B}\ \underline{G}) + \underline{Q} + \underline{G}'\underline{R}\ \underline{G} \quad . \tag{B.9}$$

With the above definition, note that $\underline{K}$ is the cost matrix associated with the gain matrix $\underline{L}^*= -\underline{R}^{-1}\underline{B}'\underline{K}$.

Consequently we see that the cost difference, Eq. (B.6) is

$$\Delta J(\underline{x}_o) = \underline{x}_o'[\underline{V}_G - \underline{K}]\ \underline{x}_o \qquad (B.10)$$

so that studying the cost difference between $\underline{u} = -\underline{G}\ \underline{x}$ and $\underline{u} = -\underline{L}^*\underline{x}$ is tantamount to studying the difference in their respective cost matrices.

We now obtain an equation for $\underline{V}_G - \underline{K} \triangleq \underline{S}_G$. We rewrite Eq. (B.4) as

$$\underline{0} = \underline{K}(\underline{A} - \underline{B}\ \underline{G}) + (\underline{A} - \underline{B}\ \underline{G})'\underline{K} + \underline{Q} - \underline{L}^{*\prime}\underline{R}\ \underline{L}^* + \underline{K}\ \underline{B}\ \underline{G} + \underline{G}'\underline{B}'\underline{K} \quad .$$

But $\underline{B}'\underline{K} = \underline{R}\ \underline{L}^*$ so that

$$\underline{0} = \underline{K}(\underline{A} - \underline{B}\ \underline{G}) + (\underline{A} - \underline{B}\ \underline{G})'\underline{K} + \underline{Q} - \underline{L}^{*\prime}\underline{R}\ \underline{L}^* + \underline{L}^{*\prime}\underline{R}\ \underline{G} + \underline{G}'\underline{R}\ \underline{L}^* \quad . \qquad (B.11)$$

We subtract Eq. (B.11) from Eq. (B.9) to obtain

$$\underline{0} = \underline{S}_G(\underline{A} - \underline{B}\ \underline{G}) + (\underline{A} - \underline{B}\ \underline{G})'\underline{S}_G + (\underline{G} - \underline{L}^*)'\underline{R}(\underline{G} - \underline{L}^*) \quad . \qquad (B.12)$$

Since the eigenvalues of $(\underline{A} - \underline{B}\ \underline{G})$ have negative real parts, $\underline{S}_G$ is given explicitly by

$$\underline{S}_G = \int_0^\infty e^{(\underline{A} - \underline{B}\ \underline{G})'t} [\underline{G} - \underline{L}^*]'\underline{R}[\underline{G} - \underline{L}^*]\, e^{(\underline{A} - \underline{B}\ \underline{G})t}\, dt \quad . \qquad (B.13)$$

We shall henceforth call the matrix $\underline{S}_G$ the *sensitivity matrix* (associated with the gains $\underline{G}$) since

$$\Delta J(\underline{x}_o) = \underline{x}_o'\ \underline{S}_G\ \underline{x}_o \quad . \qquad (B.14)$$

Note that $\underline{S}_G$ is a positive definite matrix for all $\underline{G} \neq \underline{L}^*$. This expresses the condition that $\underline{L}^*$ is the optimal gain matrix for our regulator problem. Furthermore, the cost increase [Eq. (B.14)] is finite if and only if the eigenvalues of $(\underline{A}-\underline{B}\ \underline{G})$ have negative real parts.

In summary then, we have shown that the cost increase resulting from the control $\underline{u} = -\underline{G}\ \underline{x}$ is given by Eq. (B.14) where $\underline{S}_G$ is given by Eq. (B.13).

B. INPUT NOISE DISTURBANCE CASE

We now consider the noise input case for which the linear system is characterized by

$$\dot{\underline{x}}(t) = \underline{A}\ \underline{x}(t) + \underline{B}\ \underline{u}(t) + \underline{w}(t) \qquad \underline{x}(o) = \underline{0} \tag{B.15}$$

where $\underline{w}(t)$ is a zero-mean, white gaussian noise process with covariance matrix $\underline{W}$,

$$\text{cov}[\underline{w}(t)] = E[\underline{w}(t)\ \underline{w}'(\tau)] = \underline{W}\ \delta(t-\tau) \quad . \tag{B.16}$$

The cost functional for this case is the mean squared criteria

$$J[\underline{u}(\cdot)] = E_{\underline{w}(\cdot)}\left\{ \lim_{t_1 \to \infty} \frac{1}{t_1} \int_0^{t_1} [\underline{x}'(t)\ \underline{Q}\ \underline{x}(t) + \underline{u}'(t)\ \underline{R}\ \underline{u}(t)]dt \right\} . \tag{B.17}$$

It has been shown [see Ref. 19] that the control $\underline{u}^*(\cdot)$ which minimizes Eq. (B.17) is

$$\underline{u}^*(t) = -\underline{L}^*\ \underline{x}(t) = -\underline{R}^{-1}\underline{B}'\underline{K}\ \underline{x}(t) \tag{B.18}$$

which is the same control law which was optimal for the deterministic problem. The optimal cost associated with $\underline{L}^*$ is

$$J[\underline{u}^*(\cdot)] = J^* = \text{tr}[\underline{K}\ \underline{W}] \quad . \tag{B.19}$$

We again let $\underline{u}_G = -\underline{G}\ \underline{x}$ be a control law differing from $\underline{u}^*$. We wish to calculate the cost increase

$$\Delta J(\underline{G}) = J[\underline{u}_G(\cdot)] - J[\underline{u}^*(\cdot)] \quad . \tag{B.20}$$

To avoid mathematical subtleties we shall assume that $\underline{G}$ is such that $\lambda_i(\underline{A}-\underline{B}\ \underline{G})<0$. The cost associated with $\underline{u}_G$ is obtained by substituting in Eq. (B.17) with the result

$$J[\underline{u}_G(\cdot)] = \mathrm{tr}\left\{(\underline{Q}+\underline{G}'\underline{R}\ \underline{G}) \cdot \lim_{t_1\to\infty} \frac{1}{t_1}\int_0^{t_1} \mathrm{cov}[\underline{x}(t)]dt\right\} \quad . \tag{B.21}$$

But, the covariance matrix of $\underline{x}(t)$, $E[\underline{x}(t)\underline{x}'(t)]$, is given by

$$\mathrm{cov}[\underline{x}(t)] = \int_0^t e^{(\underline{A}-\underline{B}\ \underline{G})\tau}\ \underline{W}\ e^{(\underline{A}-\underline{B}\ \underline{G})'\tau} d\tau = \underline{\Sigma}(t) \quad . \tag{B.22}$$

$\underline{\Sigma}(t)$ has a limit $\overline{\underline{\Sigma}}$ as $t\to\infty$ since $(\underline{A}-\underline{B}\ \underline{G})$ is stable. $\overline{\underline{\Sigma}}$ is given by

$$\overline{\underline{\Sigma}} = \int_0^\infty e^{(\underline{A}-\underline{B}\ \underline{G})\tau}\ \underline{W}\ e^{(\underline{A}-\underline{B}\ \underline{G})'\tau} d\tau \tag{B.23}$$

and satisfies

$$(\underline{A}-\underline{B}\ \underline{G})\ \underline{\Sigma} + \underline{\Sigma}(\underline{A}-\underline{B}\ \underline{G})' = -\underline{W} \quad . \tag{B.24}$$

Thus,

$$J[\underline{u}_G(\cdot)] = \mathrm{tr}[(\underline{Q}+\underline{G}'\underline{R}\ \underline{G})\ \overline{\underline{\Sigma}}] \quad . \tag{B.25}$$

We may write Eq. (B.25) in another form by noting from Eq. (B.9) that the cost matrix $\underline{V}_G$ satisfies

$$\underline{Q} + \underline{G}'\underline{R}\ \underline{G} = -(\underline{A}-\underline{B}\ \underline{G})'\underline{V}_G - \underline{V}_G(\underline{A}-\underline{B}\ \underline{G}) \quad . \tag{B.26}$$

Hence,

$$J[\underline{u}_G(\cdot)] = \mathrm{tr}\{-(\underline{A}-\underline{B}\ \underline{G})'\underline{V}_G\ \underline{\Sigma} - \underline{V}_G\ (\underline{A}-\underline{B}\ \underline{G})\ \underline{\Sigma}\}$$

$$= \mathrm{tr}\{\underline{V}_G \cdot [-\underline{\Sigma}(\underline{A}-\underline{B}\ \underline{G})' - (\underline{A}-\underline{B}\ \underline{G})\ \underline{\Sigma}]\}$$

$$= \mathrm{tr}[\underline{V}_G\ \underline{W}] \quad . \tag{B.27}$$

Therefore,

$$\Delta J(\underline{G}) = \mathrm{tr}(\underline{V}_G\underline{W}) - \mathrm{tr}(\underline{K}\ \underline{W}) = \mathrm{tr}[(\underline{V}_G-\underline{K}) \cdot \underline{W}] \quad . \tag{B.28}$$

But $(\underline{V}_G-\underline{K})=\underline{S}_G$ as defined in Eq. (B.13) so that we obtain the result

$$\Delta J(\underline{G}) = \mathrm{tr}[\underline{S}_G\ \underline{W}] \quad . \tag{B.29}$$

C. COMPARISON OF BOTH CASES

If we compare Eqs. (B.29) and (B.14) for the noise input case and deterministic case respectively, we notice a certain similarity. This is evident by writing Eq. (B.14) as

$$\Delta J(\underline{x}_o) = \underline{x}_o'\ \underline{S}_G\ \underline{x}_o = \mathrm{tr}[\underline{S}_G\ \underline{x}_o\ \underline{x}_o'] \quad . \tag{B.30}$$

Consequently if $\underline{x}_o$ is a random vector, uniformly distributed over the surface of the ellipsoid

$$\underline{x}'\ \underline{W}\ \underline{x} = 1$$

we would have that

$$E_{x_o}\{\Delta J(\underline{x}_o)\} = tr[S_G\ \underline{W}] \qquad (B.31)$$

which is just the cost increase for the noise input regulator.

Thus, the initial state $\underline{x}_o$ and the input noise $\underline{w}(t)$ play equivalent roles in the two related cases. Note that it is always possible to find a set of initial condition vectors which will have the same effect on system performance and sensitivity as would the input noise $\underline{W}$. To see this we note that if $\underline{W}$ is of rank $p \leq n$, there exists a set of p vectors $\underline{\xi}_1, \underline{\xi}_2, \ldots \underline{\xi}_p$ such that

$$\underline{W} = \underline{\xi}_1\underline{\xi}_1' + \underline{\xi}_2\underline{\xi}_2' + \cdots + \underline{\xi}_p\underline{\xi}_p' \quad .$$

Then, by linearity of the trace functional we have

$$tr[\underline{S}_G\ \underline{W}] = \sum_{i=1}^{p} tr[\underline{S}_G\ \underline{\xi}_i\underline{\xi}_i'] = \sum_{i=1}^{p} \Delta J(\underline{\xi}_i) = \Delta J(\underline{G}) \quad . \qquad (B.32)$$

Thus it is possible to simulate the effect of white noise by suitable initial conditions. This artifice is often used for analog computation.

APPENDIX C

AN ITERATIVE TECHNIQUE FOR RICCATI EQUATION COMPUTATIONS

In this appendix an iterative technique for solving the matrix Riccati equation

$$\underline{O} = \underline{K}\,\underline{A} + \underline{A}'\underline{K} + \underline{Q} - \underline{K}\,\underline{B}\,\underline{R}^{-1}\underline{B}'\underline{K} \qquad (C.1)$$

is presented. The scheme is based on the method of successive approximations and is discussed in greater detail in Refs. 17 and 25 by using the concept of a "cost matrix". Below, the main result of the analysis is presented and discussed. We then present the actual computer program which was used to implement the iterative scheme.

A. METHOD OF SUCCESSIVE SUBSTITUTIONS

The main theoretical result which we need is:

Theorem: Let $\underline{V}_K$, K=0,1, ... , be the (unique) positive definite solution of the linear algebraic equation

$$\underline{O} = \underline{A}_K'\,\underline{V}_K + \underline{V}_K\,\underline{A}_K + \underline{Q} + \underline{L}_K'\,\underline{R}\,\underline{L}_K \qquad (C.2)$$

where, recursively

$$\underline{L}_K = \underline{R}^{-1}\underline{B}'\underline{V}_{K-1} \qquad K=1,2, \ldots$$

$$\underline{A}_K = \underline{A} - \underline{B}\,\underline{L}_K$$

and where $\underline{L}_o$ is chosen such that the matrix $\underline{A}_o = \underline{A} - \underline{B}\,\underline{L}_o$ has eigenvalues with negative real parts. Then,

(a) $\underline{K} \leq \underline{V}_{K+1} \leq \underline{V}_K \leq \ldots$ for K=0,1, ...

(b) $\lim_{K\to\infty} \underline{V}_K = \underline{K}$.

(The notation $\underline{X} \geq \underline{Y}$ means that the matrix $\underline{X}-\underline{Y}$ is positive definite.) The proof of this result may be found in Ref. 17.

B. REMARKS

1. Since the pair $(\underline{A},\underline{B})$ is assumed to be completely controllable it is always possible to pick an $\underline{L}_o$ such that $\mathrm{Re}\{\lambda_i(\underline{A}_o)\}<0$. (See Ref. 26). This is necessary to insure that $\underline{V}_o$ will be positive definite. Otherwise the iterations may converge to an indefinite solution of Eq. (C.1), if they converge at all.

2. It can be shown that the iterative scheme embodied in the theorem is precisely that which is obtained by applying Newton's method (in function spaces) to solve Eq. (C.1). [See Appendix E of Ref.17]. However, Newton's method alone will not provide conditions which will insure monotone convergence.

3. In addition to their being monotonically convergent, the iterates $\underline{V}_K$ are also quadratically convergent. This is a basic property of Newton's method. Thus

$$\| \underline{V}_{K+1} - \underline{K} \|^2 \leq c_2 \| \underline{V}_K - \underline{K} \|^2 \quad . \tag{C.3}$$

Therefore, convergence of $\underline{V}_K$ to $\underline{K}$ is extremely rapid in the vicinity of $\underline{K}$. This is not the case in most other iterative schemes for solving Eq. (C.1) (ASP method, Runge-Kutta, etc.) which display only linear convergence to $\underline{K}$.

C. THE RICCATI EQUATION PROGRAM

The theorem provides a useful iterative scheme for the numerical solution of Eq. (C.1) and hence the solution of the associated optimal linear regulator problem. A computer program for finding $\underline{K}$ in this manner has been written for the SDS 940 computer using Fortran II. The symbolics are included. The elements of the program are

1. Main Program: Requires the input data $\underline{A}$, $\underline{B}$, $\underline{Q}$ and $\underline{R}$. The main program then calls the subroutine RICSOL.
2. RICSOL: Solves Eq. (C.1) by the above algorithm. A suitable matrix $\underline{L}_o$ is found by using the results of Ref. 26. For each iteration, $\underline{V}_K$ is obtained by solving an $n(n+1)/2$ dimensional linear vector equation. This task is accomplished by the subroutine LINSOL. The subroutine MAT5 is simply for matrix multiplication.
3. Returned Quantities: RICSOL returns the matrix $\underline{K}$, the optimal feedback gains $\underline{L}^*=\underline{R}^{-1}\underline{B}'\underline{K}$ and the closed-loop system matrix $\underline{A}-\underline{B}\ \underline{R}^{-1}\underline{B}'\underline{K}$. These are outputed by the main program.

The computer program can handle up to 10 state variables (i.e. $\underline{K}=10 \times 10$) with the existing SDS 940 storage facilities. Experience has shown that the convergence to $\underline{K}$ is rapid with approximately 10 iterations of Eq. (C.2) needed in most cases.

```
C       RICCATI EQUAT  N PROGRAM--7/25/67

        DIMENSION A(6,6),B(6,6),Q(6),R(6),X(6,6),Y(6,6),Z(6,6)
        LA=1HA
        LB=1HB
        LQ=1HQ
        LR=1HR
        TYPE 1
1       FORMAT(/$NO. OF STATE VBLES.=$)
        ACCEPT 2,N
2       FORMAT(I2)
        TYPE 3
3       FORMAT(/$NO. OF CONTROL VBLES.=$)
        ACCEPT 2,M
        DO 5 I=1,N
        DO 5 J=1,N
        TYPE 6,LA,I,J
6       FORMAT(/A1,$(,I2,$,$,I2,$)=$)
        ACCEPT 7,A(I,J)
7       FORMAT(F15.5)
5       CONTINUE
        DO 8, I=1,N
        TYPE 6,LQ,I,I
        ACCEPT 7 ,Q(I)
8       CONTINUE
        DO 10 I=1,M
        TYPE 6,LR,I,I
        ACCEPT 7,R(I)
10      CONTINUE
        DO 9 I=1,N
        DO 9 J=1,M
        TYPE 6,LB,I,J
        ACCEPT 7 , B(I,J)
9       B(I,J)=B(I,J)/SQRT(R(J))
        OPEN(2,OUTPUT,/DATA/)
        WRITE 2,2,N,M
        WRITE 2,67,A,B,Q,R
        CLOSE(2)
        GO TO 75
69      OPEN(2,INPUT,/DATA/)
        READ 2,2,N,M
        READ 2,67,A,B,Q,R
        CLOSE(2)
67      FORMAT(6(E15.7))
75      CALL RICSOL(N,M,A,B,Q,X,Y,Z)
        TYPE 82
82      FORMAT(//$THE SOLUTION OF KA+A'K+Q-KB(RINV)B'K=0 IS:$/)
        DO 83 I=1,N
83      TYPE 84,(X(I,J),J=1,N)
84      FORMAT(/,6(E11.5,1X))
        DO 86 I=1,M
        DO 86 J=1,N
86      X(I,J)=Y(J,I)/SQRT(R(I))
C               X=(R)-1 B'P
        TYPE 87
87      FORMAT(//$THE OPTIMAL FEEDBACK GAINS L=(RINV)B'K ARE:$/)
        DO 88 I=1,M
88      TYPE 84,(X(I,J),J=1,N)
        TYPE 89
89      FORMAT(//$THE OPTIMAL CLOSED LOOP MATRIX A-BL IS:$/)
        DO 90 I=1,N
90      TYPE 84,(Z(I,J),J=1,N)
100     CONTINUE
        END
```

```
      SUBROUTINE RICSOL(N,M,A,B,Q,X,Y,Z)
      DIMENSION A(6,6),B(6,6),Q(6),V(21,21),W(6,6),X(6,6),Z(6,6)
     1 Y(6,6),MM(6),MS(6)
      S1=0
      S2=0
      DO 80 I=1,N
      DO 81 J=1,M
81    S2=S2+B(I,J)**2
80    S1=S1+DIM(Q(I),S1)
      C1=-SQRT(S1*S2/(N*M))
      MR=0
      DO 31 I=1,M
31    MM(I)=0
      DO 34 L=1,M
      DO 30 I=1,N
30    Y(I,L)=B(I,L)

      DO 38 JJ=1,N
      IMR=MR+1
      DO 35 I=1,N
      X(I,L)=Y(I,L)
35    W(I,IMR)=Y(I,L)
      DO 33 I=1,IMR
      DO 33 J=1,IMR
      Y(I,J)=0
      DO 33 K=1,N
33    Y(I,J)=Y(I,J)+W(K,I)*W(K,J)

      CALL MATINV(IMR,Y,Z,D,MRANK,MTYPE)
      IF(ABS(D)-10E-4) 34,34,37
37    IF(MRANK-IMR) 34,39,39
39    MR=MR+1
      MM(L)=MM(L)+1
      IF(MR-N) 36,11,11
36    DO 38 I=1,N
      Y(I,L)=0
      DO 38 K=1,N
38    Y(I,L)=Y(I,L)+A(I,K)*X(K,L)
34    CONTINUE

      TYPE 32
32    FORMAT(/$ THE PAIR [A,B] IS UNCONTROLLABLE$)
      GO TO 54
11    MR=0
      IMR=0
      JJ=0
      CALL MATINV(N,W,Z,D,MRANK,MTYPE)

      DO 13 K=1,M
      JJ=JJ+MM(K)
      IMR=IMR+IDIM(MM(K),IMR)
      IF(MM(K)) 13,13,14
14    MR=MR+1
      MS(MR)=MM(K)
      DO 15 I=1,N
      W(MR,I)=Z(JJ,I)
      Y(MR,I)=W(MR,I)
15    X(I,MR)=B(I,K)
      IF(MM(K)-1) 13,13,16
16    DO 13 L=1,MM(K)-1
      DO 17 I=1,N
      Z(JJ,I)=0
```

```
      DO 18 I=1,N
18    Y(MR,I)=Z(J,  )
13    CONTINUE
      S=1.0
      CALL MAT5(Y,X,MR,N,MR,Z)
      CALL MATINV(MR,Z,Y,D,MRANK,MTYPE)
      DO 27 I=1,N
      DO 21 J=1,N
      Z(I,J)=0
21    V(I,J)=0
27    V(N+1,I)=0
      DO 23 J=1,MR
      ID=MS(J)
      JJ=1
      DO 22 I=1,MS(J)
      V(I,J)=-JJ*(-C1)**ID
      JJ=ID*JJ/I
22    ID=ID-1
23    V(MS(J)+1,J)=-1.0
      DO 24 L=0,IMR
      DO 25 I=1,MR
      DO 25 J=1,N
      X(I,J)=W(I,J)
25    Z(I,J)=Z(I,J)+V(L+1,I)*W(I,J)
      CALL MAT5(X,A,MR,N,N,W)
24    CONTINUE

      CALL MAT5(Y,Z,MR,MR,N,W)
      JJ=0
      DO 41 I=1,M
      IF(MM(I)) 44,44,42
42    JJ=JJ+1
      DO 43 J=1,N
43    Y(J,I)=-W(JJ,J)
      GO TO 41
44    DO 45 J=1,N
45    Y(J,I)=0
41    CONTINUE
      S=1.0
50    DO 57 I=1,N
      DO 51 J=1,N
      X(I,J)=Z(I,J)
      Z(I,J)=A(I,J)
      W(I,J)=0
      DO 51 K=1,M
      Z(I,J)=Z(I,J)-B(I,K)*Y(J,K)
51    W(I,J)=W(I,J)+Y(I,K)*Y(J,K)
57    W(I,I)=W(I,I)+Q(I)
      IF(S-10E-5)54,54,55
55    CALL LINSOL(Z,W,N,Z,V)

      CALL MAT5(Z,B,N,N,M,Y)

      S2=0.0
      DO 53 I=1,N
53    S2=S2+Z(I,I)
      S=ABS(S1-S2)
      S1=S2
      GO TO 50
54    CONTINUE
      RETURN
      END
*
```

APPENDIX D

CALIBRATION OF THE ANALYSIS PROCEDURE

A series of calibrations was performed in order to determine the ability of the analysis techniques to (a) identify the controller's effective time delay, (b) identify the full set of five controller gains, and (c) identify two sets of gains when switching of foveal attention was simulated. In addition, the effect of simulated human controller remnant on the measured gains was investigated.

The time delay "identified" by the analysis procedure was defined as the time delay for which the residual was a minimum. The calibration was performed using an analog simulation of the man-vehicle system. The pilot was simulated by a time delay of 0.2 seconds cascaded with the corresponding set of five optimal gains. The time delay was realized by a first-order Pade approximation. Switching of attention was not simulated. The lowest residual was yielded when the time delay used for the computation of the gains was 0.176 seconds.† Table D-1a shows that the computed gains were within 6% of the true values.

The calibration procedure was repeated with the addition of noise added to the simulated stick output in order to simulate controller remnant. The additive noise, which was uncorrelated with the system forcing function, was approximately white noise filtered by a third-order Butterworth filter having a break frequency of 30 rad/sec. The residual indicated by the analysis

---

†The time delays employed in the regression analysis were constrained by the digital computing system to be integral multiples of 0.044 sec.

procedure was 0.26, which was within the range obtained from the manual control data. The time delay yielding the lowest residual was 0.132 sec. Table D-1b shows that four of the five gains were within 10% of the correct value; the largest error (26%) occurred in the measurement having the smallest numerical value.

The ability of the analysis procedure to identify two sets of gains, when switching of attention was simulated, was investigated using an analog simulation of a problem having two state variables. (Limited computing facilities prohibited this test with the XV-5A simulation.) A "foveal" and "peripheral" feedback gain were programmed for each state variable. The feedback gains were cascaded with a pure time delay of 0.2 sec which was realized by means of a magnetic tape loop. Switching between the two pairs of gains was controlled by a periodic rectangular waveform uncorrelated with the system forcing function. The pair of gains labelled "A" were connected for 1.4 sec per switching cycle; pair "B" were connected for 0.6 sec. Controller remnant was not simulated in this calibration. Table D-1c shows that all gains were measured to within an accuracy of 12%, when a time delay of 0.176 sec was used in the analysis. This time delay yielded the lowest residual.

We conclude from this set of calibrations that our analysis procedure will yield a value for the controller's effective time delay that is correct to within 0.1 sec. Except for some of the lower valued gains, the analysis procedure appears capable of given estimates of the controller gains that are accurate to within 10%, when a moderate amount of controller remnant is present.

TABLE D-1

Calibration of Linear Regression Procedure:
Comparison of Measured and True Values of Gain

a. Five states, no controller remnant simulated

Variable	Gain on:					
	$\dot{u}$	u	x	q	θ	Residual
Correct Value	1.76	1.95	.86	-1.09	-0.23	0.00
Measured Value	1.73	1.83	.86	-1.04	-0.23	0.00
Fractional Difference	0.02	0.06	0.00	0.05	0.00	——

b. Five states, controller remnant simulated

Variable	Gain on:					
	$\dot{u}$	u	x	q	θ	Residual
Correct Value	1.76	1.95	0.86	-1.09	-0.23	——
Measured Value	1.92	1.81	0.83	-1.03	-0.17	0.26
Fractional Difference	0.09	0.07	0.04	0.03	0.26	——

c. Two states, switching of attention

State of Switch	A			B		
Variable	K_1	K_2	Residual	K_1	K_2	Residual
Correct Value	1.60	0.28	0.00	0.57	1.14	0.00
Measured Value	1.55	0.29	0.01	0.64	1.04	0.03
Fractional Difference	0.03	0.04	——	0.12	0.09	——

APPENDIX E

EXPERIMENTAL RESULTS FOR INDIVIDUAL SUBJECTS

TABLE E-1

Effect of Velocity Display on Performance Scores

		α=0.24 rad/sec		α=8.0 rad/sec	
		u	ü	u	ü
Mean-squared position error (x)(ft^2)	JM	15.3	26.1	15.1	20.3
	WW	18.2	31.5	27.2	19.2
	RW	20.5	42.2	27.9	31.6
	Average	18.0	33.3	23.4	23.7
Mean-squared control (δ_θ) ($degrees^2$)	JM	3.04	2.70	2.75	3.88
	WW	1.82	3.83	2.78	2.28
	RW	4.89	3.11	5.25	3.02
	Average	3.25	3.21	3.59	3.06
Total performance measure	JM	18.4	28.8	17.9	24.1
	WW	20.1	35.3	29.9	21.4
	RW	25.4	45.3	33.1	34.6
	Average	21.3	36.5	27.0	26.7

TABLE E-2

Effect of Velocity Display on Mean Observation Time and Allocation of Attention

		α=0.24 rad/sec		α=8.0 rad/sec	
		u	ʉ	u	ʉ
Mean observation time on position display (sec)	JM	1.06	.904	.961	.873
	WW	1.49	1.65	1.56	1.09
	RW	1.75	.964	1.38	.878
	Average	1.43	1.17	1.30	.948
Mean observation time on pitch display (sec)	JM	.591	.581	.612	.515
	WW	.498	.621	.582	.670
	RW	.734	.819	.757	.804
	Average	.608	.673	.650	.663
Mean scan period (sec)	JM	1.65	1.48	1.57	1.39
	WW	1.99	2.27	2.15	1.76
	RW	2.49	1.78	2.13	1.68
	Average	2.04	1.85	1.95	1.61
Fraction of attention devoted to pitch display	JM	.358	.392	.388	.373
	WW	.257	.280	.272	.383
	RW	.307	.461	.376	.479
	Average	.307	.378	.345	.412

TABLE E-3

Effect of Rate Display on Individual Pilot Gains

Experimental Conditions			DISPLAY FIXATED													
			Position						Pitch							
			Gain on:						Gain on:							
α	Rate Display	Sub-ject	$\dot{u}$	u	x	q	θ	Residual	$\dot{u}$	u	x	q	θ	Residual	Aθ	Score
0.24	ON	JM	-.483	-.280	-.070	.620	.055	.278	-.112	-.167	-.096	.489	.256	.204	.338	21.0
		WW	-.620	-.308	-.057	.602	-.010	.235	-.046	-.321	-.197	.622	.479	.154	.151	15.6
		RW	-.567	-.318	-.101	.682	.092	.297	.251	-.117	-.048	.630	.394	.309	.257	22.4
		AVG	-.557	-.302	-.076	.635	.046	.270	.031	-.202	-.113	.580	.376	.222	.249	19.7
	OFF	JM	-.214	-.263	-.121	.481	.228	.215	-.007	-.117	-.090	.426	.223	.134	.436	28.1
		WW	-.289	-.244	-.081	.505	.137	.262	.040	-.251	-.200	.650	.466	.122	.268	36.7
		RW	-.314	-.213	-.092	.475	.181	.369	-.189	-.126	-.051	.568	.285	.223	.431	43.4
		AVG	-.272	-.240	-.098	.487	.182	.282	-.052	-.165	-.114	.548	.324	.160	.378	36.1
8.0	ON	JM	-.106	-.221	-.149	.437	.369	.381	-.018	-.158	-.063	.547	.244	.156	.348	21.9
		WW	-.151	-.204	-.110	.444	.241	.155	-.017	-.038	-.072	.400	.284	.108	.233	29.7
		RW	-.145	-.268	-.084	.532	.199	.427	-.017	-.143	-.033	.672	.169	.196	.442	26.1
		AVG	-.134	-.231	-.114	.471	.270	.321	-.017	-.113	-.056	.540	.232	.153	.341	25.9
	OFF	JM	-.046	-.465	-.172	.649	.355	.247	.001	-.203	-.051	.493	.271	.141	.350	20.0
		WW	-.064	-.317	-.079	.604	.220	.299	.018	-.254	-.118	.678	.312	.103	.317	24.6
		RW	-.002	-.179	-.066	.501	.299	.449	.032	-.025	-.123	.594	.360	.267	.508	19.9
		AVG	-.037	-.320	-.105	.584	.291	.332	.017	-.161	-.097	.570	.314	.170	.392	21.5

T_e = 0.5 sec

TABLE E-4

Effect of Pitch Display Gain on
Performance Score

		Gain=0.2 deg/deg		Gain=0.1 deg/deg	
		u	ü	u	ü
Mean-squared positional error (ft^2)	JM	12.1	13.5	12.3	18.1
	WW	28.9	37.4	24.0	38.8
	RW	17.6	29.6	20.3	35.3
	Average	19.6	26.8	18.8	30.8
Mean-squared control deflection ($degrees^2$)	JM	1.79	3.46	7.61	7.75
	WW	1.49	1.00	1.37	1.12
	RW	4.02	5.55	1.20	11.5
	Average	2.43	3.34	7.00	6.79
Total performance measure	JM	13.9	17.0	19.9	25.9
	WW	30.4	38.4	25.0	39.9
	RW	21.6	35.2	32.3	46.8
	Average	22.0	30.2	25.7	37.5

TABLE E-5

Effect of Pitch Display Gain on Mean Observation Time and Allocation of Attention

		Gain=0.2 deg/deg		Gain=0.1 deg/deg	
		u	~~u~~	u	~~u~~
Mean observation time on position display (sec)	JM	.692	.625	.679	.660
	WW	1.36	1.09	1.18	.971
	RW	1.19	.922	.857	.884
	Average	1.08	.880	.905	.838
Mean observation time on pitch display (sec)	JM	.459	.413	.503	.584
	WW	.522	.678	.610	.763
	RW	.692	.869	.799	.926
	Average	.558	.653	.637	.758
Mean scan period (sec)	JM	1.16	1.04	1.15	1.24
	WW	2.21	1.77	1.79	1.73
	RW	1.88	1.79	1.66	1.74
	Average	1.75	1.53	1.53	1.57
Fraction of attention devoted to pitch display	JM	.396	.398	.425	.469
	WW	.252	.382	.343	.442
	RW	.368	.486	.483	.531
	Average	.339	.422	.417	.491

TABLE E-6

Effect of Pitch Display Gain on Individual Pilot Gain

Experimental Conditions			DISPLAY FIXATED													
			Position						Pitch							
			Gain on:						Gain on:							
Pitch Gain	Rate Display	Subject	$\dot{u}$	u	x	q	θ	Residual	$\dot{u}$	u	x	q	θ	Residual	Aθ	Score
0.2	ON	JM	-.361	-.442	-.128	.684	.145	.253	-.078	-.269	-.149	.554	.320	.178	.377	14.7
		WW	-.323	-.118	-.057	.472	.096	.214	-.086	-.115	-.070	.471	.208	.270	.321	21.9
		RW	-.608	-.260	-.131	.647	.066	.269	-.081	-.234	-.081	.666	.304	.174	.423	21.3
		AVG	-.431	-.273	-.105	.601	.102	.245	-.081	-.206	-.100	.564	.277	.207	.374	19.3
	OFF	JM	-.167	-.450	-.149	.728	.266	.286	.099	-.294	-.214	.593	.439	.224	.373	16.5
		WW	-.161	-.211	-.071	.647	.178	.459	-.0353	-.147	-.035	.657	.166	.163	.368	34.4
		RW	-.348	-.330	-.164	.697	.262	.267	.125	-.158	-.060	.652	.299	.198	.488	34.6
		AVG	-.225	-.330	-.128	.691	.235	.337	.003	-.200	-.103	.634	.301	.195	.410	28.5
0.1	ON	JM	-.249	-.579	-.163	.618	.278	.178	-.051	-.263	-.153	.475	.334	.158	.431	26.1
		WW	-.357	-.143	-.066	.386	.062	.203	-.132	-.119	-.067	.403	.144	.124	.300	23.8
		RW	-.530	-.531	-.123	.625	.132	.229	.063	-.433	-.238	.690	.450	.136	.421	22.0
		AVG	-.379	-.418	-.117	.543	.157	.203	-.040	-.272	-.153	.523	.309	.139	.384	24.0
	OFF	JM	-.176	-.350	-.225	.535	.324	.216	.090	-.360	-.215	.550	.418	.128	.475	29.3
		WW	-.122	.013	-.032	.316	.095	.121	-.213	-.004	-.025	.289	.060	.286	.497	35.3
		RW	-.413	-.387	-.219	.588	.243	.311	.098	-.325	-.170	.661	.467	.173	.534	35.8
		AVG	-.237	-.242	-.159	.480	.221	.216	-.008	-.230	-.137	.500	.315	.196	.502	33.5

APPENDIX F

XV-5A EQUATIONS OF MOTION

The linearized equations of motion of the XV-5A lift fan vehicle near hover are:[18]

$$\begin{bmatrix} \dot{u} \\ \dot{\theta} \\ \dot{q} \\ \dot{w} \end{bmatrix} = \begin{bmatrix} X_u & -g & 0 & 0 \\ 0 & 0 & 1 & 0 \\ M_u & 0 & M_q & M_w \\ 0 & 0 & Z_q & Z_w \end{bmatrix} \begin{bmatrix} u \\ \theta \\ q \\ w \end{bmatrix} + \begin{bmatrix} X_{\beta_v} & 0 & 0 \\ 0 & 0 & 0 \\ M_{\beta_v} & 0 & M_{NF} \\ 0 & Z_{\beta_s} & Z_{NF} \end{bmatrix} \begin{bmatrix} \beta_{cv} \\ \beta_{cs} \\ \theta_{NF} \end{bmatrix} \qquad \text{(Fl long.)}$$

$$\begin{bmatrix} \dot{v} \\ \dot{\phi} \\ \dot{p} \\ \dot{r} \end{bmatrix} = \begin{bmatrix} Y_v & g & 0 & Y_r \\ 0 & 0 & 1 & 0 \\ L_v & 0 & L_p & 0 \\ N_v & 0 & 0 & N_r \end{bmatrix} \begin{bmatrix} v \\ \phi \\ p \\ r \end{bmatrix} + \begin{bmatrix} 0 & 0 \\ 0 & 0 \\ L_{\beta_s} & 0 \\ 0 & N_{\beta_v} \end{bmatrix} \begin{bmatrix} \beta_{ds} \\ \beta_{dv} \end{bmatrix} \qquad \text{(Fl lat.)}$$

where:

u,v,w	components of incremental translational velocity along X, Y, and Z axes of aircraft
p,q,r	components of angular velocity about the X, Y, and Z axes (i.e., roll, pitch, and yaw rates)
θ,ϕ,ψ	the pitch, roll, and yaw angles
g	gravitational acceleration
X_u	drag damping
Z_w	vertical damping
Z_q	lift due to pitch rate
M_u	velocity stability
M_w	angle of attack stability

M_q	pitch damping
$Y_v v$	sideforce due to sideslip
$Y_r r$	sideforce due to yaw rate
L_v	dihedral effect
L_p	damping in roll
N_v	directional stability
N_r	yaw damping

and where the control inputs β_{cv}, β_{cs}, θ_{NF}, β_{dv} and β_{ds} are

β_{cv}	collective vector angle (the direction of the thrust vector from both wing fans)
β_{cs}	collective stagger angle (the exit louver stagger of both wing fans; the stagger determines the thrust)
θ_{NF}	nose fan thrust modulator door angle (the nose fan thrust is controlled by θ_{NF})
β_{dv}	differential vector angle (the direction of the differential thrust vector, the two wing fans directed oppositely to produce a yawing moment)
β_{ds}	differential stagger angle (the stagger angle of the two wing fans changed by equal and opposite amounts to produce a rolling moment).

X_{β_v}, M_{β_v}, Z_{β_s}, M_{NF}, Z_{NF}, L_{β_s} and N_{β_v} are coefficients relating the components of the linear and angular acceleration vector of the vehicle to the control inputs.

We will assume as does Ryan[18] that $\beta_{cv}=0°$ in a nominal hover condition, which will simplify (F1) even further. Moreover, we shall deal only with the longitudinal equations of motion. If we examine these equations (with $\beta_{cv}=0°$), then we note that the nose fan θ_{NF} affects both pitching moment and lift and that the collective stagger angle affects lift. Thus, it is possible (and desirable from a flight control point of view) to obtain independent control of pitch and lift by introducing a coupling between the pilot's control of pitch and both the nose fan and the collective stagger. Denoting the pilot's pitch control by δ_θ and the pilot's lift control by δ_Z, we can accomplish this by letting

$$\theta_{NF} = \delta_\theta \quad , \quad \beta_{cs} = K_1\delta_\theta + \delta_Z$$

where the constant K_1 is chosen in such a fashion that control movements of δ_θ do not affect lift, i.e.

$$Z_{\beta_s} K_1\delta_\theta + Z_{NF}\delta_\theta = 0$$

or,

$$K_1 = -Z_{NF}/Z_{\beta_s} \quad .$$

In terms of δ_θ and δ_Z, the (simplified) longitudinal equations of motion become

$$\begin{bmatrix} \dot{u} \\ \dot{\theta} \\ \dot{q} \\ \dot{w} \end{bmatrix} = \begin{bmatrix} X_u & -g & 0 & 0 \\ 0 & 0 & 1 & 0 \\ M_u & 0 & M_q & M_w \\ 0 & 0 & Z_q & Z_w \end{bmatrix} \begin{bmatrix} u \\ \theta \\ q \\ w \end{bmatrix} + \begin{bmatrix} 0 & 0 \\ 0 & 0 \\ 0 & M_{NF} \\ Z_{\beta_s} & 0 \end{bmatrix} \begin{bmatrix} \delta_Z \\ \delta_\theta \end{bmatrix} \qquad \text{(F2)}$$

Equation (F2) describes the longitudinal motion of the XV-5A in a vehicle referenced coordinate system without the presence of disturbances (e.g., windgusts). To determine the motion relative to the earth, we introduce an earth referenced (inertial) coordinate system X', Y', Z'

$$\dot{X}' = u - v\psi + w\theta$$

$$\dot{Y}' = u\psi + v - w\phi$$

$$\dot{Z}' = u\theta - v\phi + w$$

for small angles θ, ϕ, ψ. Since we consider longitudinal motion (without sideslip), we treat only the equations

$$\dot{X}' = u + w\theta \quad , \quad \dot{Z}' = u\theta + w \quad .$$

Letting X and Z denote the incremental position and altitude errors, respectively, and noting that θ is assumed small, we neglect the product terms and obtain

$$\dot{X} = u \quad , \quad \dot{Z} = w \quad .$$

Therefore, the system of longitudinal equations takes the form

$$\begin{bmatrix} \dot{u} \\ \dot{x} \\ \dot{q} \\ \dot{\theta} \\ \dot{w} \\ \dot{z} \end{bmatrix} = \begin{bmatrix} X_u & 0 & 0 & -g & 0 & 0 \\ 1 & 0 & 0 & 0 & 0 & 0 \\ M_u & 0 & M_q & 0 & M_w & 0 \\ 0 & 0 & 1 & 0 & 0 & 0 \\ 0 & 0 & Z_q & 0 & Z_w & 0 \\ 0 & 0 & 0 & 0 & 1 & 0 \end{bmatrix} \begin{bmatrix} u \\ x \\ q \\ \theta \\ w \\ z \end{bmatrix} + \begin{bmatrix} 0 & 0 \\ 0 & 0 \\ 0 & M_{NF} \\ 0 & 0 \\ Z_{\beta_s} & 0 \\ 0 & 0 \end{bmatrix} \begin{bmatrix} \delta_Z \\ \delta_\theta \end{bmatrix} \qquad \text{(F3)}$$

If we introduce a disturbance added to $\dot{u}$ of the form

$$u_w(s) = w_1(s)/(s+\alpha)$$

so that

$$\dot{u}_w(t) + \alpha u_w(t) = w_1(t)$$

the equations of the disturbed system become

$$\begin{bmatrix} \ddot{u} \\ \dot{u} \\ \dot{x} \\ \dot{q} \\ \dot{\theta} \\ \dot{w} \\ \dot{z} \end{bmatrix} = \begin{bmatrix} X_u-\alpha & \alpha X_u & 0 & -g & -\alpha g & 0 & 0 \\ 1 & 0 & 0 & 0 & 0 & 0 & 0 \\ 0 & 1 & 0 & 0 & 0 & 0 & 0 \\ 0 & M_u & 0 & M_q & 0 & M_w & 0 \\ 0 & 0 & 0 & 1 & 0 & 0 & 0 \\ 0 & 0 & 0 & Z_q & 0 & Z_w & 0 \\ 0 & 0 & 0 & 0 & 0 & 1 & 0 \end{bmatrix} \begin{bmatrix} \dot{u} \\ u \\ x \\ q \\ \theta \\ w \\ z \end{bmatrix} +$$

$$\begin{bmatrix} 0 & 0 \\ 0 & 0 \\ 0 & 0 \\ 0 & M_{NF} \\ 0 & 0 \\ Z_{\beta_s} & 0 \\ 0 & 0 \end{bmatrix} \begin{bmatrix} \delta_Z \\ \delta_\theta \end{bmatrix} + \begin{bmatrix} 1 \\ 0 \\ 0 \\ 0 \\ 0 \\ 0 \\ 0 \end{bmatrix} w_1 \qquad \text{(F4)}$$

3. Stability Derivatives

We need to calculate the relevant stability derivatives appearing in the equations of motion. The Ryan reports[18] give the requisite quantities for the nominal hover conditions:

$\bar{g}$ = g/57.3 =	.561 ft/deg.sec^2	gravitational constant (converted)
m = 28.5	slugs	mass
I_x = 4,252	slug-ft^2	moment of inertia
I_y = 15,139	slug-ft^2	moment of inertia
I_z = 17,418	slug-ft^2	moment of inertia
A_F = 42.6	ft^2	main fan area
q^s = 202	lbs	nominal hover condition of slipstream dynamic pressure
$\bar{y}_f$ = 5.07	ft	wing fan moment arm
$\bar{x}_{NF}$ = 15.6	ft	nose fan moment arm
T_{NF} = 1,500	lbs	nose fan thrust (nominal hover condition)
$\dot{m}_{NF}$ = 4.38	slugs/sec	nose fan mass flow rate

$\dot{m}_{MF}$	= 12.56	slugs/sec	main fan mass flow rate
$\Delta K_{N_{NF}}$	= 1.7	deg^{-1}	function describing variation of nose fan thrust with thrust reverser door position

The force coefficients used are:

$\Delta C_{X_{\beta_s}} \doteq 0$

$\Delta C_{m_{\beta_v}} \doteq .005$

$\Delta C_{X_{\beta_v}} \doteq .02$ (computed from Fig. 3 of Ref. 18)

$\Delta C_{N_{\beta_s}} \doteq -.008$ (computed from Fig. 2 of Ref. 18)

$\Delta C_{N_{\beta_c}} \doteq 0$

$\beta_{cv} = 0°$, $\beta_{cs} = 20°$ (nominal hover conditions)

Using the data in the reports, we thus obtain:

$X_u = -31.8/m = -.11 \text{ sec}^{-1}$

$M_u = 134/I_y = 5.10 \times 10^{-1} \text{ deg/ft.sec}$

$M_q = -4.38\bar{x}^2_{NF}/I_y$ $= -7.04 \times 10^{-2}$ sec^{-1}

$M_w = -4.38\bar{x}_{NF}/I_y$ $= -2.87 \times 10^{-1}$ deg/ft-sec

$Z_q = +4.38\bar{x}_{NF}/m$ $= 4 \times 10^{-3}$ ft/sec-deg

$Z_w = 4.38/m$ $= 1.5 \times 10^{-2}$ sec^{-1}

$Y_v = -31.8/m$ $= 1.1 \times 10^{-1}$ sec^{-1}

$Y_r = -4.38\dot{m}_{NF}\bar{x}_{NM}/m$ $= -4 \times 10^{-3}$ ft/deg-sec

$L_v = -134/I_x$ $= -1.79$ deg/ft-sec

$L_p = -2\dot{m}_{MF}\bar{y}^2_f/I_x$ $= -1.52 \times 10^{-1}$ sec^{-1}

$N_v = 47/I_z$ $= 1.56 \times 10^{-1}$ deg/ft-sec

$N_r = \left(m_{NF}\bar{x}^2_{NF}+2m_{MF}\bar{y}^2_f\right)/I_z$ $= -9.8 \times 10^{-2}$ sec^{-1}

$X_{\beta_v} = q^s A_F \Delta C_{x_{\beta_v}}/2m$ $= 5.25 \times 10^{-3}$ ft/deg-sec^2

$M_{NF} = T_{NF}\bar{x}_{NF}\Delta K_{N_{NF}}/I_y$ $= 2.66$ sec^{-2}

$M_{\beta_v} = q\ A_F D_F \Delta C_{m_{\beta_v}}/2I_y$ $= 7.4 \times 10^{-2}$ sec^{-2}

$Z_{\beta_s} = q\ A_F \Delta C_{N_{\beta_s}}/2m$ $= -2.1 \times 10^{-3}$ ft/deg-sec^2

$$Z_{NF} = T_{NF}\Delta K_{NF}/m \qquad = 4.28 \text{ ft/deg-sec}^2$$

$$L_{\beta_s} = q^s A_F \Delta C_{N_{\beta_s}} \bar{y}_f/2I_x \qquad = -5.15 \times 10^{-2} \text{ sec}^{-2}$$

$$N_{\beta_v} = q^s A_F \Delta C_{X_{\beta_v}} \bar{y}_f/2I_z \qquad = 2.5 \times 10^{-2} \text{ sec}^{-2}$$

REFERENCES

1. D. T. McRuer and E. S. Krendel, "Dynamic Response of Human Operators," WADC TR-56-524, Oct. 1957.

2. J. W. Senders, J. I. Elkind, M. C. Grignetti, and R. P. Smallwood, "An Investigation of the Visual Sampling Behaviour of Human Observers," NASA CR-434 (Apr. 1966).

3. J. I. Elkind, "A Survey of the Development of Models for The Human Controller," in *Progress in Astronautics and Aeronautics*, R. C. Langford and C. J. Mundo, Eds. (Academic Press, New York, N. Y., 1964), Guidance and Control II 13:623-643.

4. D. T. McRuer, D. Graham, E. S. Krendel and W. Reisener, Jr., "Human Pilot Dynamics in Compensatory Systems: Theory, Models and Experiments with Controlled-Element and Forcing Function Variations," AFFDL-TR-65-15, July 1965.

5. R. E. Kalman, T. S. Englar and R. S. Bucy, "Fundamental Study of Adaptive Control Systems," ASD-TR-61-27 (1962).

6. M. Athans and P. L. Falb, *Optimal Control: An Introduction to the Theory and Its Applications* (McGraw-Hill Book Co., Inc., New York, N. Y., 1966).

7. W. H. Levison, and J. I. Elkind, "Studies of Multivariable Manual Control Systems: Two-Axis Compensatory Systems with Separated Displays and Controls," Bolt Beranek and Newman Inc., Rept. 1459, Feb. 1962.

8. H. M. James, N. B. Nichols and R. S. Phillips, "Manual Tracking" in *Theory of Servomechanisms* (McGraw-Hill Book Co., Inc., New York, N. Y., 1947), pp. 360-368.

9. J. I. Elkind, "Characteristics of Simple Manual Control Systems," M.I.T., Lincoln Lab. Rept. TR 111, Apr. 1956.

10. N. Wiener, *Extrapolation, Interpolation, and Smoothing of Stationary Time Series* (The M.I.T. Press & John Wiley and Sons, Inc., New York, N. Y., 1950).

11. R. W. Roig, "A Comparison Between Human Operator and Optimum Linear Controller RMS-Error Performance," IRE Trans. Human Factors Electron. HFE-3:18-22 (1962).

12. T. Leonard, "Optimizing Linear Dynamics for Human-Operated Systems by Minimizing the Mean-Squared Tracking Error," WESCON, Vol. 4, Pt. 4, 57-62 (1960).

13. R. W. Obermayer, F. A. Muckler, "On the Inverse Optimal Control Problem in Manual Control Systems," NASA CR-208 (1965).

14. J. Wolkovitch, "A Simple Test for Optimality," IEEE Trans. Human Factors Electron. HFE-8:282-285, No. 4 (Dec. 1967).

15. D. C. Miller, "The Effects of Performance-Scoring Criteria on Compensator Tracking Behavior," IEEE Trans. Human Factors Electron. HFE-6:62-65 (1965).

16. J. D. Burchfield, J. I. Elkind and D. C. Miller, "On the Optimal Behavior of the Human Controller: A Pilot Study Comparing the Human Controller with Optimal Control Models," Bolt Beranek and Newman Inc., Rept. 1532, Aug. 1967.

17. D. L. Kleinman, "Sub-Optimal Design of Linear Regulator Systems Subject to Computer Storage Limitations," M.I.T. Electronic Systems Lab. Rept. 297, Feb. 1967.

18a. H. J. Shear, Jr., and V. A. Utgoff, "Final Systems Analysis and Flight Simulation Report U. S. Army XV-5A," Rept. 64B129, Vol. I.

18b. H. J. Shear, Jr., and V. A. Utgoff, "Final Systems Analysis and Flight Simulation Report U. S. Army XV-5A Lift Fan Research Aircraft," Rept. 64B129, Vol. II.

19. W. M. Wonham, "Lecture Notes on Stochastic Control," Brown University Center for Dynamical Systems, Feb. 1967.

20. E. C. Kris, "A Technique for Electrically Recording Eye Position," WADC-TR-58-660, Dec. 1958.

21. J. I. Elkind and D. M. Green, "Measurement of Time-Varying and Nonlinear Dynamic Characteristics of Human Pilots," ASD-TR-61-225, Dec. 1961.

22. M. C. Grignetti, R. V. Payne and J. I. Elkind, "Signal Analyzer I. A Signal Analysis System for Manual Control Studies," in IEEE Intern. Conv. Record 13, Pt. 6, 143-151, (1965).

23. J. W. Cooley and J. W. Tukey, "An Algorithm for The Machine Calculation of Complex Fourier Series," in Mathematics and Computation 10:297-301, Apr. 1965.

24. R. B. Blackman and J. W. Tukey, *The Measurement of Power Spectra* (Dover Publications, Inc., New York, N. Y., 1959).

25. D. L. Kleinman, "On an Iterative Technique for Riccati Equation Computations," IEEE Trans. on Autom. Control (to be published).

26. W. A. Wolovich, "On the Stabilization of Controllable Systems," (to be published).

27. S. Baron and D. Kleinman, "The Human as an Optimal Controller and Information Processor," Bolt Beranek and Newman Inc., Rept. 1571 (Dec. 1967).

28. C. E. Shannon and W. Weaver, *The Mathematical Theory of Communication* (The University of Illinois Press, Urbana, Illinois, 1949).

29. W. Levison and D. Kleinman, "A Model for Human Controller Remnant," Presented at NASA Conference on Manual Control, University of Michigan (Mar. 1968).

30. P. G. Hoel, *Introduction of Mathematical Statistics* (John Wiley and Sons, New York, N. Y., 1947).

31. W. B. Davenport and W. L. Root, *Random Signals and Noise* (McGraw-Hill Book Co., Inc., New York, N. Y., 1958).

32. R. Bellman and Cooke, K. L., *Differential-Difference Equations* (Academic Press, New York, N. Y., 1963).

Unclassified
Security Classification

DOCUMENT CONTROL DATA - R & D

(Security classification of title, body of abstract and indexing annotation must be entered when the overall report is classified)

1. ORIGINATING ACTIVITY (Corporate author)
Bolt Beranek and Newman Inc.
50 Moulton Street
Cambridge, Massachusetts 02138

2a. REPORT SECURITY CLASSIFICATION
Unclassified

2b. GROUP
N/A

3. REPORT TITLE
AN OPTIMAL CONTROL METHOD FOR PREDICTING CONTROL CHARACTERISTICS AND DISPLAY REQUIREMENTS OF MANNED-VEHICLE SYSTEMS

4. DESCRIPTIVE NOTES (Type of report and inclusive dates)
Final Report Period from 1 July 1966 to 31 August 1967

5. AUTHOR(S) (First name, middle initial, last name)
Jerome I. Elkind, Peter L. Falb, David Kleinman, and William H. Levison

6. REPORT DATE
June 1968

7a. TOTAL NO. OF PAGES
170

7b. NO. OF REFS
30

8a. CONTRACT OR GRANT NO.
Contract No. AF 33(615)-5160

b. PROJECT NO.
#8219

c.
Task No. 821910

d.

9a. ORIGINATOR'S REPORT NUMBER(S)
BBN Report No. 1559

9b. OTHER REPORT NO(S) (Any other numbers that may be assigned this report)
AFFDL-TR-67-187

10. DISTRIBUTION STATEMENT
This document has been approved for public release and sale; its distribution is unlimited.

11. SUPPLEMENTARY NOTES

12. SPONSORING MILITARY ACTIVITY
AF Flight Dynamics Laboratory
Wright-Patterson AFB, Ohio 45433

13. ABSTRACT
An analytic procedure for determining information display requirements and human control and instrument monitoring characteristics for complex multivariable vehicular control systems is developed. The method is based upon the assumption that the human controller will act in a near optimal manner. Optimal control theory and its associated state-space representation is used as the basis for the analytic procedure. A model for the human controller is developed in which the controller's inherent limitations are approximated by a time delay. The model includes a predictor for compensating for this time delay, a controller for producing the control inputs to the vehicle and a cost functional that is to be minimimized. The controller is assumed to be optimal. Several suboptimal predictors are investigated. Only quadratic cost functionals are considered. The analytic procedure assumes that the human operator's control characteristics can be represented by a set of gains operating on the delayed state variables of the system. These gains are predicted from the gains of optimal controller and from the characteristics of the predictor. It is further postulated that the information display requirements and instrument monitoring behavior can be determined from the sensitivity of the cost to changes in gain of the controller.

DD FORM 1 NOV 65 1473 (PAGE 1)
S/N 0101-807-6811

Unclassified
Security Classification

A-3140R

14. KEY WORDS	LINK A		LINK B		LINK C	
	ROLE	WT	ROLE	WT	ROLE	WT
1. Optimal Control						
2. Manual Control Systems						
3. Display Requirements Prediction						